Chapter 4

The Kinetics of Pressure-Dependent Reactions

Hans-Heinrich Carstensen and Anthony M. Dean

1 INTRODUCTION

Commonly used reaction mechanisms for atmospheric or combustion systems contain a significant fraction of unimolecular and chemically activated reactions. Each of these reactions is in principle both temperature and pressure dependent, although the pressure dependence might vanish under certain conditions. Consequently, in order to achieve accurate kinetic predictions of complex chemical systems, it is necessary to incorporate this pressure and temperature dependence into kinetic models. This leads to the need to develop tools which allow the kineticist to analyze these types of reactions and which yield apparent time-independent rate constants that can be used in modeling studies.

Among the reaction types that display pressure dependence are radical–radical recombination reactions, addition reactions of radicals to multiple bonds, insertions of species with empty orbitals (e.g., carbenes) into single bonds, elimination reactions, dissociation reactions (e.g., β-scission), and isomerization reactions. All these reactions can be thought of as a sequence of at least two steps with one of them being an excitation process followed either by a deactivation step, in which excess energy has to be removed by the bath gas to stabilize a molecule, or by a reaction producing generally[1] two or more products. We shall clarify this in the following section and note for the moment that it is energy transfer to or from a molecule or intermediate that distinguishes a pressure-dependent reaction from a pressure-independent one.

In this chapter we will first review the underlying theory of unimolecular and recombination reactions, starting with single-channel single-well systems and then considering complex multi-well systems. We then briefly discuss a few program packages, which allow a kinetic analysis of

[1]Pure isomerization reactions are an exception, because only one product (the isomer) is formed per reaction channel.

Comprehensive Chemical Kinetics, Volume 42, 101–184

ISSN: 0069-8040/doi:10.1016/S0069-8040(07)42004-0

pressure-dependent reactions, and also describe some methods to obtain the required input parameters. Finally, we present results of the kinetic analysis of several example reactions. These detailed calculations allow a comparison of the predictions with experimental data and a discussion of the accuracy of different methods and the input parameters they need. We conclude with an outlook of anticipated future research directions.

2 REVIEW OF PRESSURE-DEPENDENT REACTIONS

2.1 Unimolecular reactions

In this section we try to provide a short introduction of unimolecular reactions to set the stage for the practical applications that are discussed later in this chapter. For a more detailed discussion, the reader is referred to kinetics textbooks, e.g., those by Holbrook *et al.* [1] or Gilbert and Smith [2], which served as a guide for the following discussion.

Consider the unimolecular reaction $AB \rightarrow A + B$, which designates either a dissociation or an elimination reaction. The simplest model to qualitatively describe this reaction was proposed by Lindemann. It splits the overall process into two steps:

$$AB + M \underset{k_{-1}}{\overset{k_1}{\rightleftharpoons}} AB^* + M$$

$$AB^* \xrightarrow{k_2} A + B$$

The first step, a ''strong'' collision between a bath gas molecule (M) and a reactant AB, transfers enough energy to AB to reach a state above the reaction barrier (excitation step). This energized state AB^* then either rearranges to the products $A + B$ (reaction) or it loses energy in a subsequent collision to re-form AB (deactivation). After a short time, formation and consumption of AB^* will be in balance, or in other words the concentration of AB^* (symbolized as $[AB^*]$) reaches a constant value, called the steady-state concentration. At this time the condition $d[AB^*]_{ss}/dt = 0$ holds. If we assume that the time required to achieve the steady-state condition is negligible compared to the total reaction time, then the apparent unimolecular rate constant, k_{uni}, for the reaction $AB \rightarrow A + B$ can be derived as follows:

$$\frac{d[AB^*]_{ss}}{dt} = k_1[M][AB] - \{k_{-1}[M] + k_2\}[AB^*]_{ss} = 0 \qquad (1)$$

$$[AB^*]_{ss} = \frac{k_1[M]}{k_{-1}[M] + k_2}\ [AB] \tag{2}$$

$$-\frac{d[AB]}{dt} = \frac{d[A]}{dt} = \frac{d[B]}{dt} \equiv k_{uni}[AB] = k_2[AB^*] \cong k_2[AB^*]_{ss} \tag{3}$$

$$k_{uni} = \frac{k_1 k_2[M]}{k_{-1}[M] + k_2} \tag{4}$$

The two limiting cases of low ($[M] \to 0$) and high ($[M] \to \infty$) collider concentrations lead to expressions for the low-pressure rate constant k_0 and the high-pressure rate constant k_∞:

$$[M] \to 0, \quad k_{uni} \to k_{uni,0} \equiv k_0 = k_1[M] \tag{5}$$

$$[M] \to \infty, \quad k_{uni} \to k_{uni,\infty} \equiv k_\infty = \frac{k_1 k_2}{k_{-1}} \tag{6}$$

Fig. 1 schematically shows a double logarithmic plot of k_{uni} as a function of the total pressure, a so-called fall-off plot. If we use the low-pressure region as reference point, we observe that k_{uni} departs at a certain pressure from the linear relationship and "falls off" to the high-pressure limit. The transition region, in which k_{uni} switches from the low-pressure to the high-pressure rate regime, is called the fall-off region.[2] Its location may be characterized by the pressure $p_{1/2}$, at which k_{uni} equals $1/2k_\infty$. By substituting k_∞ in equation (4) with $1/2k_\infty$ and substituting k_∞ with the expression in equation (6) it follows after rearranging that at $p_{1/2}$ the condition $k_2 = k_{-1}[M]_{1/2}$ holds. This relationship allows one to determine how the location of the fall-off region shifts as a function of temperature. Typically k_2 grows faster with temperature than k_{-1} does; hence, with increasing temperature a larger concentration $[M]_{1/2}$ is required to fulfill the $k_2 = k_{-1}[M]_{1/2}$ condition. Further, since $[M]_{1/2} = p_{1/2}/RT$, the pressure required to maintain the same $[M]_{1/2}$ concentration scales with T. Both effects cause the fall-off region to shift with increasing temperature toward higher pressure. The magnitude of shift when going from low to high temperature conditions can be substantial, e.g., a reaction which at room temperature is at or near its high-pressure limit might be deep in the fall-off region at combustion temperatures. This explains why the pressure dependence of rate constants is especially important for the modeling of combustion systems.

[2] An alternative definition of the fall-off is possible by choosing the high-pressure limit as reference point. In the high-pressure regime, $k_{uni}/k_\infty = 1$. Some authors refer the fall-off region as the pressure range for which this ratio declines ("falls off"). According to this definition a rate is in a fall-off region as long as the high-pressure limit is not reached.

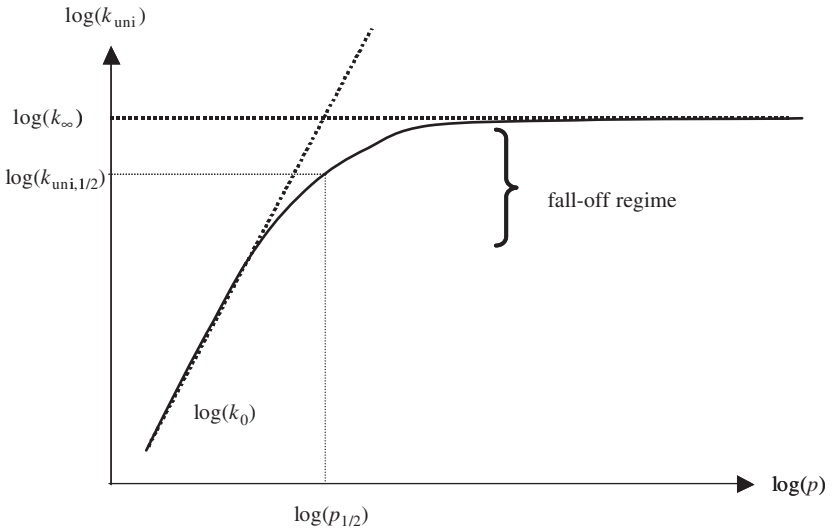

Fig. 1. A schematic fall-off plot for a unimolecular rate constant as function of pressure.

The unimolecular rate constant k_{uni} is usually expressed in terms of k_0 and k_∞, or, alternatively, in terms of the reduced pressure p_{r}, defined as

$$p_{\text{r}} = \frac{k_0[\text{M}]}{k_\infty} \tag{7}$$

$$k_{\text{uni}} = k_\infty \frac{p_{\text{r}}}{1 + p_{\text{r}}} \tag{8}$$

In the simplest form, the Lindemann mechanism assumes that the rate constants for the activation and deactivation steps, k_1 and k_{-1}, do not depend on energy and can directly be calculated from kinetic collision theory. With the probability for the AB species to obtain energy $\geqslant E_0$ being $\exp(-E_0/RT)$, we obtain

$$k_1 = Z_{\text{col}}\, \text{e}^{-E_0/RT} \tag{9}$$

$$k_{-1} = Z_{\text{col}} \tag{10}$$

The rate constant k_2 was initially also assumed to be independent of the energy in AB* and its value should be comparable to or smaller than a vibrational frequency ($10^{13}\,\text{sec}^{-1}$). For cases in which the high-pressure rate constant k_∞ is known from experiments one can calculate k_2 by rearranging equation (6),

$$k_2 = \frac{k_\infty k_{-1}}{k_1} \tag{11}$$

Although the Lindemann model can explain the occurrence of a fall-off region, it predicts its location to occur at several orders of magnitude higher pressures than experimentally observed. Related to this, calculated k_2 rate constants from experimental high-pressure rate constants were found to be unrealistically large. One major cause of these problems is the inherent assumption that AB and AB* can be treated as different species. If so, then we obtain with $\Delta G \approx E_0$

$$\frac{k_1}{k_{-1}} = K_{\text{eq}} = \text{e}^{-E_0/RT} \tag{12}$$

which leads to equation (9). In reality, AB* is the same species as AB with the difference that it contains additional internal energy, mainly stored in vibrational modes. A given amount of excess energy can be stored in many different combinations of vibrations (states) and the number of states increases rapidly with energy. Since AB* therefore exists in many different states, the probability to excite AB to AB* increases (it scales with the number of states). Hinshelwood derived an expression for this probability[3] based on the assumption that all vibrations are classical oscillators at equilibrium:

$$f(E) = \frac{(E/kT)^{s-1}}{(s-1)!}\text{e}^{-E/kT} \tag{13}$$

If this probability is incorporated into equation (9), one obtains

$$k_1 = Z_{\text{col}}\frac{(E_0/kT)^{s-1}}{(s-1)!}\text{e}^{-E_0/kT} \tag{14}$$

The ratio $(E/kT)^{s-1}/(s-1)!$ is usually significantly larger than unity; hence, k_1 increases compared to the initial Lindemann model. k_{-1} remains unchanged, because within the "strong" collision assumption every collision will still deactivate AB*. From equation (11) we see that an increase of k_1 leads to a smaller k_2 rate constant, which in turn reduces the bath gas density $[\text{M}]_{1/2}$ required to fulfill $k_2 = k_{-1}[\text{M}]_{1/2}$, our definition of the location of the fall-off region. Therefore, this modification improves both issues with the original model: it moves the fall-off regime to a lower pressure range and it leads to a more realistic value for k_2.

An important consequence of the Hinshelwood–Lindemann treatment is that the probability to find AB at the energy E depends now on the number of oscillators, s, or in other words on the size of the reacting

[3]We are using three different symbols for the energy distribution function: f(E) denotes the Boltzmann (equilibrium) distribution function, g(E) refers to an unspecified distribution function, and h(E) describes the overall energy distribution of reactants in chemically activated systems.

molecule AB. Larger species are more easily activated to energies above E_0 than small molecules.

In general, the Hinshelwood–Lindemann model reproduces the location of the fall-off region well, though the shapes of experimental fall-off curves are still not accurately captured. To further improve the theory, a modified reaction scheme proves to be helpful:

$$AB + M \underset{k_{-1}}{\overset{k_1}{\rightleftharpoons}} AB^* + M$$

$$AB^* \xrightarrow{k_2} AB^{\#}$$

$$AB^{\#} \rightarrow A + B$$

The conversion of AB^* to products is now thought to proceed *via* a critical geometry $AB^{\#}$. AB^* and $AB^{\#}$ have the same energy, E, with $E \geqslant E_0$, but in AB^* this energy is randomly distributed among all oscillators, while in $AB^{\#}$ an amount $E_m \geqslant E_0$ is localized in the reactive mode. This is the basic idea of the RRK theory (Rice–Ramsperger–Kassel). The assumption of random energy distribution among all modes allows the calculation of statistical weights for AB^* and $AB^{\#}$. To do so, Kassel assigned—in the quantum version of this theory—a single average frequency, v, to all oscillators of AB. Now, the total distributable energy E is made up by n quanta and the threshold energy E_0 by m quanta ($n \geqslant m$) of v. Statistically, the probability w to distribute n quanta of energy among s oscillators is given by

$$w(AB^*) = \frac{(n+s-1)!}{n!(s-1)!} \tag{15}$$

In the case of $AB^{\#}$ only n–m quanta are freely distributable, which leads to

$$w(AB^{\#}) = \frac{(n-m+s-1)!}{(n-m)!(s-1)!} \tag{16}$$

The rate constant k_2 is proportional to the ratio of these probabilities

$$k_2(E) \sim \frac{w(AB^{\#})}{w(AB^*)} = \frac{(n-m+s-1)!/\{(n-m)!(s-1)!\}}{(n+s-1)!/\{n!(s-1)!\}} \tag{17}$$

$$k_2(E) = A_{2,\infty} \frac{n!(n-m+s-1)!}{(n-m)!(n+s-1)!} \tag{18}$$

Now, k_2 is a function of the total energy E stored in AB*. The proportionality constant, $A_{2,\infty}$, can be identified as the high-pressure pre-exponential factor of $k_{2,\infty}$. The single frequency model also leads to a description of the ratio between $k_1(E)$ and k_{-1}:

$$\frac{k_1(E = nhv)}{k_{-1}} = \frac{(n + s - 1)!}{n!(s - 1)!}(1 - e^{-hv/kT})^s e^{-nhv/kT} \tag{19}$$

Written in this way, $k_2(E)$ and $k_1(E)/k_{-1}$ are step functions because n is an integer. This problem can easily be overcome by replacing $n!$ with the gamma function $\Gamma(n+1)$, which transforms them into continuous functions.

The single frequency versions of RRK and QRRK[4] theories predict experimental fall-off curves in most cases reasonably well if s is identified with the number of "effective" oscillators, which is often about one-half of the number of actual oscillators. Several ways to calculate the number of effective oscillators s are suggested in the literature. For example, Troe and Wagner [3] use

$$s = \frac{E_{\text{vib}}}{kT} \tag{20}$$

and Golden *et al.* [4] recommend

$$s = \frac{C_{\text{vib}}}{R} \tag{21}$$

A related question is how to determine the representative frequency. Investigations by, e.g., Weston [5] revealed that results obtained by using the geometric mean frequency agree "invariably better" with exact rate calculations compared to results from calculations employing the average mean frequency. Nevertheless, rate expressions obtained with RRK theory in its single frequency version often deviate substantially from experimental data. Kassel already pointed out that it is possible to extend RRK theory to a multi-frequency version, and Schranz *et al.* [6] demonstrated that a two-frequency model leads to improved accuracy. Later Chang *et al.* [7] reported the implementation of a three-frequency QRRK model with non-integer degeneracies of the representative frequencies. This method is useful for cases in which the complete sets of frequencies of the reacting species are not available, but their thermodynamic properties can be estimated *via*, e.g., group additivity methods. The representative frequencies are then obtained from fits to the $C_p(T)$ values [8].

[4]The name QRRK is not clearly defined. Here, we use QRRK to denote the quantum version of RRK theory, also referred as quantum Kassel theory.

Marcus modified the RRK theory to what is known as *RRKM* theory. RRKM theory is the microcanonical[5] version of transition state theory, and $AB^{\#}$ is identified as the transition state of the reaction. A transition state is defined as the "dividing surface" between reactants and products, and its location is determined by the condition that every trajectory (flux), which passes this surface, will form the products without recrossing. The second major assumption of RRKM theory, the ergodicity assumption, requires fast and complete randomization of the available freely distributable energy among all active modes after excitation. This assumption recognizes that only a part of the internal energy can freely be distributed among different modes. Examples of contributions to the internal energy that are assigned to a particular mode and hence not distributable are (1) the zero-point energy of vibrations and (2) a fraction of the rotational energy, which is bound to rotational modes due to the conservation law of total angular momentum. Hence, the distributable energy is mainly vibrational energy (excluding the zero-point energy) stored in oscillators and to a small extent rotational energy. It is common to consider all vibrations and one rotation (the so-called K-rotor) as active modes.

The rate constant $k_2(E)$ will depend on the transition frequency ($v^{\#}$) with which a trajectory passes through the transition state, $v^{\#} = kT/h$, and the probability (statistical weight ratio) to form the transition state geometry from all AB^*. This probability can be determined from the sum of states, $W(E)$ of $AB^{\#}$, and the number of states of AB^* at the energy E. Because the number of states of AB^* is generally enormously high, it is expressed *via* its density of states ($\rho(E)$, number of states per energy interval). The final expression[6] for $k_2(E)$ in the RRKM theory is

$$k_2(E) = \frac{kT}{h}\frac{W^{\#}(E - E_0)}{\rho(E)kT} = \frac{W^{\#}(E - E_0)}{h\rho(E)} \tag{22}$$

The unimolecular rate constant is obtained by integrating over all energy levels above E_0, weighted by the population distribution, $g(E)$:

$$k_{\text{uni}} = \int_{E_0}^{\infty} \frac{k_2(E)k_1(E)/k_{-1}}{1 + k_2(E)/k_{-1}[\text{M}]} g(E)\,\mathrm{d}E \tag{23}$$

[5]A microcanonical system is characterized by the number of particles (N), its volume (V), and the energy (E). Therefore, a microcanonical rate constant is a function of energy. On the other hand, a system defined by its temperature instead of its energy is called a canonical system and consequently, canonical rate constants are functions of T.

[6]For a detailed derivation of the RRKM theory, please refer to textbooks on chemical kinetics.

The ratio $k_1(E)/k_{-1}$ is easily evaluated for the condition of equilibrium

$$\frac{k_1(E)}{k_{-1}} = K_{eq} = \frac{Q_{AB^*}(E)}{Q_{AB}} \tag{24}$$

By applying the definition of a partition function Q,

$$Q = \sum_{i=0}^{\infty} g_i \, e^{-E_i/kT} \tag{25}$$

to a "species" existing only at the energy E (more precisely in the range E, $E + dE$),

$$Q(E) = \left(\sum_{E}^{E+dE} g(E) \right) e^{-E/kT} = \rho(E) e^{-E/kT} \tag{26}$$

we obtain

$$\frac{k_1(E)}{k_{-1}} = \frac{\rho(E)}{Q_{AB}} e^{-E/kT} \tag{27}$$

This points to the key role of the density of states, $\rho(E)$, in RRKM theory, as it is not only needed to calculate k_2, but also for the ratio between the activation and the deactivation rate constants.

At the high-pressure limit, equation (23) can be integrated analytically and it can be shown that $k_{uni}(T)$ obtained from RRKM theory as described here is similar but not equal to the high-pressure rate obtained *via* canonical transition state theory[7]

$$k_{uni,[M]\to\infty} = \frac{kT}{h} \frac{Q^{\#}_{vib}}{Q_{vib}} e^{-E_0/kT} \tag{28}$$

$$k_{TST} = \frac{kT}{h} \frac{Q^{\#}_{rot} Q^{\#}_{vib}}{Q_{rot} Q_{vib}} e^{-E_0/kT} \tag{29}$$

Equations (28) and (29) differ in that latter contains contributions from the rotational partition functions. This contribution is lost in a RRKM analysis unless one includes the total angular momentum, J, and thus formulates the microcanonical rate constants as $k(E, J)$. In many cases, the geometries of the transition state and the reactant are very similar and consequently the ratio of the rotational partition functions is very

[7]The transition state theory developed by Eyring and by Evans and Polanyi yields high-pressure rate constants $k(T)$. Since it is based on the same assumptions as the RRKM theory (existence of a transition state and fast complete energy distribution), the results from both theories should coincide. See textbooks for more details on TS theory.

close to unity. Then equations (28) and (29) lead to the same result. Reactions with loose transition states, e.g., those involving ionic species, are examples for which a simple $k(E)$ treatment is not accurate and a $k(E, J)$ analysis required.

In summary, an adequate kinetic description of unimolecular reactions requires knowledge of the rate constants for the individual processes of activation, deactivation, and transformation to products. In addition, the population distribution function for the reactant as a function of the internal energy E is needed. Within the framework of the steady-state treatment and strong collisions, the key property describing the population distribution is the density of states, $\rho(E)$. Both QRRK and RRKM theories are statistical methods and assume that excess energy is rapidly distributed among all active modes. Besides the barrier height and the pre-exponential factor of the high-pressure rate constant, QRRK theory only requires knowledge of the representative frequency(ies) of the reacting molecule and its collision parameters. This information is easily obtained from the literature or estimation methods, so that QRRK calculations can be performed with comparatively little effort. In contrast, detailed frequency and rotational data for the stable species as well as for the transition state are needed as input for RRKM theory. If such information is available, however, RRKM theory is more fundamental and precise and the method of choice.

2.2 Chemically activated reactions

The recombination $A + B \rightarrow AB$ is the reverse reaction of the unimolecular dissociation of AB. The principle of detailed balancing ties both reactions together by the thermodynamic equilibrium constant

$$\frac{k_{\text{uni}}}{k_{\text{rec}}} = K_{\text{eq}} \tag{30}$$

Consequently, k_{rec} is—like k_{uni}—pressure dependent. This is obvious for the high-pressure limit when collisions with the bath gas quickly establish a Boltzmann distribution of the population, but Smith *et al.* [9,10] argue that equation (30) also holds for lower pressures.

In the introduction we characterized a pressure-dependent reaction as a process that is composed of an excitation step followed by either deactivation or reaction to (often multiple) products. A closer look at the recombination in terms of the underlying scheme of elementary reactions

$$A + B \underset{k_2}{\overset{k_{-2}}{\rightleftharpoons}} AB^*$$

$$AB^* + M \xrightarrow{k_{-1}} AB + M$$

reveals that these criteria are met. The excitation step is called *chemical activation*, since energized AB^* molecules are created when a new bond is formed during the recombination process. Previously we discussed excitation due to collisions with the bath gas or so-called thermal activation. The energy distribution of initially formed AB^* with respect to non-activated AB is determined by two contributions: (1) the energy released from the newly formed bond and (2) the thermal energy content in both reactants, which is commonly assumed to follow a Boltzmann distribution. Redissociation of the excited complex leads back to the reactants (hence special type of products) and collisions with the bath gas to stabilization. Thus, all elements of a pressure-dependent reaction are present.

Application of the steady-state assumption for $[AB^*]$ yields the apparent recombination rate constant for stabilization, defined as $d[AB]/dt = k_{rec}[A][B]$,

$$k_{rec} = \frac{k_{-1}k_{-2}[M]}{k_{-1}[M] + k_2} \tag{31}$$

$$[M] \to 0, \quad k_{rec} \to k_{rec,0} \equiv k_0 = \frac{k_{-1}k_{-2}}{k_2}\ [M] \tag{32}$$

$$[M] \to \infty, \quad k_{rec} \to k_{rec,\infty} \equiv k_\infty = k_{-2} \tag{33}$$

If we combine equations (4) and (31) we can show that equation (30) is obtained:

$$\frac{k_{uni}}{k_{rec}} = \frac{k_1k_2[M]/\{k_{-1}[M] + k_2\}}{k_{-1}k_{-2}[M]/\{k_{-1}[M] + k_2\}} = \frac{k_1k_2}{k_{-1}k_{-2}} = \frac{[AB][AB^*]}{[AB^*][A][B]}$$
$$= K_{eq} \tag{34}$$

In other words, if a steady-state population of the energized complex AB^* is formed, then the recombination and corresponding dissociation reactions always obey detailed balancing. Deviations from this principle may only occur in situations in which the steady-state condition is not (yet) reached.

Building on our definition for pressure dependence one might wonder about the impact of additional product channels. Adding just one additional product channel leads to the following scheme:

$$A + B \underset{k_2}{\overset{k_{-2}}{\rightleftharpoons}} AB^*$$

$$AB^* + M \xrightarrow{k_{-1}} AB + M$$

$$AB^* \xrightarrow{k_3} C + D$$

An example for such a case is the reaction between C_2H_5 radicals and H atoms. The C + D channel would then refer to the products $CH_3 + CH_3$, and AB can be identified with C_2H_6. The expression for the steady-state concentration of AB^*

$$[AB^*]_{ss} = \frac{k_{-2}[A][B]}{k_{-1}[M] + k_2 + k_3} \tag{35}$$

contains one additional term ($+k_3$) in the denominator compared to the previous scheme. However, we now need two apparent rate constants to fully describe this chemically activated reaction: one to describe the stabilization step and the second one for the formation channel of the new products.

$$A + B \xrightarrow{k_{stab}} AB \Rightarrow \frac{d[AB]}{dt} = k_{stab}[A][B]$$

$$A + B \xrightarrow{k_{prod}} C + D \Rightarrow \frac{d[C]}{dt} = \frac{d[D]}{dt} = k_{prod}[A][B]$$

If we formulate the formation of AB or C + D in terms of $[AB^*]_{ss}$, we obtain expressions for k_{stab} and k_{prod}

$$\begin{aligned} &\frac{d[AB]}{dt} = k_{-1}[M][AB^*]_{ss} = k_{-1}[M]\frac{k_{-2}[A][B]}{k_{-1}[M] + k_2 + k_3} \\ &\Rightarrow k_{stab} = \frac{k_{-1}k_{-2}[M]}{k_{-1}[M] + k_2 + k_3} \end{aligned} \tag{36}$$

$$\begin{aligned} &\frac{d[C]}{dt} = \frac{d[D]}{dt} = k_3[AB^*]_{ss} = k_3\frac{k_{-2}[A][B]}{k_{-1}[M] + k_2 + k_3} \\ &\Rightarrow k_{prod} = \frac{k_3k_{-2}}{k_{-1}[M] + k_2 + k_3} \end{aligned} \tag{37}$$

By considering the limiting case of high pressure, we again find that the high-pressure rate constant for stabilization is independent of [M]. More interesting is to examine the pressure dependence of the apparent rate constant for the C + D product channel. This rate constant at its high-pressure limit is inversely proportional to pressure. This is also true for the redissociation reaction, which is just a special product channel.

$$\Rightarrow k_{redis} = \frac{k_2k_{-2}}{k_{-1}[M] + k_2 + k_3} \tag{38}$$

By combining equations (36)–(38) it is easy to show that the sum of all three apparent rate constants equals k_{-2}, or in other words that the rate for the formation of the excited complex equals the sum of all complex consuming rates (as it should be).

2.3 *Energy transfer models*

(*i*) *The modified strong collision assumption*

Before continuing the discussion of more complicated reaction systems we will consider the energy transfer process. So far the discussion was based on the assumption that all collisions are "strong," meaning that a single collision with a collider species completely activates AB or deactivates AB*. This assumption leads to a bimodal energy distribution and ignores the fact that depending on the collision angle, relative velocities of the colliding species, and energy distribution in the colliders a wide range of interactions is possible. Certainly, in the real world, not each "collision" will lead to complete exchange of energy. In order to keep the simplicity of the strong collision assumption, the "modified strong collision (MSC)" approach was developed. It basically assumes that only a fraction of all collisions is "strong" while the remaining collisions are elastic (no transfer of internal energy). The collision parameter β_c describes the fraction of "successful" collisions as a function of collider properties and the temperature. If we express the collision frequency ω, defined as the number of collisions per time, in terms of the Lennard–Jones diameters σ_R and σ_M for a reactant R and bath gas M, we obtain

$$\omega_{LJ} = N_A \left(\frac{\sigma_R + \sigma_M}{2}\right)^2 \sqrt{\frac{8\pi kT}{\mu}}\, \Omega^{*(2,2)}(T)\,[M] \tag{39}$$

where N_A is the Avogadro number, μ the reduced mass, and $\Omega^{*(2,2)}$ the collision integral. In the framework of the MSC assumption, the stabilization rate constant is then given as

$$k_{MSC} = \beta_c \omega_{LJ} \tag{40}$$

Based on solutions of the master equation (ME) (see below) for model systems, Troe [11,12] developed a relationship between the collision efficiency parameter (β_c) and the average energy transferred per collision, $\langle \Delta E_{all} \rangle$

$$\frac{\beta_c}{1 - \sqrt{\beta_c}} \cong \frac{-\langle \Delta E_{all} \rangle}{F_E kT} \tag{41}$$

The "energy-dependence factor" of the density of states F_E is a function introduced by Troe [13] and it is defined for vibrational densities of

states as

$$F_E(T) = \frac{\int_{E_0}^{\infty} \rho_{\text{vib}}(E)\text{e}^{-E/kT}\,\text{d}E}{kT\rho_{\text{vib}}(E_0)\text{e}^{-E_0/kT}} \tag{42}$$

In this equation we explicitly write F_E as a function of temperature to emphasize that it is not a constant number. Evaluation of F_E requires knowledge of $\rho_{\text{vib}}(E)$ and in a later section we will describe methods to accurately calculate this function.

Gilbert *et al.* [14] showed that the approximation given by equation (41) leads to inaccurate results for high values of F_E and suggested the following alternative formulation:

$$\beta_{\text{c}} = \left(\frac{\alpha_{\text{c}}}{\alpha_{\text{c}} + F_E kT}\right)^2 \frac{1}{\Delta} \tag{43}$$

In this equation α_{c} represents the average energy transferred in deactivating (''down'') collisions. α_{c} is related to $\langle \Delta E_{\text{all}} \rangle$ *via*

$$\langle \Delta E_{\text{all}} \rangle = \gamma_{\text{c}} - \alpha_{\text{c}} \tag{44}$$

and

$$\gamma_{\text{c}} = \frac{\alpha_{\text{c}} F_E kT}{\alpha_{\text{c}} + F_E kT} \tag{45}$$

where γ_{c} represents the average energy transferred in activating (''up'') collisions. Notice that because the average energy transferred in down collisions is always larger than that for up collisions, $\langle \Delta E_{\text{all}} \rangle$ is defined as a negative property. This explains the negative sign in equation (41) to ensure $0 < \beta_{\text{c}} \leq 1$.

The property Δ in equation (43) can again be calculated if the functions F_E and $\rho_{\text{vib}}(E)$ are known:

$$\Delta = \Delta_1 - \left[\frac{F_E kT}{\alpha_{\text{c}} + F_E kT}\right]\Delta_2 \tag{46}$$

$$\Delta_1 = \frac{\int_0^{E_0} \rho_{\text{vib}}(E)\text{e}^{-E/kT}\text{d}E}{\Delta_N} \tag{47}$$

$$\Delta_2 = \frac{\int_0^{E_0} \rho_{\text{vib}}(E)\text{e}^{-E/kT}\,\text{e}^{-(E_0-E)/F_E kT}\,\text{d}E}{\Delta_N} \tag{48}$$

$$\Delta_N = \int_0^{\infty} \rho_{\text{vib}}(E)\text{e}^{-E/kT}\,\text{d}E \tag{49}$$

Although these integrals might look complicated, they can easily be evaluated if the density of states function is given in an analytic way as introduced by Whitten and Rabinovitch [15]. Essentially ρ_{vib} (E) is expressed as a polynomial in E and the above integrals have analytic solutions (see, e.g., Ref. [16]).

(*ii*) *The master equation*

A realistic description of energy transfer would include all possible states or energy levels of a molecule AB with AB* being a subset of AB. In a collision, energy can be transferred as translational, vibrational, and rotational energy. Since the rate constants of pressure-dependent reactions depend only on the energy content in active modes, we can ignore changes in translational energy in this context. Due to the restriction of total angular momentum conservation, only a small part of rotational energy is freely distributable and available for reaction. Consequently, the transfer of energy as vibrational energy is most important. In reality, vibrations and rotations are coupled, meaning that they are not completely independent of each other. However, a separation of modes is often a good assumption and generally internal modes are treated as independent harmonic oscillators and rigid rotors (HO–RR approximation).

A collision between two colliders will not depend on previous collisions if we assume rapid energy redistribution among all active modes in-between collisions. In other words, "collisions" are independent events, and they depend only on the initial states of the two colliding partners. Therefore, we can describe them as Markovian or "random walk" processes, and we can assign time-independent rate constants for the transition of a species AB from a state of energy E' to a state of energy E:

$$\frac{\mathrm{d}[\mathrm{AB}(E)]}{\mathrm{d}t} = k(E, E')[\mathrm{AB}(E')] \tag{50}$$

Looking at the evolution of the population of states of energy E with time t, we obtain

$$\frac{\partial \rho(E,t)}{\partial t} = \int_{E'} k(E, E')\rho(E', t)\mathrm{d}E' - \int_{E'} k(E', E)\rho(E, t)\mathrm{d}E' \tag{51}$$

$$\frac{\partial \rho(E,t)}{\partial t} = \sum_{E'} k(E, E')\rho(E', t) - \sum_{E'} k(E', E)\rho(E, t) \tag{52}$$

The first term of the right-hand side of either the continuous (51) or discrete (52) formulation describes the increase of $\rho(E, t)$ *via* transitions from levels E' to E while the second term represents depletion of $\rho(E, t)$ to states of energy E'. In the following, we will focus on the discrete

description since it is the basis for implementation into computer codes. $\rho(E', t)$ may also be thought of as a population density function (population per energy interval), in which case equations (51) and (52) are descriptions of the evolution of the population density with time. If the transfer of AB from a state E to E' is exclusively caused by collisions, we can define the collision frequency $\omega(E)$ as

$$\omega(E) = \sum_{E'} k(E', E) \tag{53}$$

and equation (52) becomes

$$\frac{\partial \rho(E,t)}{\partial t} = \sum_{E'} k(E, E')\rho(E', t) - \omega(E)\rho(E, t) \tag{54}$$

It is desirable to define a normalized transition probability $P(E, E')$

$$P(E, E') = \frac{k(E, E')}{\sum\limits_{E} k(E, E')} = \frac{k(E, E')}{\omega(E')} \tag{55}$$

which allows us to rewrite equation (54) to

$$\frac{\partial \rho(E,t)}{\partial t} = \omega(E') \sum_{E'} P(E, E')\rho(E', t) - \omega(E)\rho(E, t) \tag{56}$$

This latest transformation is only valid with the assumption that the collision frequency $\omega(E')$ is only a weak function of E and hence can be treated as a constant. This assumption holds well if, for example, Lennard–Jones collision frequencies are used.

The detailed balancing requirement puts a constraint on the reverse energy transfer rates ($f(E)$ is again the equilibrium distribution function):

$$k(E, E')f(E') = k(E', E)f(E) \tag{57}$$

or in terms of transition probabilities:

$$\omega(E')P(E, E')f(E') = \omega(E)P(E', E)f(E) \tag{58}$$

Again utilizing $\omega(E) \cong \omega(E')$, the detailed balancing requirement simplifies to

$$P(E, E')f(E') = P(E', E)f(E) \tag{59}$$

Numerous energy transfer models for $P(E, E')$ are discussed in the literature [17]; the most widely known and used one is the "exponential down model." It assumes that the probability to transfer energy in a single collision event depends exponentially on the energy amount that is transferred. Small amounts of energy are more likely transferred than

large quantities. If the probability is expressed as

$$P(E', E) = A(E')e^{-\alpha(E-E')}, \quad \text{for } E \geq E' \tag{60}$$

then we can identify the parameter α to be inversely proportional to the average energy transferred in deactivating collisions:

$$\alpha = \frac{1}{\langle E_{\text{down}} \rangle} \tag{61}$$

$\langle E_{\text{down}} \rangle$ values range from $\sim 100\,\text{cm}^{-1}$ to $200\,\text{cm}^{-1}$ for weak colliders such as He and can take values $> 1000\,\text{cm}^{-1}$ if the bath gas belongs to the group of very strong colliders. Equation (60) defines only the energy transfer probabilities of deactivating collisions. The complementary probability function for activating collisions,

$$P(E, E') = A(E')e^{-\alpha(E-E')}\frac{f(E)}{f(E')}, \quad \text{for} \quad E > E' \tag{62}$$

is obtained by substituting equation (60) into equation (59) and rearranging. Note that this time the condition $E > E'$ does not include equality of E and E' to avoid double-counting. Finally, the normalization factor $A(E')$ is determined *via* the criteria

$$\sum_{E} P(E', E) = 1 \tag{63}$$

Besides being a normalization factor, $A(E')$ can also be interpreted as the probability that a collision is elastic, or in other words it is the fraction of collisions that do not lead to energy transfer. This can be seen from equation (60) by setting $E = E'$.

Having specified the energy transfer probabilities $P(E', E)$, we notice that the right-hand side of equation (56) is linear in $\rho(E, t)$. This allows us to rewrite equation (56) as an eigenvalue problem

$$\frac{\partial \rho(E, t)}{\partial t} = \hat{M}\rho(E, t) \tag{64}$$

The operator $\hat{M}$ describes the collision and reaction terms. The solutions of eigenvalue problems are eigenvalues λ_i and the corresponding eigenfunctions ψ_i. A convenient way to define those is *via*

$$\rho(E, t) = \sum_{i} c_i \psi_i(E) e^{\lambda_i t} \tag{65}$$

The population distribution function is described as an expansion of the eigenfunctions and the eigenvalues define their exponential decays. The expansion coefficients c_i are given by the density distribution at $t = 0\,\text{sec}$. The number of chosen energy intervals determines the number of

expansion terms. Since all density distributions are finite and the total mass is conserved, all eigenvalues λ_i must be real and of negative or zero value. They have the physical meaning of relaxation rates. At long times the energy distribution will reach thermal equilibrium. Hence, the largest eigenvalue for pure collision systems must be zero and the second largest eigenvalue describes the slowest relaxation rate. The eigenfunctions ψ_i are most conveniently chosen to be δ-functions. They then define the individual energy intervals of AB used in the discrete expressions of the ME.

2.4 The master equation approach for single-well systems

The review of pressure-dependent reactions, which so far was based on the strong collision assumption, is readily adapted to more sophisticated collision models. Here, we discuss the description of unimolecular reactions in form of the ME. Our initial scheme

$$\mathrm{AB} + \mathrm{M} \underset{P(E,E')}{\overset{P(E',E)}{\rightleftharpoons}} \mathrm{AB}^*$$

$$\mathrm{AB}^* \xrightarrow{k_2(E)} \mathrm{A} + \mathrm{B}$$

translates into the following ME (assuming ω is independent of E):

$$\frac{\partial \rho(E,t)}{\partial t} = \omega \sum_{E'} P(E,E')\rho(E',t) - \omega\rho(E,t) - k_2(E)\rho(E,t) \quad (66)$$

The rate constants k_1 and k_{-1} of the (modified) strong collision model have been replaced by state specific energy transitions as discussed above. The first right-hand term describes the increase of the population density $\rho(E, t)$ by collisions that transfer species which contain the energy E' to states of energy E. Note that the sum includes the case $E' = E$ although it does not increase $\rho(E, t)$. The second term describes the removal of species at energy E by collisions. Again, elastic collisions are included even though they do not lead to depletion of $\rho(E, t)$. The net effect is that the elastic collisions in both terms annihilate each other. Finally, the third term describes the consumption of $\rho(E, t)$ *via* chemical reaction (to form the products A + B). If we label discrete energy intervals with i and j, we can rewrite equation (66) to

$$\frac{\partial \rho_i(t)}{\partial t} = \omega \sum_{E'} P_{ij}\rho_j(t) - \omega\rho_i(t) - k_{2i}\rho_i(t) \quad (67)$$

Written as eigenvalue problem (see equation (64)) we can identify the matrix elements

$$\begin{aligned} M_{ij} &= \omega P_{ij} \\ M_{ii} &= \omega P_{ii} - \omega - k_{2i} \end{aligned} \tag{68}$$

As mentioned before, the solution of this eigenvalue problem provides a set of negative eigenvalues, which contain all kinetic and dynamic information. In most cases collisional relaxation is fast compared to chemical reactions, and if this is the case then the smallest negative eigenvalues will be clearly separated in magnitude from the remaining ones. Since the product formation is irreversible, no thermal equilibrium is reached and the smallest negative eigenvalue is less than zero. Its negative value represents the unimolecular rate constant for the chemical reaction.

The eigenvalues of this eigenvalue problem are found by diagonalizing the matrix $\hat{M}$. The situation is more complicated if collisional relaxation is not fast compared to chemical reaction. In that case, the solution will yield more than one small negative eigenvalues and the overall reaction will proceed on a non-exponential time scale. In other words, if collisional relaxation interferes with unimolecular reaction, the reaction process cannot be described by a time-independent rate constant k_{uni}.

We now take a look at the corresponding chemically activated reaction,

$$\begin{aligned} &\mathrm{A} + \mathrm{B} \underset{k_2(E)}{\overset{k_{-2}(E)}{\rightleftharpoons}} \mathrm{AB}^* \\ &\mathrm{AB}^* + \mathrm{M} \underset{P(E',E)}{\overset{P(E,E')}{\rightleftharpoons}} \mathrm{AB} + \mathrm{M} \end{aligned}$$

This system is described by the following ME:

$$\begin{aligned} \frac{\partial \rho(E,t)}{\partial t} = \omega \sum_{E'} P(E,E')\rho(E',t) - \omega\rho(E,t) \\ - k_2(E)\rho(E,t) + k_{-2,\infty} h(E)[\mathrm{A}][\mathrm{B}] \end{aligned} \tag{69}$$

Several features of this equation make the solution more challenging compared to the dissociation: (1) The last term on the right-hand side makes equation (69) non-linear, because [A] and [B] are both time dependent. (2) Often, the association or recombination rate is only known as high-pressure rate $k_{-2,\infty}(T)$. (3) The deactivation of energized AB is reversible so that stabilized AB can be reactivated. Starting with the second problem, it can be resolved by introducing a new function $h(E)$ to convert $k_{-2,\infty}(T)$ to an energy-dependent rate constant. This function

$h(E)$ is easily determined from considerations at equilibrium, with

$$\frac{k_{-2,\infty}}{k_{2,\infty}} = \frac{[\mathrm{AB}]}{[\mathrm{A}][\mathrm{B}]} = K_{\mathrm{eq}} \tag{70}$$

Under the same conditions, detailed balancing requires

$$k_{-2,\infty} h(\mathrm{E})[\mathrm{A}][\mathrm{B}] = k_2(\mathrm{E}) f(\mathrm{E})[\mathrm{AB}] \tag{71}$$

Both equations combined yield

$$k_{-2,\infty} h(E) = k_2(E) f(E) K_{\mathrm{eq}} \tag{72}$$

Hence

$$\frac{\partial \rho(E,t)}{\partial t} = \omega \sum_{E'} P(E,E')\rho(E',t) - \omega\rho(E,t) - k_2(E)\rho(E,t) + k_2(E) f(E) K_{\mathrm{eq}}[\mathrm{A}][\mathrm{B}] \tag{73}$$

An alternative would have been to substitute only $h(E)$ by

$$h(E) = \frac{k_2(E) f(E)}{\sum\limits_{E > E_0} k_2(E) f(E)} \tag{74}$$

which follows straightforwardly from equations (70) and (71) together with

$$k_2 = \sum_{E \geq E_0} k_2(E) f(E) \tag{75}$$

The first problem with equation (69) is also easily fixed by requiring $[\mathrm{B}] \gg [A]$. Now only the concentration of [A] will vary during the reaction and $[\mathrm{B}] = [\mathrm{B}]_0$ and the ME is linearized.

$$\frac{\partial \rho(E,t)}{\partial t} = \omega \sum_{E'} P(E,E')\rho(E',t) - \omega\rho(E,t) - k_2(E)\rho(E,t) + k_2(E) f(E)[\mathrm{B}]_0 K_{\mathrm{eq}}[\mathrm{A}] \tag{76}$$

If we consider $[\mathrm{A}](t)$ as an additional element in the population vector $\rho(E,\ t)$, equation (76) is again an eigenvalue problem and can be re-written in the same form as equation (64) with similar matrix elements, except for the additional source term.

There are several options to solve either (76) or (64): first, equation (76) may be integrated numerically. The results are time-dependent populations of all energy levels based on the initial conditions. If conditions change, a new integration is needed. The advantage of this method is that the population profiles are exact; however, it does not directly provide rate constants suitable for modeling. To obtain these

rate constants for the association reaction

$$A + B \rightarrow AB$$

one can evaluate the formation of AB at short reaction times, when the redissociation (the third problem discussed in connection with equation (69)) of AB is still insignificant, but relaxation of the individual energy levels is already complete. The reverse rate can be obtained from the final concentrations at long times when equilibrium is reached. This method will work well for systems with deep wells relative to the thermal energy. Under these conditions redissociation will occur on a long time scale that is clearly separated from the association process. Another but similar way to obtain the association rate constant is to prevent redissociation by making the stabilization process irreversible. AB molecules are "frozen out" when reaching a low-lying energy level. This technique is known as introducing an "absorbing boundary" to the system. The boundary will be located sufficiently below the barrier (for example, 10 kT below E_0). In general, this method works also for shallow wells for which a temporal separation of the reactions is not possible.

Both methods essentially rely on reaching steady-state concentrations for the energized AB molecules relative to the concentration of [A](t). Otherwise, the obtained rate constants would vary with time, because the population distribution would change. In terms of the eigenvalue approach of this reaction system, the smallest negative eigenvalues must be clearly separated from those that describe energy relaxation. As written above, the largest eigenvalue is obviously zero, because the system eventually reaches equilibrium. Thus, the second largest eigenvalue (the second smallest negative eigenvalue) will contain the desired kinetic information.

2.5 Complex pressure-dependent systems

So far, we only considered single-well and single-channel reactions. Often pressure-dependent reactions proceed *via* several isomerization steps and have many different product channels. In the following we will discuss such systems and the specific problems arising from them.

(*i*) *Two-well isomerization*

Consider the irreversible isomerization reaction

$$A \xrightarrow{k_A} B$$

The (modified) strong collision assumption allows us to separate this reaction into several steps

$$\mathrm{A} + \mathrm{M} \underset{k_{\mathrm{deact,A^*}}}{\overset{k_{\mathrm{act,A}}(E)}{\rightleftharpoons}} \mathrm{A^*} + \mathrm{M}$$

$$\mathrm{A^*} \underset{k_{\mathrm{BA}}(E)}{\overset{k_{\mathrm{AB}}(E)}{\rightleftharpoons}} \mathrm{B^*}$$

$$\mathrm{B^*} + \mathrm{M} \overset{k_{\mathrm{deact,B^*}}}{\longrightarrow} \mathrm{B} + \mathrm{M}$$

The steady-state assumption for $\mathrm{A^*}$ and $\mathrm{B^*}$ yields

$$\frac{\mathrm{d}[\mathrm{A^*}](E)}{\mathrm{d}t} = 0 = k_{\mathrm{act,A}}(E)[\mathrm{M}][\mathrm{A}] + k_{\mathrm{BA}}(E)[\mathrm{B^*}](E) - \{k_{\mathrm{deact,A^*}}[\mathrm{M}] + k_{\mathrm{AB}}(E)\}[\mathrm{A^*}](E) \tag{77}$$

$$\frac{\mathrm{d}[\mathrm{B^*}](E)}{\mathrm{d}t} = 0 = k_{\mathrm{AB}}(E)[\mathrm{A^*}](E) - \{k_{\mathrm{BA}}(E) + k_{\mathrm{deact,B^*}}[\mathrm{M}]\}[\mathrm{B^*}](E) \tag{78}$$

$$[\mathrm{B^*}](E) = \frac{k_{\mathrm{AB}}(E)}{k_{\mathrm{AB}}(E) + k_{\mathrm{deact,B^*}}[\mathrm{M}]}[\mathrm{A^*}](E) \tag{79}$$

$$[\mathrm{A^*}](E) = \frac{k_{\mathrm{act,A}}(E)[\mathrm{M}]}{k_{\mathrm{deact,A^*}}[\mathrm{M}] + k_{\mathrm{AB}}(E) - k_{\mathrm{BA}}(E)((k_{\mathrm{AB}}(E))/x}\ [\mathrm{A}] \quad \text{where } x = (k_{\mathrm{BA}}(E) + k_{\mathrm{deact,B^*}}[\mathrm{M}]) \tag{80}$$

Note that we treat the species $\mathrm{A^*}$ and $\mathrm{B^*}$ in energy-resolved form but deal with A and B as bulk species. This allows us to consider the deactivation steps as energy independent. With the steady-state concentrations of $\mathrm{A^*}$ and $\mathrm{B^*}$ determined, the rate constant $k_{\mathrm{iso,A}}$ is given by

$$\frac{\mathrm{d}[\mathrm{B}]}{\mathrm{d}t} \equiv k_{\mathrm{iso,A}}[\mathrm{A}] = \sum_E k_{\mathrm{deact,B^*}}[\mathrm{M}][\mathrm{B^*}](E) = \sum_E k_{\mathrm{deact,B^*}}[\mathrm{M}] \frac{k_{\mathrm{AB}}(E)}{k_{\mathrm{BA}}(E) + k_{\mathrm{deact,B^*}}[\mathrm{M}]} \times \frac{k_{\mathrm{act,A}}(E)[\mathrm{M}]}{k_{\mathrm{deact,A^*}}[\mathrm{M}] + k_{\mathrm{AB}}(E) - k_{\mathrm{BA}}(E)[k_{\mathrm{AB}}(E)/x]}\ [\mathrm{A}] \quad \text{where } x = (k_{\mathrm{BA}}(E) + k_{\mathrm{deact,B^*}}[\mathrm{M}]) \tag{81}$$

At the high-pressure limit ($[\mathrm{M}] \to \infty$) the pressure dependence cancels out and we obtain the same result as for unimolecular reactions forming

products, namely

$$k_{\mathrm{iso,A},\infty} = \sum_E k_{\mathrm{AB}}(E) \frac{k_{\mathrm{act,A}}(E)}{k_{\mathrm{deact,A^*}}} \tag{82}$$

For [M]$\rightarrow$0 we find a linear dependence of the low-pressure rate constant on [M]

$$k_{\mathrm{iso,A},0} = \sum_E \frac{k_{\mathrm{AB}}(E)}{k_{\mathrm{BA}}(E)} \frac{k_{\mathrm{act,A}}(E)}{k_{\mathrm{deact,A^*}}} k_{\mathrm{deact,B^*}}[\mathrm{M}] \tag{83}$$

but this time an additional term $k_{\mathrm{AB}}(E)/k_{\mathrm{BA}}(E)$ takes into account that the overall population of excited molecules is divided between [A*] and [B*]. This makes sense because at low pressures the reversible isomerization A$^* \rightleftharpoons$ B* leads to a partially equilibrated distribution among the excited states. Although collisions with M are required to produce A* and deactivate B*, we find only a linear dependence on [M]. This can be explained with the fact that collisions with [M] also deactivate A* and thus reduce the rate of production of B. Having obtained the rate constant for the irreversible isomerization of A to B, we could either repeat this procedure for B isomerizing to A or, alternatively, use the thermal equilibrium constant to calculate the reverse rate constant.

It should be clear at this point that all required elementary rate constants $k(E)$ for activation, deactivation, and isomerization can be obtained with either (Q)RRK or RRKM theory as discussed earlier.

We will now analyze the same isomerization reaction using the ME approach [18] to demonstrate differences and similarities. For the population densities of isomer A, $\rho^{\mathrm{A}}(E, t)$, we construct the ME

$$\begin{aligned} \frac{\partial}{\partial t}\rho^{\mathrm{A}}(E,t) = \omega \sum_{E'} P(E,E')\rho^{\mathrm{A}}(E',t) - \omega\rho^{\mathrm{A}}(E,t) \\ - k_{\mathrm{AB}}(E)\rho^{\mathrm{A}}(E,t) + k_{\mathrm{BA}}(E)\rho^{\mathrm{B}}(E,t) \end{aligned} \tag{84}$$

It contains two $\rho^{\mathrm{A}}(E, t)$ producing terms (either from different energy levels of A, term 1, or from $\rho^{\mathrm{B}}(E, t)$, term 4) and two consuming terms, in which $\rho^{\mathrm{A}}(E, t)$ is lost to other energy levels of A (term 2) or to B (term 3). For the population density of B an analogous ME exists. Both populations are coupled by the mass conservation requirement and therefore the set of coupled differential equations contains both species. We can define a new vector $\rho(E, t)$ which contains the populations of both isomers. This leads to the same eigenvalue equation as discussed earlier,

$$\frac{\partial}{\partial t}\rho(E,t) = \hat{M}\rho(E,t) \tag{85}$$

However, the matrix elements of the operator $\hat{M}$, which describes the evolution of the combined states, are different for each problem and distinguish one reaction system from the other. Provided that energy relaxation is fast compared to the reaction time or in other words that reaction takes place on a much longer time scale than energy transfer between individual levels, the solution of this eigenvalue problem will yield two chemically relevant eigenvalues which are much larger than and well separated from all other eigenvalues. The largest eigenvalue is zero reflecting that this reaction system will finally reach equilibrium. The second largest eigenvalue determines the approach to equilibrium and can be shown [19] to be equal to

$$-\lambda_2 = k_{\text{iso,A}} + k_{\text{iso,B}} \tag{86}$$

Since at equilibrium

$$K_{\text{eq}} = \frac{k_{\text{iso,A}}}{k_{\text{iso,B}}} \tag{87}$$

we obtain for the phenomenological rate constants

$$k_{\text{iso,A}} = \frac{-\lambda_2}{1 + 1/K_{\text{eq}}} \tag{88}$$

$$k_{\text{iso,B}} = \frac{-\lambda_2}{K_{\text{eq}} + 1} \tag{89}$$

The condition that the largest two eigenvalues must be well separated from all others implies that steady state is reached. Otherwise the isomerization reaction would depend on several eigenvalues describing the interaction between energy relaxation and chemical reaction. This would lead to time-dependent "rate constants" or non-exponential behavior.

(*ii*) *Multi-well, multi-channel systems*

Consider as an example for a multi-well, multi-channel problem the following chemically activated reaction system:

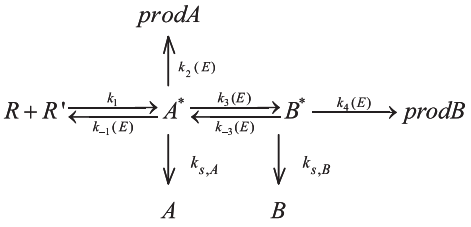

It describes the reaction of two reactants R and R′ to form the excited species A*, which can stabilize *via* collisions with bath gas molecules M, react to products (prodA), or isomerize to B*. Similarly, B* can undergo

collisional stabilization, isomerize back to A*, or form other products named prodB. If R and R′ were radicals, this scheme could represent a recombination reaction (e.g., $C_2H_5 + O_2$ if one considers O_2 as biradical, or $CH_3 + C_2H_3$), while if R′ were a molecule with multiple bonds, this scheme would represent an addition reaction (e.g., $CH_3 + C_2H_4$). R′ could also be a species with an empty orbital and then this example could describe an insertion reaction (e.g., $^1CH_2 + H_2O$).

(*a*) *The modified strong collision approach* In the following we will present the steady-state analysis of this system based on the MSC assumption. All product channels and stabilization reactions are treated as irreversible processes, and thermal dissociation of either A or B is considered as a separate process. Hence, the implicit assumption is made that the overall reaction system can be divided into two independent additive steps: (a) reactions originating directly from the reactants as shown in the scheme and (b) thermal dissociation reactions originating from stabilized intermediates.

The chemically activated reaction R + R′ yields four different products: A, B, prodA, and prodB. The goal is to obtain apparent[8] rate constants for these four channels, defined as

$$\frac{d[A]}{dt} = k_{stab,A}[R][R'] \tag{90}$$

$$\frac{d[B]}{dt} = k_{stab,B}[R][R'] \tag{91}$$

$$\frac{d[prodA]}{dt} = k_{prod,A}[R][R'] \tag{92}$$

$$\frac{d[prodB]}{dt} = k_{prod,B}[R][R'] \tag{93}$$

By applying the steady-state condition for A* and B* at all energy levels

$$\begin{aligned}\frac{d[A^*(E)]_{ss}}{dt} &= 0 \\ &= k_1 h(E)[R][R'] + k_{-3}(E)[B^*(E)]_{ss} \\ &\quad - \{k_{-1}(E) + k_2(E) + k_{s,A} + k_3(E)\}[A^*(E)]_{ss}\end{aligned} \tag{94}$$

$$\begin{aligned}\frac{d[B^*(E)]_{ss}}{dt} &= 0 = k_3(E)[A^*(E)]_{ss} \\ &\quad - \{k_{-3}(E) + k_4(E) + k_{s,B}\}[B^*(E)]_{ss}\end{aligned} \tag{95}$$

[8]The rate constants are called "apparent" because they refer to complex reactions. In contrast, "regular" rate constants correspond to elementary (one-step) reactions.

$$[\mathrm{B}^*(E)]_{\mathrm{ss}} = \frac{k_3(E)}{k_{-3}(E) + k_4(E) + k_{s,\mathrm{B}}}[\mathrm{A}^*(E)]_{\mathrm{ss}} \tag{96}$$

we obtain the steady-state concentrations of $[\mathrm{A}^*(E)]_{\mathrm{ss}}$ and $[\mathrm{B}^*(E)]_{\mathrm{ss}}$

$$[\mathrm{A}^*(E)]_{\mathrm{ss}} = \frac{k_1 h(E)}{k_{w1}(E) - k_{-3}(E)k_3(E)/k_{w2}(E)}[\mathrm{R}][\mathrm{R}'] \tag{97}$$

$$[\mathrm{B}^*(E)]_{\mathrm{ss}} = \frac{k_3(E)}{k_{w2}(E)}\frac{k_1 h(E)}{k_{w1}(E) - k_{-3}(E)k_3(E)/k_{w2}(E)}[\mathrm{R}][\mathrm{R}'] \tag{98}$$

with $k_{w1}(E)$ and $k_{w2}(E)$ defined as

$$k_{w1}(E) = k_{-1}(E) + k_2(E) + k_{s,\mathrm{A}} + k_3(E) \tag{99}$$

$$k_{w2}(E) = k_{-3}(E) + k_4(E) + k_{s,\mathrm{B}} \tag{100}$$

In this derivation the rate constant k_1 presents the temperature-dependent high-pressure rate constant for the addition reaction and the function $h(E)$ is used (as before) to calculate the energy distribution of the initial complex AB(E).

The apparent rate constants are given as:

$$\frac{\mathrm{d}[\mathrm{A}(E)]}{\mathrm{d}t} = k_{s,\mathrm{A}}[\mathrm{A}^*(E)]_{\mathrm{ss}} = k_{s,\mathrm{A}}\frac{k_1 h(E)}{k_{w1}(E) - k_{-3}(E)k_3(E)/k_{w2}(E)}[\mathrm{R}][\mathrm{R}'] \tag{101}$$

$$\frac{\mathrm{d}[\mathrm{prodA}(E)]}{\mathrm{d}t} = k_2(E)[\mathrm{A}^*(E)]_{\mathrm{ss}} = k_2(E)\frac{k_1 h(E)}{k_{w1}(E) - k_{-3}(E)k_3(E)/k_{w2}(E)}[\mathrm{R}][\mathrm{R}'] \tag{102}$$

$$\frac{\mathrm{d}[\mathrm{B}(E)]}{\mathrm{d}t} = k_{s,\mathrm{B}}[B^*(E)]_{\mathrm{ss}} = k_{s,\mathrm{B}}\frac{k_3(E)}{k_{w2}(E)}\frac{k_1 h(E)}{k_{w1}(E) - k_{-3}(E)k_3(E)/k_{w2}(E)}[\mathrm{R}][\mathrm{R}'] \tag{103}$$

$$\frac{\mathrm{d}[\mathrm{prodB}]}{\mathrm{d}t} = k_4(E)[\mathrm{B}^*(E)]_{\mathrm{ss}} = k_4(E)\frac{k_3(E)}{k_{w2}(E)}\frac{k_1 h(E)}{k_{w1}(E) - k_{-3}(E)k_3(E)/k_{w2}(E)}[\mathrm{R}][\mathrm{R}'] \tag{104}$$

Finally, integration (or summation in the discrete form) over all energy levels above the energy threshold for reaction (E_0) yields the total

apparent rate constants, e.g., for $k_{\mathrm{stab,A}}$:

$$k_{\mathrm{stab,A}} = k_1 \int_{E_0}^{\infty} \frac{k_{s,\mathrm{A}}}{k_{w1}(E) - k_{-3}(E)k_3(E)/k_{w2}(E)} h(E)\mathrm{d}E \qquad (105)$$

The normalized distribution function $h(E)$ is calculated similar to equation (74)

$$h(E) = \frac{k_{-1}(E)f(E)}{\int_{E_0}^{\infty} k_{-1}(E)f(E)\mathrm{d}E} \qquad (106)$$

Total apparent rate expressions for $k_{\mathrm{stab,B}}$, k_{prodA}, and k_{prodB} are obtained in an analogous way.

$$k_{\mathrm{prodA}} = k_1 \int_{E_0}^{\infty} \frac{k_2(E)}{k_{w1}(E) - k_{-3}(E)k_3(E)/k_{w2}(E)} h(E)\mathrm{d}E \qquad (107)$$

$$k_{\mathrm{stab,B}} = k_1 \int_{E_0}^{\infty} \frac{k_{s,\mathrm{B}}k_3(E)/k_{w2}(E)}{k_{w1}(E) - k_{-3}(E)k_3(E)/k_{w2}(E)} h(E)\mathrm{d}E \qquad (108)$$

$$k_{\mathrm{prodB}} = k_1 \int_{E_0}^{\infty} \frac{k_4(E)k_3(E)/k_{w2}(E)}{k_{w1}(E) - k_{-3}(E)k_3(E)/k_{w2}(E)} h(E)\mathrm{d}E \qquad (109)$$

In equations (105) and (107)–(109), the terms $k_{s,\mathrm{A}}$, $k_{s,\mathrm{B}}$, k_{w1}, and k_{w2} depend linearly on [M]. All other rates $k_i(E)$ are pressure independent. This allows us to analyze the pressure dependence of the four apparent rates. In the high-pressure limit we obtain

$$[\mathrm{M}] \to \infty \Rightarrow k_{\mathrm{stab,A}} \to k_1 \qquad (110)$$

$$[\mathrm{M}] \to \infty \Rightarrow k_{\mathrm{prodA}} \to k_1 \int_{E_0}^{\infty} \frac{k_2(E)}{k_{s,\mathrm{A}}} h(E)\mathrm{d}E \qquad (111)$$

$$[\mathrm{M}] \to \infty \Rightarrow k_{\mathrm{stabB}} \to k_1 \int_{E_0}^{\infty} \frac{k_3(E)}{k_{s,\mathrm{A}}} h(E)\mathrm{d}E \qquad (112)$$

$$[\mathrm{M}] \to \infty \Rightarrow k_{\mathrm{prodB}} \to k_1 \int_{E_0}^{\infty} \frac{k_3(E)k_4(E)}{k_{s,\mathrm{A}}k_{s,\mathrm{B}}} h(E)\mathrm{d}E \qquad (113)$$

The important point to notice is that the pressure dependence of the apparent rate constants at their high-pressure limits depends on the "distance" of the channels from the entrance channel (reactants). With "distance" we mean the number of isomerization steps needed to form the isomer, which then reacts to the products described by the apparent rate constant. With respect to our example system, all product channels originating from B are one isomerization step further away from the initial complex than products formed from A (the initial complex). Thus,

the corresponding apparent rate constant of the product channel of B exposes a different order of pressure dependence than that of the product channel of A. The same general conclusions can be drawn for the stabilization rate constants.

A look at the equations (110)–(113) clarifies this conclusion: the apparent high-pressure rate constant for stabilization of A is obviously pressure independent and the high-pressure rate constant for product formation from A^* is inversely proportional to [M] (due to $k_{s,A}$). This is reasonable because product formation competes with collisional stabilization. The high-pressure stabilization rate constant for B formation ($k_{stab,B}$) also depends inversely on [M] for the same reason and thus its dependence of [M] differs from $k_{stab,A}$ by $[M]^{-1}$. The same $[M]^{-1}$ difference is observed between k_{prodA} and k_{prodB}, since latter high-pressure rate constant shows a quadratic inverse dependence on [M].

It is also interesting to look at the low-pressure limits:

$$[M] \to 0 \Rightarrow k_{stab,A} \to k_1 \int_{E_0}^{\infty} \frac{k_{s,A}}{k_{-1}(E) + k_2(E) + k_3(E) - (k_{-3}(E)k_3(E)/(k_{-3}(E) + k_4(E))} h(E)\mathrm{d}E \tag{114}$$

$$[M] \to 0 \Rightarrow k_{prodA} \to k_1 \int_{E_0}^{\infty} \frac{k_2(E)}{k_{-1}(E) + k_2(E) + k_3(E) - (k_{-3}(E)k_3(E)/(k_{-3}(E) + k_4(E))} h(E)\mathrm{d}E \tag{115}$$

$$[M] \to 0 \Rightarrow k_{stab,B} \to k_1 \int_{E_0}^{\infty} \frac{k_{s,B}k_3(E)/(k_{-3}(E) + k_4(E))}{k_{-1}(E) + k_2(E) + k_3(E) - k_{-3}(E)k_3(E)/(k_{-3}(E) + k_4(E))} h(E)\mathrm{d}E \tag{116}$$

$$[M] \to 0 \Rightarrow k_{prodB} \to k_1 \int_{E_0}^{\infty} \frac{k_4(E)k_3(E)/(k_{-3}(E) + k_4(E))}{k_{-1}(E) + k_2(E) + k_3(E) - k_{-3}(E)k_3(E)/(k_{-3}(E) + k_4(E))} h(E)\mathrm{d}E \tag{117}$$

Within their low-pressure limits both stabilization rate constants depend linearly on [M] (incorporated in $k_{s,A}$ and $k_{s,B}$), while the rate constants for product formation are both pressure independent under these conditions.

The discussion so far dealt with apparent product formation and stabilization rates for $R + R'$ and we ignored the fact that the stabilized intermediates can thermally dissociate. We now briefly look at the latter

process. The underlying reaction system for the dissociation of the intermediate A looks very similar to the chemical activation part:

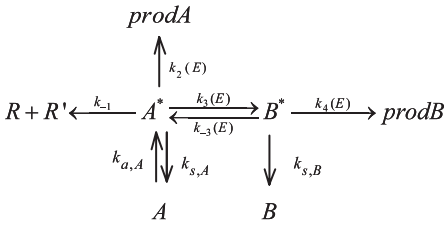

There are only two changes compared to the association part: first, collisional activation of the intermediate A is included, and second, the production of the former reactants R and R′ is now an irreversible channel. Apparent rate constants are expressed by analogy to those for the chemically activated reaction, e.g.,

$$\frac{\mathrm{d[R]}}{\mathrm{d}t} = k_{\mathrm{react,A}}[\mathrm{A}] \tag{118}$$

$$\frac{\mathrm{d[prodA]}}{\mathrm{d}t} = k_{\mathrm{prodA,A}}[\mathrm{A}] \tag{119}$$

and similar expressions can be derived if steady-state assumptions for A^* and B^* are made. The thermal dissociation of B can be treated in the same way.

If we compare the schemes for the chemically activated part ($R + R'$) and the thermal dissociation parts (unimolecular reactions of A and B), we will notice that several apparent rate constants are defined twice. For example, we obtain apparent rate constants not only for $R + R' \xrightarrow{k_{\mathrm{stab,A}}} A$, but also for $A \xrightarrow{k_{\mathrm{react,A}}} R + R'$. The principle of detailed balancing requires that both rate constants must be thermodynamically consistent and this can be used as internal check of the kinetic analysis.

A generalization of this example to multi-well and multi-channel systems is straightforward and easily implemented in kinetic software (discussed later). All integrals are replaced by finite sums and energy graining will be one important input parameter to such codes.

(*b*) *The master equation approach* There are several ways to extract apparent time-independent rate constants from the solution of the ME for a multi-channel, multi-well system. Based on the earlier discussion of the isomerization reaction $A \rightleftharpoons B$, one could use the "absorbing layer" method to make the formation of intermediates irreversible if they occupy energy levels significantly below the lowest reaction barrier. The thermal dissociations of stabilized intermediates could then be treated as

separate processes similar to the discussion above of the steady-state MSC approach.

Alternatively, apparent rate constants can be obtained by analyzing the results of the ME at short reaction times. Based on the starting conditions, the rate constants for the consumption of the reactants or for the thermal dissociation of intermediates can be found. A realization of this concept is described by Klippenstein and Miller [20,21], and we will discuss this method now for the two-well, two-channel example. To simplify the analysis, we assume that pseudo-first-order conditions apply ($[R'] \gg [R]$, where R is the minor reactant) and further lump all products together. The reaction scheme thus is:

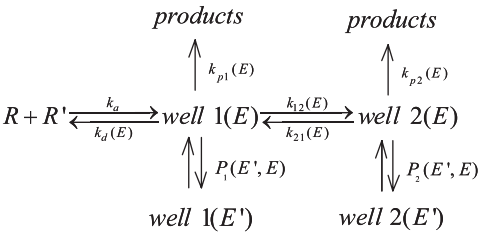

The corresponding MEs are

$$\frac{\partial n_{\mathrm{R}}}{\mathrm{d}t} = \sum_{i=1}^{M} \int_{E_{0i}}^{\infty} k_{\mathrm{d}i}(E) n_i(E) \mathrm{d}E - n_{\mathrm{R}} n_{\mathrm{R}'_0} \sum_{i}^{M} K_{\mathrm{eq},i} \int_{E_{0i}}^{\infty} k_{\mathrm{d}i}(E) f_i(E) \mathrm{d}E \tag{120}$$

for the minor reactant and

$$\begin{aligned} \frac{\partial n_i(E)}{\mathrm{d}t} = {} & \omega \int_{E_{0i}}^{\infty} P_i(E, E') n_i(E') \mathrm{d}E' - \omega n_i(E) \\ & + \sum_{j \neq i}^{M} k_{ij}(E) n_j(E) - \sum_{j \neq i}^{M} k_{ji}(E) n_i(E) \\ & + K_{\mathrm{eq},i} k_{\mathrm{d}i}(E) f_i(E) n_{\mathrm{R}} n_{\mathrm{R}'_0} - k_{\mathrm{p}i}(E) n_i(E) \end{aligned} \tag{121}$$

for the *isomer i*. Here, $n_i(E)$ is the concentration of *isomer i* at energy E, n_{R} the concentration of the minor reactant R, $n_{\mathrm{R}'_0}$ the time-independent concentration of the excess reactant R′, $k_{ij}(E)$ the microcanonical rate constants for isomerization from *well i* to *well j*, $K_{\mathrm{eq},i}$ the equilibrium constant for the system $\mathrm{R} + \mathrm{R}' \rightleftharpoons$ isomer i, $k_{\mathrm{p}i}(E)$ and $k_{\mathrm{d}i}(E)$ the energy-dependent rate constants for the product and reactant channels, respectively, and $f_i(E)$ the equilibrium energy distribution for *well i*. For our particular two-well example it follows that $M = 2$ and that all $k_{\mathrm{d}2}(E)$ rates are zero. The integrals can be replaced by sums if we divide the

continuous energy distribution into discrete energy "bins" of width δE. By doing so and by envisioning a vector $|w(t)\rangle$, which contains the population of isomer 1 in its first N_1 components, those of isomer 2 in its elements N_1+1 to N_1+N_2, and so on, and the population of n_R in its last element, we can formulate the eigenvalue problem

$$\frac{\mathrm{d}|w(t)\rangle}{\mathrm{d}t} = G\big|w(t)\big\rangle \tag{122}$$

Here, G is the transition matrix and is formed from the kinetic and energy transfer rates expressions in equations (120) and (121). It is a square matrix with $N = 1 + \sum_{i=1}^{M} N_i$ elements, if N_i is the number of discrete energy levels of *isomer i*. One possible solution to equation (122) is

$$|w(t)\rangle = \sum_{j=1}^{N} \mathrm{e}^{\lambda_j t}\ \big|g_j\big\rangle\big\langle g_j\big|w(0)\big\rangle \tag{123}$$

which introduces the eigenvalues λ_j and eigenvectors $\big|g_j\big\rangle$. This definition of the eigenvectors $\big|g_j\big\rangle$ has the advantage that the population vector can now easily be calculated from the initial conditions stored in $\big|w(0)\big\rangle$. However, the solution is independent of the initial conditions and equation (123) can be used for any starting conditions. This allows one to use equation (123) to calculate apparent rate constants.

As mentioned earlier, apparent rate constants are only defined if energy relaxation processes are completed before chemical transformations become significant. This means that most of the eigenvalues are very small and clearly separated from the few chemically relevant ones. After a small lag time, all energy levels of the same isomer are relaxed (equilibrated) and contributions of the corresponding eigenvalues to the sum vanish. Assuming that the eigenvalues are sorted in decreasing order, we obtain

$$|w(t)\rangle = \sum_{j=1}^{N_{\mathrm{chem}}} \mathrm{e}^{\lambda_j t}\big|g_j\big\rangle\big\langle g_j\big|w(0)\big\rangle, \quad \text{for } t > t_{\text{energy relaxation}} \tag{124}$$

or, if we only consider the lth component of the population vector,

$$w_l(t) = \sum_{j=1}^{N_{\mathrm{chem}}} \mathrm{e}^{\lambda_j t}\ g_{jl}\big\langle g_j\big|w(0)\big\rangle \tag{125}$$

In order to obtain the desired apparent rate constants we choose the appropriate initial conditions and evaluate the formation rate at $t = 0$

(actually at a time that is short on the chemical time scale but long enough to allow complete energy relaxation). The number of independent apparent rate constants N_R needed to describe a multi-well, multi-channel system completely depends on the number of distinguishable "species", S. A system with N_W wells (intermediates), N_P *different* product channels, and one reactant channel has $S = 1 + N_W + N_p$ species. For our example with $N_P = 1$ and $N_W = 2$ we calculate $S = 4$. With this information we can calculate N_R:

$$N_R = \frac{S(S-1)}{2} - \frac{N_P(N_P-1)}{2} \tag{126}$$

which yields $N_R = 6$ for the example.[9] These six independent reactions and apparent rate constants are

$$\mathrm{R} \rightarrow \text{well 1} : \frac{\mathrm{d}[\text{well 1}]}{\mathrm{d}t} = k_{\text{stab1}}[\mathrm{R}]$$

$$\mathrm{R} \rightarrow \text{well 2} : \frac{\mathrm{d}[\text{well 2}]}{\mathrm{d}t} = k_{\text{stab2}}[\mathrm{R}]$$

$$\mathrm{R} \rightarrow \text{products} : \frac{\mathrm{d}[\text{products}]}{\mathrm{d}t} = k_{\text{prod,R}}[\mathrm{R}]$$

$$\text{well 1} \rightarrow \text{well 2} : \frac{\mathrm{d}[\text{well 2}]}{\mathrm{d}t} = k_{\text{iso12}}[\text{well 1}]$$

$$\text{well 1} \rightarrow \text{products} : \frac{\mathrm{d}[\text{products}]}{\mathrm{d}t} = k_{\text{prod,1}}[\text{well 1}]$$

$$\text{well 2} \rightarrow \text{products} : \frac{\mathrm{d}[\text{products}]}{\mathrm{d}t} = k_{\text{prod,2}}[\text{well 2}]$$

To obtain rates for the first three reactions, we select the $|w(0)\rangle$ such that all states are unpopulated with exception of the reactant R. We indicate this initial condition as $|w^{\mathrm{R}}(0)\rangle$. Similarly, $|w^1(0)\rangle$ stands for the initial condition at which all population is Boltzmann distributed in *well* 1, and so on. The total population of R is given in a single vector element $(N_1 + N_2 + 1)$, but the total population of wells 1 and 2 has to be calculated by adding the populations of all individual energy levels. For well 1 as example,

$$w^1(t) = \sum_{l=1}^{N_1} w_l(t) = \sum_{l=1}^{N_1} \sum_{j=1}^{N_{\text{chem}}} \mathrm{e}^{\lambda_j t}\, g_{jl} \langle g_j | w(0) \rangle \tag{127}$$

[9] Klippenstein *et al.* derived the simpler equation $N_R = S(S-1)/2$, because they considered chemically activated systems with just one product channel so that the second term vanishes.

Differentiation with respect to time yields

$$\frac{\mathrm{d}w^1(t)}{\mathrm{d}t} = \sum_{l=1}^{N_1} \frac{\mathrm{d}w_l(t)}{\mathrm{d}t} = \sum_{l=1}^{N_1} \sum_{j=1}^{N_{\mathrm{chem}}} \lambda_j \, \mathrm{e}^{\lambda_j t} \, g_{jl} \langle g_j | w^{\mathrm{R}}(0) \rangle$$
$$\equiv \mathrm{const} \cdot k_{\mathrm{stab1}} | w^{\mathrm{R}}(0) \rangle \tag{128}$$

The vector $|w^{\mathrm{R}}(0)\rangle$ in equation (128) indicates that we start with pure reactant $w^{\mathrm{R}}(0) = 1$, so that

$$k_{\mathrm{stab1}} = \frac{1}{\mathrm{const}} \sum_{l=1}^{N_1} \sum_{j=1}^{N_{\mathrm{chem}}} \lambda_j \, \mathrm{e}^{\lambda_j t} \, g_{jl} \langle g_j | w^{\mathrm{R}}(0) \rangle \tag{129}$$

Note that since all λ_j are negative but rate constants are defined to be positive, it follows that

$$\langle g_j | w^{\mathrm{R}}(0) \rangle \sum_{i=1}^{N_1} g_{jl} = -\Delta w_j^{1,\mathrm{R}} \tag{130}$$

where $\Delta w_j^{1,\mathrm{R}}$ is a positive number and it is a measure of the formation of w^1 *via* the relaxation process described by λ_j if the reaction started with pure R. The validity of equation (130) can be assured by evaluating equation (125) for $t = 0$ and ∞ and equating the difference to $\Delta w_j^{1,\mathrm{R}}$.

Equation (129) allows the calculation of the apparent rate constant k_{stab1} from the calculated chemically significant eigenvectors and eigenvalues. The constant "const" was introduced because the population vector does not contain concentrations, so that the rate constant defined in (128) is only proportional to the apparent rate constant defined above. In an analogous way, k_{stab2} and the total rate of consumption of R can be obtained. Since the product channel is not a part of the population vector, $k_{\mathrm{prod,R}}$ is calculated as the difference between the total rate and the rates to form stabilized intermediates. Apparent rate constants for the reactions of *wells* 1 and 2 are obtained with the same strategy. For a more detailed derivation and for a discussion of a second method see Klippenstein and Miller [20]. More details on the strategy to numerically solve the eigenvalue problem may be found in Bedanov *et al.* [22], who essentially use the same strategy as Klippenstein and coworkers.

To complete the discussion of techniques to obtain time-independent rate constants for complex reaction systems, the "virtual components" approach of Knyazev and Tsang [23] should be mentioned. This approach is based on earlier work by Schranz and Nordholm [24] and Smith *et al.* [9]. It envisions the total population of an isomer being partitioned into ("virtual") components from each eigenvector/eigenvalue pair of the solution of the ME. Each component will be in steady state and can be described by time-independent rate constants for

formation and consumption into different channels. The total rate constants are the sums of these rate constants for all virtual components. Knyazev *et al.* have demonstrated that this approach can be used for very complex systems in which activated complexes do not just undergo unimolecular but also bimolecular consumption reactions.

(*c*) *The stochastic approach* Stochastic simulations of complex reaction systems address the basic physical problem that chemical reactions are not continuous and that they may not be describable in a deterministic way. Instead, on a molecular level, reactions depend on randomly occurring collisions and the events can be seen as a ''random walk'' from one state to another. The most accurate method to describe complex chemical reactions in this way is to use a stochastic approach. Gillespie [25] developed algorithms that—in the limit of infinite trials—describe these systems exactly by statistical probing of random events. Two different approaches are possible: in the first case [26], a swarm of molecules is initially placed in a set of energy bins and at each time step one molecule is moved to a different bin. The vector of all populations is updated for each time step and the evolution of the distribution is followed. This approach is feasible for linear and non-linear problems. If the ME contains only linear terms, a second method [27] is beneficial. Here, a single molecule per trial is followed in time, and snapshots of its properties are taken at defined time intervals. This reduces the memory requirements, because only averaged results are stored. The final results of a stochastically solved ME are temporal distribution functions and derived information such as time profiles of average vibrational energy and time-dependent stochastic rate constants.

The Gillespie method requires two random numbers. One random number, r_1, defines the next time step, τ, *via*

$$\tau = \frac{-\ln(r_1)}{k_{\text{total}}} \tag{131}$$

where k_{total} is the sum of all first-order rate coefficients. The second random number, r_2, is used to select the direction of the transition

$$\sum_{i=1}^{j-1} k_i < r_2 \cdot k_{\text{total}} \leq \sum_{i=j}^{n} k_i \tag{132}$$

In this equation the *j*th path is selected by r_2 among a total of n different reaction paths. After each time step the rate coefficients need to be updated because either the transition leads to isomerization and different rate constants apply or the isomer is now in a different energy level and the $k(E)$ values change.

The time requirements for a stochastic analysis depend on the pressure (collision frequency), molecule parameters, unimolecular rate constants, reaction time, and the desired accuracy. Due to the central role of random numbers, the quality of the random number generator is crucial and its range of numbers as well as its randomness strongly influences the quality of the results.

A major advantage of stochastic solutions of MEs for multi-well and multi-channel systems is that they provide time-resolved distribution functions without the need to diagonalize a large matrix and interpret the eigenvalues. The distribution functions provide direct insight into the behavior of the system, especially the energy transfer part. A severe drawback is that stochastic calculations spanning a large time range require a substantial amount of CPU time. Deterministic methods are generally orders of magnitude faster than stochastic calculations.

(*d*) *Conclusions*

Chemically activated and unimolecular reactions are on a fundamental level very complicated because they are governed by energy transfer and chemical processes that can proceed on many different time scales. The most fundamental and precise results are obtained by numerically solving the time-dependent ME. Such solutions, however, have the disadvantage that they cannot easily be incorporated into kinetic models for large reaction systems. A second approach is to solve the eigenvalue problem of the ME. This leads to a huge number of eigenpairs, which again is not a feasible result if one is only interested in the chemical kinetics part. Only if one can separate the eigenvalues describing energy relaxation from those few that are chemically relevant, it is possible to extract a set of apparent rate constants that describe the chemistry of the systems accurately for all but very short reaction times. Essentially, waiting for the energy relaxation to be completed means to assume steady-state conditions. This raises the question of why one would want to solve the time-dependent ME in the first place if the solutions will anyway later be reduced to time-independent rate constants. One good reason is that it is frequently not clear under which conditions a steady-state analysis is sufficiently accurate to describe the kinetic behavior. The discussion of the thermal decomposition of ethoxy radicals later in this chapter will hopefully make this point clearer.

By applying the steady-state assumption prior to solving the ME, finding its solutions becomes a straightforward and easy task if a so-called "absorptive boundary" is introduced. This means that all channels except for the source are made irreversible. The entire reaction system is separated into several processes including association (in case

of a chemical activation process) and isomerization reactions of all isomers. An even more drastic simplification is to describe the energy transfer process in terms of MSCs, which further simplifies the analysis. The main justification to use this approach is that our knowledge of the energy transfer process is very limited and hence the required parameters for the more detailed models are not readily available. Computational speed, which was a limiting factor 10–20 years ago, does not restrict the use of any method except, perhaps, the stochastic approach.

3 PRACTICAL METHODS TO ANALYZE PRESSURE-DEPENDENT REACTIONS

To perform a kinetic analysis of pressure-dependent reactions is in practice a straightforward task, since many codes are available. The major problem is to obtain the required input parameters. The following sections give short descriptions of several programs that allow the calculation of pressure-dependent rate constants, followed by a discussion of methods to obtain the input data.

3.1 Software for the calculation of pressure-dependent rate constants

We provide a description of computer programs for the kinetic analysis of pressure-dependent reaction systems. This list is by no means complete and certainly subject to the choice of the authors. Nevertheless, we hope that it is useful for readers who begin to work in this field.

1. Unimol: The Unimol [28] suite of programs from Gilbert and Smith [2] was provided to complement their textbook on unimolecular and recombination reactions. It consists of four program codes: (1) the program RRKM calculates $k(E)$ and generates the input file for ME analysis, (2) the ME solver MASTER, (3) the program named GEOM calculates moments of inertia, and (4) the program BRW estimates the average energy transferred in collisions based on the ''biased random walk'' model [29]. This code can be used to calculate unimolecular dissociation or recombination rate constants of one-well systems. The RRKM and ME codes can optionally calculate/utilize $k(E, J)$ data and thus are suitable for reactions with loose transition states.
2. ChemRate: ChemRate is software running under Windows developed by Mokrushin *et al.* [30] and allows the user to create molecule and kinetic databases, calculate elementary high-pressure reaction rate constants with TST theory, and perform a

RRKM-based ME analysis of pressure-dependent reaction systems consisting of multiple wells and channels. The ME is either solved time dependent or by imposing the steady-state approximation. A general description and application of this code is published [31]. The short manual warns any potential user that this software is only intended for experienced kineticists. At the time of writing, the homepage for ChemRate was accessible at http://www.nist.gov/kinetics/chemrate/chemrate.html

3. MultiWell: Written and distributed by Barker [32], MultiWell is a program package created to analyze pressure-dependent unimolecular reaction systems based on Gillespie's stochastic method. It contains four programs: "Thermo" calculates thermodynamic properties, "MomInert" calculates moments of inertia, "DenSum" calculates densities and sums of states as a function of energy, and "MultiWell" calculates—among other things—species and energy distribution profiles as function of time. The package and its application to the isomerization of 2-methylhexyl radicals have been described in the literature [33,34].
4. CARRA: CARRA, for *chemically activated reaction rate analysis*, calculates apparent rate constants for multi-well, multi-channel systems based on QRRK theory. It uses either the MSC (CARRA_MSC) or the steady-state ME (CARRA_ME) approach. The original concept was based on a single frequency representation of the active modes of each isomer [35,36]. Later, the code was updated to handle three representative frequencies. Descriptions of these earlier versions as well as applications can be found in Refs. [7,37]. CARRA is a modified version of these older codes, which is currently still under development [38].
5. Other program packages: There are many other well-known packages known in literature, e.g., Klippenstein *et al.*'s "VARIFLEX" [39], "TheRate" by Truong *et al.*, or the program suite "CHARMMRATE" [40] by Truhlar *et al.* In addition, reaction engineering platforms such as the "OpenChem Workbench" [41] project or the "CSEO" [42] project by Truong *et al.* contain RRKM and other kinetic applications.

3.2 Getting input data for the calculations

Input data are needed to calculate $k(E)$ values, density of states functions, collision frequencies, and so on. The specific type of required parameters depends on the selected method. If the goal is to do a "back

of the envelope'' calculation with emphasis of getting a quick answer rather than the most accurate prediction, a good choice would be a QRRK-based program since it requires only representative frequencies for the isomers, high-pressure rate constants for the individual reaction steps, and collision parameters. All this information can easily be obtained from estimation methods such as group additivity or rate estimation rules. The other extreme would be to perform a very detailed kinetic analysis with the most accurate and specific input data possible. This calls for a RRKM ME analysis and requires detailed molecular information for isomers as well as for the transition states. Although detailed information is nowadays often available from *ab initio* quantum mechanical calculations, such an approach is more time consuming and not feasible for every reaction in large mechanisms. Whatever the choice of analysis method will be, one should keep in mind that the results from both, QRRK and RRKM theories strongly depend on the energy transfer parameters employed, and a significant part of the remaining uncertainty from either analysis can be attributed to an inadequate description of the energy exchange processes during collisions.

A general strategy to obtain the required input parameters could involve the following sequence:

1. Maybe the best resource for input parameters are original publications, because these provide not just the data *per se* but also the context in which they were obtained and often an estimate of their uncertainties. Obvious sources for input data are, for example, kinetic studies (high-pressure rate expressions) and spectroscopic measurements (molecular properties)
2. If original papers are not available, consider the use of reviews, compilations, reference books, etc., which summarize and organize results from original publications. Thermodynamic data may, for example, be obtained from JANAF tables [43] or the NIST webbook [44]; high-pressure rate constants can be retrieved from recommendations (e.g., the UIPAC sponsored evaluation of rate expressions for atmospheric chemistry [45]) or web-based databases such as the NIST kinetic database [46], and a good source for transport properties is, for example, the reference book by Poling *et al.* [47]. Chemkin [48], a well-known modeling software, provides thermodynamic and transport databases for a set of frequently used molecules.
3. After all literature sources for input data are exhausted, consider estimating the missing parameters. This can be done intuitively by relating the unknown parameters to related data, or one can use

estimation methods and rules. We will discuss this approach in more detail in the following section.

4. Finally, use theoretical methods to calculate missing parameters. The most powerful tool in this regard are *ab initio* calculations, which provide all basic molecular parameters needed to calculate thermodynamic properties (*via* statistical mechanics methods) and kinetic data (*via* transition state theory). Some aspects of this approach will be outlined further below.

(*i*) *Input data based on estimation methods*
(*a*) *Thermodynamic data from group additivity* The basic assumption of group additivity is that certain properties, Φ, of a molecule are given as a sum of contributions of all the groups, ϕ_i, that form this molecule

$$\Phi = \sum_{i=1}^{n} \phi_i \tag{133}$$

If the contributions of all groups (defined as polyvalent atoms with its ligands) are known, the property for the entire molecule can be calculated. Ethanol, C_2H_6O, might serve as a simple example to illustrate this concept. Written as CH_3–CH_2–OH, we notice three polyvalent atoms (two C and one O) and hence three groups. The first group can be symbolized as {C/C/H3}, with the left part "{C/" presenting the central polyvalent atom and the following entries "C/" and "H3}" indicating the type of atoms, to which the central carbon is connected. Similarly, {C/C/H2/O} and {O/C/H} are representations of the other two groups. In order to get an estimate of thermodynamic properties of ethanol, we need to find the contributions of these three individual groups from tables as they can be found, e.g., in the textbook by Benson [49], who developed a group additivity scheme that is widely used in kinetics to estimate $\Delta_f H^{298}$, S^{298}, and $C_p(T)$ data. For example, we find in a database for the heat of formation the following contributions (in kcal/mol):

{C/C/H3}: −10.20
{C/C/H2/O}: −8.10
{O/C/H}: −37.90

This leads to an estimated heat of formation value for ethanol of −56.20 kcal/mol, which is essentially identical with the value found in the NIST webbook [44]. The estimations of entropies and heat capacities

are done similarly, although additional symmetry corrections make the estimation of entropies slightly more challenging.

Initially the group additivity concept was only used to estimate properties of stable molecules. Later the database was expanded to allow estimates for radicals [50,51] and transition states [52–54] as well. A widely distributed program called Therm [50] makes such estimates an easy task on a PC.

(*b*) *Representative frequencies from heat capacities* Usually molecular geometry and frequency information of a given species is used to calculate thermodynamic properties. However, it is possible to reverse this process. Estimated heat capacities as function of the temperature can serve as input to calculate representative frequencies [8] of that molecule. The basic theory for this process is as follows: from statistical mechanics we know how much one oscillator with the frequency v (or wavenumber $\tilde{\nu}$) contributes to the heat capacity:

$$c_v^{\text{vib}} = R\left(\frac{\theta}{T}\right)^2 \exp\left(\frac{\theta}{T}\right)\left[\exp\left(\frac{\theta}{T}\right) - 1\right]^{-2}, \quad \text{with } \theta = \frac{hv}{k} = \frac{hc\tilde{\nu}}{k} \tag{134}$$

Hence, if a species has s "effective" oscillators and if we wish to represent the internal modes with, let us say, three representative frequencies, the total heat capacity is given by

$$\begin{aligned} c_v(T) = {} & c_v^{\text{trans}}(T) + c_v^{\text{rot}}(T) + \alpha_1 c_{v,1}^{\text{vib}}(T) \\ & + \alpha_2 c_{v,2}^{\text{vib}}(T) + \{s - \alpha_1 - \alpha_2\} c_{v,3}^{\text{vib}}(T) \end{aligned} \tag{135}$$

The contributions from translation ($3/2R$) and external rotation ($3/2R$ for non-linear and $1R$ for linear species) are known, which leaves five adjustable parameters ($\alpha_1, \alpha_2, \tilde{\nu}_1, \tilde{\nu}_2,$ and $\tilde{\nu}_3$) that are determined *via* non-linear regression. Note that in this formulation α_1 and α_2 are not restricted to integer values. The same is true for n, which can take half-integer values, because each vibrational mode that represents an internal (hindered) rotation is counted as 1/2 oscillator. The representative frequencies together with their degeneracies are needed as input parameters for multi-frequency QRRK codes.

(*c*) *Estimation methods for high-pressure rate constants* Many research groups have provided estimation rules, which allow a quick calculation of an approximate high-pressure rate constant for a certain reaction family or class. A recent review of some methods can be found in

Ref. [55], and a widely used reference book for rate constant estimations was authored by Benson [49].

The basic idea behind estimation rules is to generalize experimentally obtained or calculated rate constants. This can be done by simply averaging a set of rate constants, or by developing systematic correlations to kinetic or thermodynamic properties.

Let us first look at C–H bond fission reactions as an example problem. To obtain an estimate of the rate constant we would use the following strategy: (1) Get a good estimate for the reverse reaction, the recombination of alkyl radicals with H atoms. (2) Calculate K_{eq} for the reactants and products. (3) Use the microscopic reversibility condition to calculate the C–H fission rate constant. Steps (2) and (3) are straightforward, if all thermodynamic data and the recombination rate constant are available. Therefore, only step (1) needs further discussion. We chose the recombination of H atoms with alkyl radicals as starting point, because we expect that the rate constant is independent of the alkyl radical. This is verified in Table 1, which contains a compilation of data for several H + alkyl recombination reactions found in the NIST kinetics database [46]. When several entries for a reaction are available, we selected those that appeared most reliable and averaged them. Except for the H + *n*-C_4H_9 reaction, nearly all rate constants are within a factor of 2 and even the rate constant for H + *n*-C_4H_9 is within a factor of 10 to most of the data.

Therefore, the average of all entries can serve as an estimate for the entire family of reactions. This average rate constant hardly changes with temperature, so that we can use a value of ~1.3E14 $cm^3/(mol\,sec)$ for all temperatures. The rate constant for the reverse reaction (the C–H fission) is not constant but depends *via* K_{eq} on the C–H bond strength.

Dean [35] provided a detailed discussion of this approach not only for bond fission, but also for β-scission reactions. Updated results of the

TABLE 1
Averaged high-pressure rate constants (in $cm^3/(mol\,sec)$) for H + *n*-alkyl recombination reactions obtained from selected entries in the NIST Kinetics Database [46]

Reaction	300 K	500 K	1000 K	1500 K	2000 K	2500 K
$H + CH_3 \rightarrow CH_4$	1.99E14	1.89E14	1.80E14	1.66E14	1.66E14	1.39E14
$H + C_2H_3 \rightarrow C_2H_4$	1.21E14		3.27E14			
$H + C_2H_5 \rightarrow C_2H_6$	1.0E14					
$H + C_3H_5 \rightarrow$ products	1.85E14	1.99E14	1.99E14	1.99E14	1.99E14	1.99E14
$H + C_3H_7 \rightarrow C_3H_8$	1.5E14					
$H + C_4H_9 \rightarrow$ products	3.01E13	3.01E13	3.01E13	3.01E13	3.01E13	3.01E13
Average	1.31E14	1.39E14	1.84E14	1.32E14	1.32E14	1.23E14

TABLE 2
Estimation rules for the addition of H or CH_3 to olefins on a per site basis

Reaction class	A (cm^3/(mol sec))	N	E (kcal/mol)
Recombination reactions			
$H + R \rightarrow R\text{-}H$	1.60×10^{14}	0.0	0.10
$CH_3 + R \rightarrow R\text{-}CH_3$	1.40×10^{13}	0.0	−0.47
$R' + R \rightarrow R\text{–}R'$	1.32×10^{13}	0.0	−0.10
Addition reactions			
$H + C_2H_4 \rightarrow C_2H_5$	1.69×10^{08}	1.61	1.0
H + olefin → primary R	1.26×10^{12}	0.29	2.8
H + olefin → secondary R	1.29×10^{15}	−0.55	3.0
H + olefin → tertiary R	1.29×10^{15}	−0.55	1.9
H + aromatics →	8.00×10^{12}	0.0	4.0
$CH_3 + C_2H_4 \rightarrow n\text{-}C_3H_7$	1.63×10^{11}	0.0	7.7
CH_3 + olefin → primary R	8.0×10^{10}	0.0	7.7
CH_3 + olefin → secondary R	8.0×10^{10}	0.0	7.0
CH_3 + olefin → tertiary R	8.0×10^{10}	0.0	6.0
CH_3 + aromatics →	8.0×10^{10}	0.0	7.5

Also provided are approximate data H or R + R recombination rate expressions.

evaluation of recombination and addition reactions for hydrocarbons yielded the estimation rules given in Table 2. We notice that—as expected—barriers for recombination reactions are very small or even negative, while addition reactions have a small positive barrier. For the recombination reactions we see that H atoms recombine about one order of magnitude faster than alkyl radicals. This can be explained with the size difference, which gives H atoms more flexibility while approaching the radical site or with the loss of active degrees of freedom[10] while the new bond is formed.

The addition reactions shown in Table 2 have small barriers that correlate roughly with the stability of the produced alkyl radical. Such correlations are more obvious for other types of reactions, e.g., abstraction reactions. They are known as linear free-energy relationships (LFER), and the most prominent correlation is the Evans–Polanyi relationship

$$\ln(k) = \ln(k_{\text{ref}}) + m(\Delta H_{\text{rxn}} - \Delta H_{\text{rxn,ref}}) \tag{136}$$

[10]The three translational degrees of freedom of a H atom are converted to three vibrations in the alkane. For methyl radicals, three translations and three rotations are lost and five vibrational and one internal rotation modes are formed. If one assumes that the vibrational modes contribute less to the total entropy than translations and rotations, the loss of entropy is larger for CH_3 than for H and the A-factor will be smaller.

Given $\ln(k) = \ln(A) - E/RT$, and assuming that the A-factor of a reaction family is constant, then this equation translates to

$$E_A = E_{A,\text{ref}} + \alpha\,\Delta H \tag{137}$$

The significance of this equation is that it provides an estimation method for the activation energy of a reaction based on a reference system and the difference in reaction enthalpies between both. α is positive and normally in the range 0–1 (often ~0.5). Its value can be determined for a family of reactions if kinetic data for two reactions of different exothermicity are available. From equation (137) it is clear that the barrier for a reaction within a reaction family increases with decreasing exothermicity.

Isomerization reactions may serve as an example to show how rate constants can be estimated based on analogy or correlations. Let us assume we are interested in a rough estimate for the 1,3-H shift reaction

$$\bullet CH_2CH_2CH_2CH_3 \rightleftharpoons CH_3CH_2CH\bullet CH_3$$

We notice that one H atom is transferred from a secondary C atom (a CH_2 group) to a primary radical site.[11] We also notice that the transition structure for this migration reaction is cyclic and that the ring contains four atoms (the three C atoms and the migrating H atom). Assuming that we have some information about bimolecular H abstraction reactions, then a possible strategy to approximate this unknown rate expression could involve the following steps: (1) identify a bimolecular reaction that is similar to our 1,3-H shift reaction and use the activation energy of this reaction as starting point; (2) estimate the pre-exponential factor (A-factor) based on a simple analysis of the reaction mechanism; (3) correct the A-factor and activation energy for ring strain effects.

Step 1: A good choice of a bimolecular reaction resembling our target reaction is the H abstraction from a CH_2 moiety by ethyl radicals.

$$C_2H_5\bullet + \text{R-CH}_2\text{-R}' \rightleftharpoons C_2H_6 + \text{R-CH}\bullet\text{-R}'$$

An evaluation of abstraction reactions by Dean (unpublished) leads to the following Arrhenius parameters:

$$K(T) = AT^n \exp\left(-\frac{E}{RT}\right) \tag{138}$$

[11]The terms primary, secondary, and tertiary distinguish in this context C atom with one, two, or three C–C bonds. The type of a C atom determines the strength of the C–H bonds it forms.

where

$$A = 6.6E3\ \mathrm{cm}^3/(\mathrm{mol\ sec});\quad n = 2.51;\quad E = 9.9\ \mathrm{kcal/mol}$$

Since we wish to express the rate constant for the example reaction in simple Arrhenius form

$$k(T) = A \exp\left(-\frac{E_\mathrm{A}}{RT}\right) \tag{139}$$

we need to transform the parameters of the modified Arrhenius expression to the corresponding E_A value. By applying the definition for "activation energy," E_A

$$E_\mathrm{A} = RT^2 \frac{\mathrm{d}\ln k}{\mathrm{d}T} \tag{140}$$

to equation (138), we obtain the activation energy for a given temperature,

$$E_\mathrm{A} = E + nRT \tag{141}$$

Assuming we were interested in a value for the rate constant at $\sim$1000 K we calculate

$$E_\mathrm{a} = 9.9\ \mathrm{kcal/mol} + 2.51 \times 0.001987\ \mathrm{kcal/(mol\ K)} \times 1000\ \mathrm{K} \approx 14.9\ \mathrm{kcal/mol}$$

Before concluding with step 1, we should reflect on the rather high value for n in the rate expression of the reference reaction ($n = 2.51$). This indicates strong non-Arrhenius behavior. Our attempt to describe the intramolecular H migration in form of a simple Arrhenius rate equation is therefore only valid within the small temperature range around—in this example—1000 K.

Step 2: The pre-exponential factor of the reference reaction used in step 1 describes a bimolecular reaction and is therefore of no use. To get an initial estimate for the pre-exponential factor, we compare the transition state rate expression

$$k_\mathrm{TST}(T) = \frac{kT}{h} \mathrm{e}^{\Delta S^\#/R}\, \mathrm{e}^{-\Delta H^\#/RT} \tag{142}$$

with the Arrhenius expression. Using again the definition for activation energy we find

$$E_\mathrm{A} = RT^2 \frac{\mathrm{d}k_\mathrm{TST}(T)}{\mathrm{d}T} = RT + \Delta H^\# \tag{143}$$

and we obtain

$$k(T) = A \exp\left(-\frac{RT + \Delta H^{\#}}{RT}\right) = eA \exp\left(-\frac{\Delta H^{\#}}{RT}\right) \tag{144}$$

By comparing equations (142) and (144) we finally get

$$A = \frac{ekT}{h} e^{\Delta S^{\#}/R} \tag{145}$$

During the migration process of the H atom, one C–H bond is breaking while the new bond starts to build. The partially broken (weakened) C–H bond leads to an increase of the entropy of the transition state relative to the reactant, but this increase is counterbalanced by the new partially formed C–H bond, which reduces the entropy. It is therefore reasonable to assume as a first approximation that all things considering the entropy of the transition state will be very similar to that of the reactant. Setting $\Delta S^{\#} = 0$ and focusing again on a temperature of $T = 1000\,\mathrm{K}$ we calculate $A \sim 6\mathrm{E}13\,\mathrm{sec}^{-1}$.

Step 3: Finally we apply corrections to the A-factor and activation energy that reflect the cyclic nature of the transition state. The formation of a cyclic transition state has two consequences: (1) In non-cyclic molecules, groups that are connected *via* C–C single bonds can rotate against each other. These internal rotations contribute significantly to the total entropy of a molecule. In cyclic structures, all internal rotations of C–C bonds that are part of the ring system are "frozen," which means that they do not longer behave as rotations but are converted to low-frequency vibrations. In our example, two initially "free" rotors are transformed to wagging modes (vibrations). Since these vibrations contribute less to the entropy than the rotations, it follows that a cyclic transition state will be lower in entropy than a corresponding non-cyclic transition state. The amount of entropy change depends obviously on the ring size or the number of frozen rotors. Table 3 lists approximate correction factors for transition states with up to four frozen rotors. For our example, we find that $\Delta S^{\#}$ is expected to be lower by $\sim 6.0\,\mathrm{cal/(mol\,K)}$, which translates to a correction factor of $\exp(-6.0/R)$. (2) A cyclic transition state also experiences ring strain, which is caused by less than optimal bond angles and distances. Table 3 provides approximate ring strain corrections for different ring sizes. A four-member ring is

TABLE 3
Correction values for ring strain and entropy loss in cyclic hydrocarbon transition [56]

Ring size	Ring strain (kcal/mol)	Number of frozen rotors	$\Delta S^{\#}$ (cal/(mol K))	Reduction factor for A
3 (1,2-H shift)	25	1	–3.6	6
4 (1,3-H shift)	25	2	–6.0	20
5 (1,4-H shift)	8.0	3	–12.7	600
6 (1,5-H shift)	1.0	4	–17.3	6000

~25 kcal/mol higher in energy than the corresponding non-cyclic transition state and this energy adds to the activation energy from step 1.

Putting all corrections together, we obtain our final rate constant estimate (per H atom)

$$A = 6\text{E}13\ \text{sec}^{-1} \times 0.05 = 3\text{E}12\ \text{sec}^{-1}$$
$$E_a = 14.9 + 25.0\ \text{kcal/mol} = 39.9\ \text{kcal/mol}$$

The rate estimation method discussed above might appear very rough. But even though such rate constants estimates are sometimes only accurate to one order of magnitude, they are nevertheless useful for at least two reasons: (a) they allow modelers to incorporate reactions with unknown rate constants into mechanism. By including these reactions in modeling studies and performing a rate and/or sensitivity analysis, it is possible to identify important reactions and study these later in more detail. (b) Estimation rules are also very helpful in providing a quick validation of calculated or experimentally observed rate constants and in providing a selection criterion for scattered or conflicting data.

In recent years rate estimation techniques gained substantial interest because they are needed for automated mechanism generation algorithms and new estimation approaches and improved ''rate rules'' are still currently developed. The example discussed above is only intended to provide a first glance of how such estimations can be made with rather little knowledge of the reaction details.

(*d*) *k(E) from high-pressure rate constants* High-pressure rate constants are not only useful for QRRK calculations, but can also be used in RRKM programs. In the latter case, the $k(T)$ rate constants need to be converted to microcanonical $k(E)$ rate constants. This can be achieved with the inverse Laplace transformation (ILT) technique. The temperature-dependent high-pressure rate constant is given by integrating the

$k(E)$ contributions for all E weighted by the Boltzmann distribution:

$$k(T) = \int_{E_0}^{\infty} k(E) \frac{\rho(E)}{Q_{\text{vib,rot}}(T)} \mathrm{e}^{-E/RT} \, \mathrm{d}E \tag{146}$$

This equation is known as a Laplace transformation of $k(E)$ to $k(T)$. The inverse transformation (ILT) produces $k(E)$ if $k(T)$ is given. Forst [57] has shown that if $k(T)$ can be expressed in simple Arrhenius form $k(T) = A_\infty \exp(-E_\infty/RT)$, then the ILT yields

$$k(E) = A_\infty \frac{\rho_{\text{vib,rot}}(E - E_\infty)}{\rho_{\text{vib,rot}}(E)} \tag{147}$$

In other words, knowledge of the A-factor of a high-pressure rate constant and the density of states function allows us to calculate $k(E)$ without the need to know any further detail of the transition state.

(*e*) *$\rho(E)$ based on estimated representative frequencies* If only estimated thermo data and representative frequencies are available for stable species (isomers) that are involved in pressure-dependent reactions, the corresponding density of states function can also only be calculated with limited accuracy. This is done with a modified version of the Kassel expression, in which the factorials are replaced by the gamma function to allow for continuity. The single frequency formula for $\rho(E)$ is

$$\rho(E) = N(n, s) \frac{1}{hv} = \frac{\Gamma(n + s)}{\Gamma(n + 1)\Gamma(s)} \frac{1}{hv} \tag{148}$$

Here, $n = E/(hv)$ is the number of quanta and s the number of oscillators. In Ref. [7] a detailed discussion of the function $N(n, s)$ for a multifrequency case can be found.

(*f*) *Estimation of collision parameters* Lennard–Jones parameters for stable species can be estimated if their critical properties (T_c, V_c, P_c) and dipole moment are known (see, for example, the method by Brokaw [58], as described in Ref. [47]). For polyaromatic hydrocarbons, Wang and Frenklach [59] proposed a group contribution method for the prediction of Lennard–Jones parameters. All these methods are restricted to stable molecules. To the best of our knowledge more general estimation methods, which are also applicable for radicals, are not available. The same is true for energy transfer parameters ($-\langle E_{\text{all}} \rangle$ or $\langle E_{\text{down}} \rangle$) Therefore, the common procedure is to identify a molecule of similar size or composition for which these data are available and use the same values for the species of interest.

(*ii*) *Input data based on ab initio results*

A basic description of electronic structure calculations is outside of the scope of this chapter. Instead we will restrict ourselves to a discussion of how to use such calculations to get some of the required parameters needed for pressure-dependent rate analysis.

(*a*) *Thermodynamic properties* Basic results from *ab initio* calculations include the electronic energies (E_e or with zero-point energy E_0), the optimized geometric properties of a species, the principal rotational constants, and the frequencies of molecular vibrations approximated as harmonic oscillators. Statistical mechanics [60] allow us to calculate thermal contributions to the enthalpy, the entropy, and heat capacities directly from this information within the HO–RR approximation. However, if low-frequency modes corresponding to internal rotations are present, then the entropy and $C_p(T)$ values obtained with the HO–RR method are not accurate. Instead these modes must be treated as hindered rotors. Several methods for this treatment are reported in the literature [52,61–64]. We will not discuss this issue any further except to mention that recent versions of the *ab initio* package Gaussian [65] provide an option for an automatic hindered rotor treatment (see Ref. [64] for details).

Although only relative energies are needed for an analysis of a pressure-dependent reaction system, the final goal of modelers is to incorporate these results into a reaction mechanism and perform simulations. In this case thermodynamic data of all species are needed, so we need to convert the absolute electronic energies to heats of formation. Two conversion methods are widely used: (1) atomization energies [66–68] and (2) isodesmic reactions [68,69]. The atomization method is based on the decomposition of a species into its atoms. For a species $C_xH_yO_z$ this reaction is

$$C_xH_yO_z^{(g)} \rightarrow xC^{(g)} + yH^{(g)} + zO^{(g)}$$

The reaction energy for this process can be calculated *via ab initio* calculations. With the use of literature values for the enthalpies of all involved atoms we are able to calculate the enthalpy of the species $C_xH_yO_z$ *via*

$$\begin{aligned}\Delta H^{0K}(C_xH_yO_z) = {} & E_0(C_xH_yO_z) - xE_0(C) - yE_0(H) \\ & - zE_0(O) + x\,\Delta_f H^{0K}(C) \\ & + y\,\Delta_f H^{0K}(H) + z\,\Delta_f H^{0K}(O)\end{aligned} \tag{149}$$

If spin–orbit coupling is not incorporated in the *ab initio* method, an additional SOC correction term should be added. To convert $\Delta H^{0\,K}(C_xH_yO_z)$ values to the heats of formation at 298.15 K, thermal

enthalpy corrections for the elements in standard state and the species of interest are applied:

$$\begin{aligned}\Delta_f H^{298\ K}(C_xH_yO_z) = \Delta H^{0\ K}(C_xH_yO_z) + \Delta\Delta H^{298\ K}(C_xH_yO_z) \\ - x\Delta\Delta H^{298\ K}(C_{(s)}) - y\Delta\Delta H^{298\ K}(H_2) \\ - z\Delta\Delta H^{298\ K}(O_2)\end{aligned} \quad (150)$$

The $\Delta\Delta H^{298}(i)$ values in this equation are given on per atom basis.

Isodesmic reactions such as

$$CH_4 + C_2H_5OH \rightarrow CH_3OH + C_2H_6 \quad \Delta_R H^{298}$$

have the property that the reactants and products have the same number of bonds of all bond types. For example, we have nine C–H bonds, one C–O bond, one O–H bond, and one C–C bond on both the left- and right-hand sides. If the heats of formation of all but one species in the reaction are known, the unknown value can be calculated *via*

$$\begin{aligned}\Delta_f H^{298}(CH_3OH) = \Delta_R H^{298} - \Delta_f H^{298}(C_2H_6) + \Delta_f H^{298}(CH_4) \\ + \Delta_f H^{298}(C_2H_5OH)\end{aligned} \quad (151)$$

The heat of reaction is calculated from *ab initio* results,

$$\begin{aligned}\Delta_R H^{298} = E_0(CH_3OH) + E_0(C_2H_6) - E_0(CH_4) - E_0(C_2H_5OH) \\ + \Delta\Delta H^{298}(CH_3OH) + \Delta\Delta H^{298}(C_2H_6) \\ - \Delta\Delta H^{298}(CH_4) - \Delta\Delta H^{298}(C_2H_5OH)\end{aligned} \quad (152)$$

In this equation $E_0(i)$ is zero-point corrected energy for species i and $\Delta\Delta H^{298}(i)$ the change of enthalpy for species i when the temperature is raised from 0 K to 298 K.

Both methods have advantages and disadvantages. The atomization method is well defined and can directly be used for all species including transition states. The strength of using isodesmic reactions is that they—unlike the atomization method—implicitly correct for systematic bond errors which are inherent in *ab initio* calculations. Some drawbacks of isodesmic reactions are that they are not uniquely defined and that they might contain a large number of species, which reduces the accuracy due to error propagation. By introducing bond additivity (BAC) [70,71] or atom-based [72] correction terms to the atomization method, systematic errors of atomization energies can be reduced and their accuracy significantly improved.

(*b*) *High-pressure rate constants* Given that the molecular and thermodynamic properties of all involved species (including the transition state)

are known it is straightforward to calculate the high-pressure rate constant of a reaction:

$$k_{\mathrm{TST}}(T) = \kappa(T)\frac{kT}{h}\frac{Q_{\#}}{\prod_i Q_i}\mathrm{e}^{-E_0/kT} \tag{153}$$

$$k_{\mathrm{TST}}(T) = \kappa(T)\frac{kT}{h}V_{\mathrm{mol}}^{\Delta n-1}\,\mathrm{e}^{-\Delta G^{\#}/RT} \tag{154}$$

Here, $\prod_i Q_i$ is the product of partition functions for all reactants involved, V_{mol} the molar volume, and Δn the molecularity of the reaction. All other symbols have been introduced earlier. The expressions (153) and (154) are equivalent. The appropriate equations to calculate, e.g., the partition function Q from basic molecular properties can be found in standard textbooks of statistical thermodynamics [60]; however, this information is often provided as part of the results of *ab initio* calculations. The program packages ChemRate, Unimol, and MultiWell do or can perform TST rate calculations, but sometimes external software with special features, e.g., to deal with hindered rotor modes, yield more accurate results. Equations (153) and (154) contain the function $\kappa(T)$, which corrects for contributions from quantum mechanical tunneling. The simplest correction function

$$\kappa(T) = 1 + \frac{1}{24}\left(1.44\frac{\nu_{\mathrm{imaginary}}}{T}\right)^2 \tag{155}$$

is based on the work of Wigner [73], but more sophisticated corrections are also known [74–76].

High-pressure rate constants for reactions with no pronounced barrier such as recombination reactions or bond fissions are more difficult to calculate theoretically. Part of the problem is due to the fact that the corresponding transition state or better transition state region is located at large bond distances. Most commonly used *ab initio* methods are optimized for regular (short) bonds and will lose accuracy when applied to long distance interactions. Related is the difficulty to define the exact transition state location. In tight transitions states all but the reacting mode remain well defined. Loose transition states on the other hand contain several weakened internal modes, which are difficult to describe accurately. In addition, the conservation of angular momentum becomes significant and the rate constant thus must be treated as $k(E, J)$. In short, reliable rate constants for reactions without a barrier still present a challenging task though the basic theory, variational transition state theory, is well established. Truhlar and co-workers [76–78] investigated

in many studies the use of combinations of *ab initio* methods and interpolation techniques to obtain a suitable potential energy surface (PES). The PES is then used as basis for variationally localizing the transition state. Other methods, going back to a simple model, were proposed by Gorin and later extended by Benson [49] and others [79]. In this model the transition state is assumed to be closely related to the final products. This allows the use of frequencies of the completely separated products for the TS. The remaining five (for the case of two non-linear fragments) missing frequencies or modes are estimated based on geometric constrains. One of these five modes can be approximated as an internal rotation around the breaking bond and the other four might be approximated as two-dimensional restricted rotors.

Recently, Harding *et al.* [80] and Klippenstein *et al.* [81] published calculations for the barrierless association of H atoms to alkyl radicals and for the combination of two alkyl radicals. Studies like these show that such calculations are possible but that they required significant efforts if high accuracy is required.

Programs such as Variflex [39], CHARMMRATE [40], or ChemRate [30] have the capability to calculate rate constants for reactions with no barrier, though both contain adjustable parameters and appear to work best if the rate constants can be anchored to experimental data.

(*c*) *The density of states function* $\rho(E)$ A key function required in any analysis of pressure-dependent reactions is the density of states $\rho(E)$. Related important functions are the sum of states $W(E)$ and the number of states $N(E)$. The Beyer–Swinehart (BS) algorithm allows the calculation of these functions by ''directly counting'' all states. The results are therefore exact within the framework of the given theory that determines the states. A second formalism to calculate the density of states function was developed by Whitten and Rabinovitch. This analytic method was widely used prior to the BS algorithm and it is still useful for theoretical derivations. For example, Troe's formula to calculate the collision efficiency factor for the MSC approach is based on the Whitten–Rabinovitch density of states function. We will present both methods in the following sections.

The Whitten–Rabinovitch formula [15] for the vibrational density of states function is

$$\rho_{\text{vib}}(E) = \frac{(E_0 + aE_z)^{S-1}}{(s-1)!\prod_{i=1}^{S} h\nu_i} \tag{156}$$

where E_z is the zero-point energy and a is given as

$$\begin{aligned} a &= 1 - \beta_v w \\ \log(w) &= -1.0506\left(\frac{E}{E_z}\right)^{0.25}, \quad \text{for } E > E_z \\ w &= \left[5.00\frac{E}{E_z} + 2.73\left(\frac{E}{E_z}\right) + 3.51\right]^{-1}, \quad \text{for } E < E_z \\ \beta_v &= \frac{S-1}{S}\frac{\langle v^2\rangle}{\langle v\rangle^2} \end{aligned} \tag{157}$$

This method is still used in the CARRA codes and it was until very recently an option in MultiWell.

The BS algorithm [82] was published in 1973 and in the same year extended by Stein and Rabinovitch [83]. The latter algorithm is more flexible (e.g., in addition to harmonic oscillators it can be applied to anharmonic oscillators and hindered rotors as well) and more accurate (rounding errors in the energy discretization step are reduced), but it requires one additional array to store intermediate results. The algorithm may be described as follows:

1. Set the energy range (0–$E_{\max}$) and the step size (ΔE) based on the problem requirements and the lowest vibrational mode. Set the integer value M such that $M\Delta E = E_{\max}$.
2. Declare two arrays T and TA of size $M+1$. Indexing is from 0 to M. The array element $T(j)$ with $j > 0$ contains the number of states with energy $(j-0.5)\Delta E$ to $(j+0.5)\Delta E$.
3. Initialize $T(0)$ and TA(0) with 1 and all other elements with 0. This reflects that just one state exists with $E = E_0$.
4. For any given vibrational mode with energy levels E_k, set the integer value R_k to $R_k = \text{MOD}((E_k - E_0)/\Delta E, 1)$. E_0 is the zero-point energy of this mode. Also set n to the largest integer for which $E_n < E_{\max}$ holds.
5. for $k = 1$ to n do
   for $j = 0$, M-R_k do
   TA($R_k + j$) = TA($R_k + j$) + $T(j)$
   end
   end
   for $j = 1$ to M do
   $T(j)$ = TA(j)
   end
6. Repeat step 5 for any mode.

After all iterations are done, $T(j)$ will contain the number of states in the corresponding energy interval, $N(E)$. The sum of states, $W(E)$, is calculated by adding all $T(j)$ with energies less than or equal to E. Finally, the density of states $\rho(E)$ can be calculated *via* $N(E)/\Delta E$.

How does this algorithm work? Let us assume that we have a certain state distribution (stored in the T vector) among all energy bins realized with the first $j-1$ oscillators and we add contributions from the jth oscillator. If the jth oscillator is in its ground state, it does not contribute, because the ground state corresponds to the zero-point energy. If the vibration is single excited (its quantum number $k = 1$), then it provides additional energy $R_k\Delta E$ to the system. This means that if $T(j)$ states were at energy $R_k\Delta E$ before we added this new oscillator mode, then these states will now be at energy $(j + R_k)\Delta E$. The total number of states at energy $(j + R_k)\Delta E$ is therefore given by those states which were realized without the jth oscillation, $\mathrm{TA}(j + R_k)$, plus the new contributions involving one quanta of the jth oscillator, $T(j)$. The updated total number of states is stored in TA until all overtone contributions of the jth vibration are dealt with. Then the new populations are transferred to the T vector and the $(j + 1)$th vibration is considered.

For cases in which the K-rotor contributes to the density of states, only the initialization step of above outlined algorithm needs to be changed. Both vectors are now initialized with $W_{\text{K-rotor}}$, the sum of states due to the K-rotor within 0–ΔE. This initialization is based on the assumption that the rotational energy of this rotor is significantly smaller then ΔE. Anharmonic vibrations, hindered rotors, and so on are easily incorporated since above algorithm is not restricted to equally spaced energy levels.

Utility programs to explicitly calculate the density of states function with either the BS algorithm or the Whitten–Rabinovitch formula are provided with the MultiWell program package. In addition (due to the central role of the density of states function in QRRK and RRKM theories), these calculations are integral parts of all programs that analyze pressure-dependent systems. If the energy is significantly higher than E_0 the densities of states calculated with either of the methods are very similar; agreement is generally better than a factor of 2. Only for energies that are within a few $100\,\mathrm{cm}^{-1}$ to a few $1000\,\mathrm{cm}^{-1}$ of E_0, clear deviations can be found. This is mainly because the Whitten–Rabinovitch formula is a steady function while the direct counting method leads to non-steady, stepwise behavior. This is shown in Fig. 2 for ethoxy radicals as an example.

(*d*) *Collision parameters* Following a review by Cambi *et al.* [84], electronic structure calculations can be used to estimate Lennard–Jones

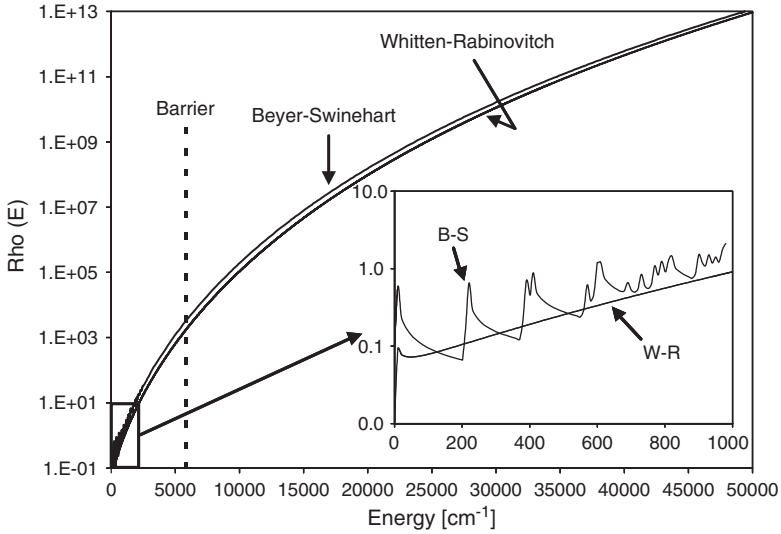

Fig. 2. Densities of states as function of the freely distributable energy for ethoxy radicals calculated with the Beyer–Swinehart (B–S) algorithm or the Whitten–Rabinovitch (W–R) equation. Calculations were done with DenSum from the MultiWell distribution.

parameters of radicals or molecules for which literature data are not available. The basic molecular property required is the average polarizability (α). In Fig. 3, we present a plot of calculated versus experimental polarizabilities for a variety of H/C/O compounds. The calculations were done at the B3LYP/6-311 + + G(3df,3pd) level of theory with geometries optimized at the B3LYP/6-31 + G(2d,p) level. Nearly all data pairs are close to the line resembling $\alpha_{exper} = \alpha_{calc}$, which shows the polarizabilities of these species can be accurately predicted with *ab initio* calculations.

Cambi *et al.* relate the LJ parameter σ_{LJ} directly to the polarizability (in $Å^3$) of a species. For the general case of two species A and B the following relation is recommended:

$$\sigma_{LJ} = 1.767 \frac{\alpha_A^{1/3} + \alpha_B^{1/3}}{(\alpha_A \alpha_B)^{0.095}} \text{ [A]} \tag{158}$$

The numerator in this equation is a measure of the molecule sizes and the product of polarizabilities in the denominator relates to the attraction of two species. The factor 1.767 and the exponent 0.095 are optimized values.

With σ_{LJ} determined and the observation that ε_{LJ} is (approximately) proportional to the product $\sigma_{LJ}^{-6} C_6^{eff}$, it is possible to estimate ε_{LJ}, if we know the long-range interaction term C_6^{eff} or if we can estimate its value.

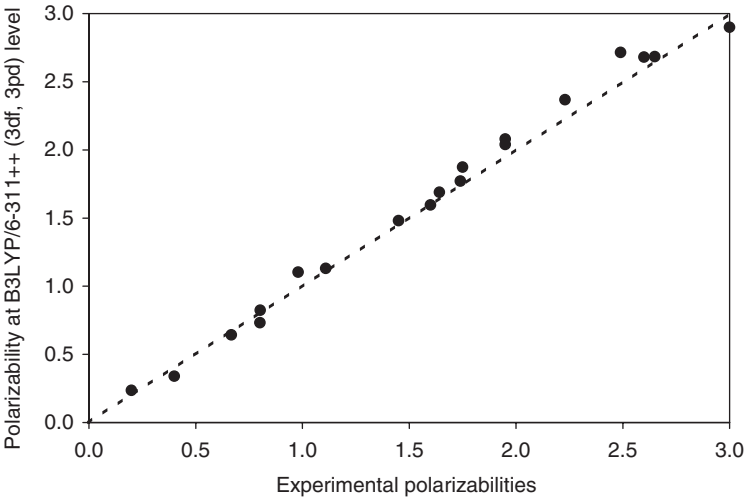

Fig. 3. Comparison between calculated and observed polarizabilities of organic compounds. The calculated polarizabilities were obtained at the B3LYP/6-311++G(3df,3pd)//B3LYP/6-31+G(2d,p) level of theory.

The C_6^{eff} parameter is usually related to the polarizability by the Slater–Kirkwood equation [85]

$$C_6^{\text{eff}} = 15.7 \times 10^3 \frac{\alpha_A \alpha_B}{\sqrt{\alpha_A/N_A} + \sqrt{\alpha_B/N_B}} \text{ [meV Å}^6\text{]}$$
$$= 1.82 \times 10^5 \frac{\alpha_A \alpha_B}{\sqrt{\alpha_A/N_A} + \sqrt{\alpha_B/N_B}} \text{ [K Å}^6\text{]} \quad (159)$$

The unknown "effective number of valence electrons," N_i, can be found with the following recipe proposed by Cambi:

$$\text{for atoms}: \quad N = N_{\text{ext}} \left\{ 1 + \left(1 - \frac{N_{\text{ext}}}{N_{\text{int}}} \right) \left(\frac{N_{\text{int}}}{N_{\text{tot}}} \right)^2 \right\} \quad (160)$$

where N_{ext} is the valence electrons, N_{int} the core electrons, $N_{\text{tot}} = N_{\text{int}} + N_{\text{ext}}$.

$$\text{for molecules}: \quad N = N_{\text{tot}} \left\{ 1 - \frac{N_b N_{nb}}{N_{\text{tot}}^2} \right\} \quad (161)$$

where N_b is the bond electrons, N_{nb} the lone-pair electrons, $N_{\text{tot}} = N_b + N_{nb}$.

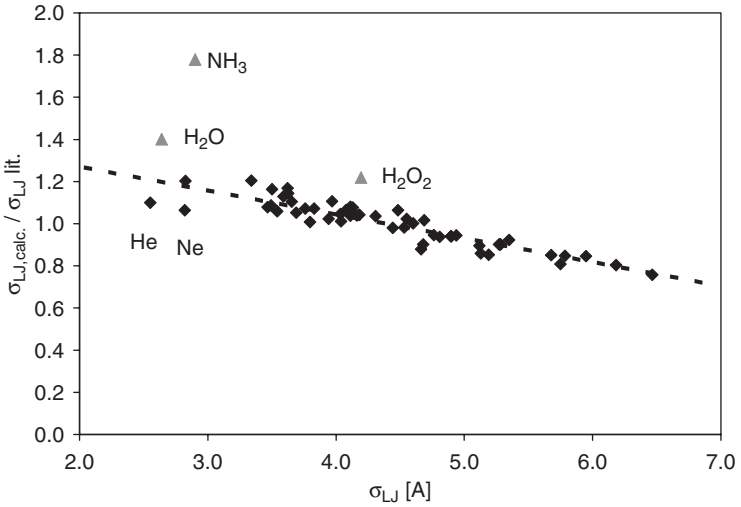

Fig. 4. Comparison of calculated and experimental σ_{LJ} values. See text for calculation details.

The final relation for the well depth is

$$\varepsilon_{LJ} = 0.720 \frac{C_6^{eff}}{\sigma_{LJ}^6}[\text{meV}] = 8.36 \frac{C_6^{eff}}{\sigma_{LJ}^6} \ [\text{K}] \tag{162}$$

It should be mentioned that the review by Cambi *et al.* is mainly based on atoms and small radicals. Though the relations are formulated in a general way, we are not aware of any comprehensive studies that validate their usefulness for large molecules or radicals. However, preliminary results of the calculations of σ_{LJ} suggest a generally good agreement with experimental data, although small systematic deviations, which scale with σ_{LJ} (Fig. 4), are observed. The agreement between calculated and tabulated ε_{LJ} values is at this point less satisfying. But it might be possible to improve this situation in future by, e.g., redefining the number of effective electrons.

A further improvement appears to be necessary if at least one of the colliding species has a permanent dipole moment. Paul and Warnatz [86] investigated correction methods in the context of transport properties. Although we will not discuss details of these corrections, the basic effect is that permanent dipole moments decrease the collision diameter slightly, while the attractive energy is strongly increased. Because the value of the collision integral $\Omega^{*(2,2)}$ depends *on* ε_{LJ}, the overall effect at low temperatures is an increase of the collision frequency.

In addition to the Lennard–Jones collision parameters, we need a measure of the energy transfer probability to describe the energy transfer

in collisions. Lim and Gilbert [2,87] published a method called the ''biased random walk'' model that calculates the average energy transferred per collision, $\langle \Delta E_{all} \rangle$. A corresponding program (BRW) is provided in the ''Unimol'' package. The program requires readily available input data: LJ parameter, the mass, specification of the composition, and so-called local LJ parameters. According to the authors, this source of energy transfer data should be used with caution since the theory for energy transfer is still in its infancy. Often, a generic value for $\langle \Delta E_{down} \rangle$ is a better choice at this stage.

4 WORKED-OUT EXAMPLES OF THE ANALYSIS OF PRESSURE-DEPENDENT REACTIONS

To complete the discussion of pressure-dependent reactions we present and discuss in this section worked-out examples for the following four reaction systems:

1. The thermal dissociation of C_2H_5O radicals to $CH_3 + CH_2O$.
2. The reversible isomerization of n-C_3H_7 to i-C_3H_7.
3. The reaction of C_2H_5 with O_2.
4. The reaction of $C_2H_3 + O_2$.

The selected examples will be used to demonstrate specific aspects of the kinetic analysis discussed earlier.

4.1 Example 1: the thermal dissociation $C_2H_5O \rightarrow CH_3 + CH_2O$

Ethoxy radicals (C_2H_5O) are rather unstable and dissociate even at temperatures as low as 400 K in less than a millisecond. Therefore, the thermal dissociation of ethoxy is suitable to demonstrate the performance of different reaction analysis programs including MultiWell. The reaction channel leading to CH_3 and CH_2O, $\Delta_R H^{298} \approx 10.5$ kcal/mol, has the lowest barrier and dominates over the second most important channel ($CH_3CHO + H$, $\Delta_R H^{298} \approx 13.8$ kcal/mol) up to at least 500 K as shown by Caralp *et al.* [88] in a recent experimental and theoretical study. Under these circumstances, the overall thermal dissociation might be thought of (in the Lindemann picture) as a two-step process:

$$C_2H_5O \overset{+M}{\rightleftharpoons} C_2H_5O^*$$
$$C_2H_5O^* \rightarrow CH_3 + CH_2O$$

We use for the high-pressure rate constant and collision parameters the following values, which are close to those given by Caralp *et al.*:

$$\sigma_{LJ}(C_2H_5O) = 4.53\text{Å}, \quad \sigma_{LJ}(He) = 2.55\text{Å}$$
$$\varepsilon_{LJ}(C_2H_5O) = 362.6\text{K}, \quad \varepsilon_{LJ}(He) = 10.0\text{K}$$
$$k_\infty = 1.0 \times 10^{13} \exp(-16.8\ \text{kcal/mol}/RT)\text{sec}^{-1}$$

Other molecular parameters are obtained from CBS-QB3 *ab initio* calculations. Since the *ab initio* data do not yield the observed *A*-factor, we adjusted the reaction path degeneracy in those applications that calculate the TST rates directly from molecular data (ChemRate, Unimol). Programs such as CARRA and MultiWell accept high-pressure rate constants in Arrhenius form as input and no adjustments were needed in these cases. The programs CARRA_MSC and CARRA_ME calculate the density of states from three characteristic frequencies instead of taking the complete set of frequencies, which we obtained with a separate fitting program.

We will present results of the thermal dissociation of ethoxy to address the following three questions:

(a) How do the predictions with the different programs compare (for an arbitrarily chosen $\langle E_{down} \rangle$ value)?
(b) How sensitive are these predictions to:
    the energy transfer treatment (MSC approach versus ME approach);
    the value for $\langle E_{down} \rangle$;
    the functional form for $P(E, E')$?
(c) Can the steady-state approximation be justified?

In Fig. 5 we present predictions of fall-off curves for the unimolecular dissociation of C_2H_5O in He with (a) Unimol, (b) ChemRate, (c) MultiWell, and (d) CARRA_ME. The $\langle E_{down} \rangle$ value was set to $200\,\text{cm}^{-1}$, which is a frequently used "standard" value for He as collider. It can be seen that the predictions with all programs are quite similar but not identical. The first two calculations slightly over-predict the unimolecular dissociation at low pressure, while MultiWell results in this region are on the low side. Finally, results obtained with CARRA_ME reproduce the data well. Since the $\langle \Delta E_{down} \rangle$ value was arbitrarily chosen, a good or bad agreement with the experimental data does not necessarily indicate that one program performs better than another. It only shows that the predictions are sensitive to specifics of the implementation of the theory in these programs. These include the treatment of internal rotations, the default energy grain size, differences in the calculation of $k(E)$, and so on. Everything else

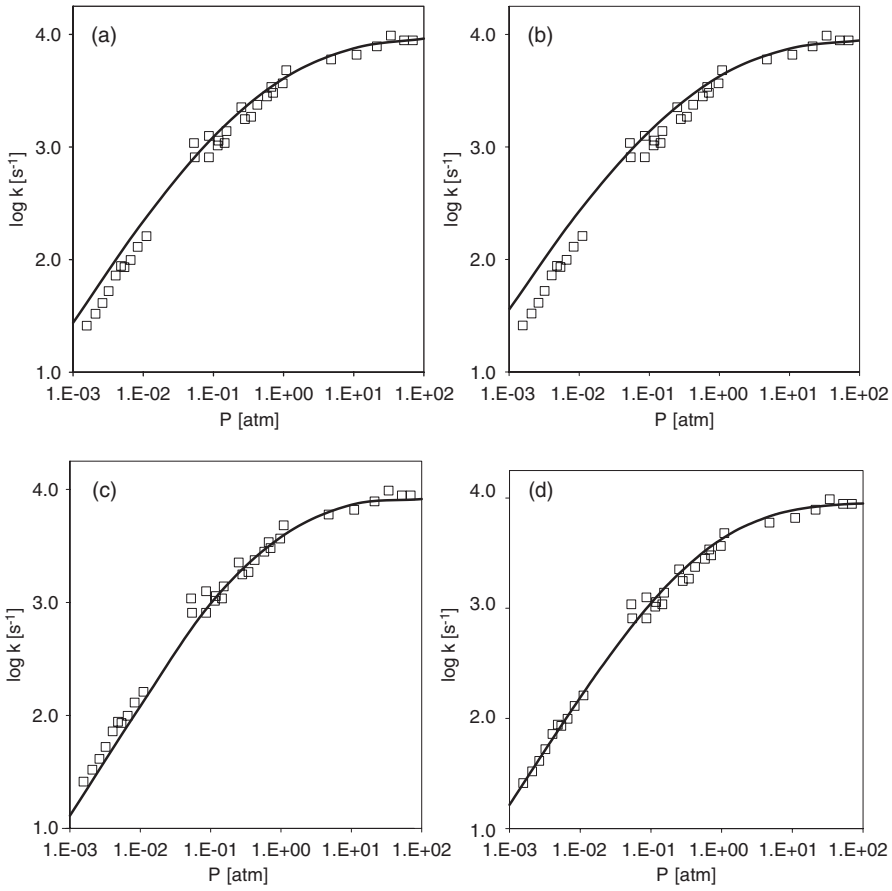

Fig. 5. Comparison of predicted fall-off curves for the thermal dissociation of C_2H_5O radicals forming $CH_3 + CH_2O$ at 406 K with experimental data. All calculations use the exponential down model with $\langle E_{down} \rangle = 200\,cm^{-1}$. (a) Unimol, (b) ChemRate (steady-state and time-dependent calculations yield similar results), (c) MultiWell, and (d) CARRA_ME.

being equal, results from CARRA_ME using QRRK theory and a three-frequency representation of the internal modes are expected to be less accurate, so the good agreement observed here is fortunate.

Next we compare collision parameters and models. In Fig. 6a, we present results obtained with CARRA_MSC and CARRA_ME. Except for the energy transfer values, all input data are identical. The CARRA_ME results are the same as shown in Fig. 5, using $\langle E_{down} \rangle = 200\,cm^{-1}$ (or 573 cal/mol). An equivalent $\langle E_{all} \rangle$ value of -273 cal/mol (or $95\,cm^{-1}$), calculated *via* equations (44) and (45), is used in CARRA_MSC. The results from both calculations compare well

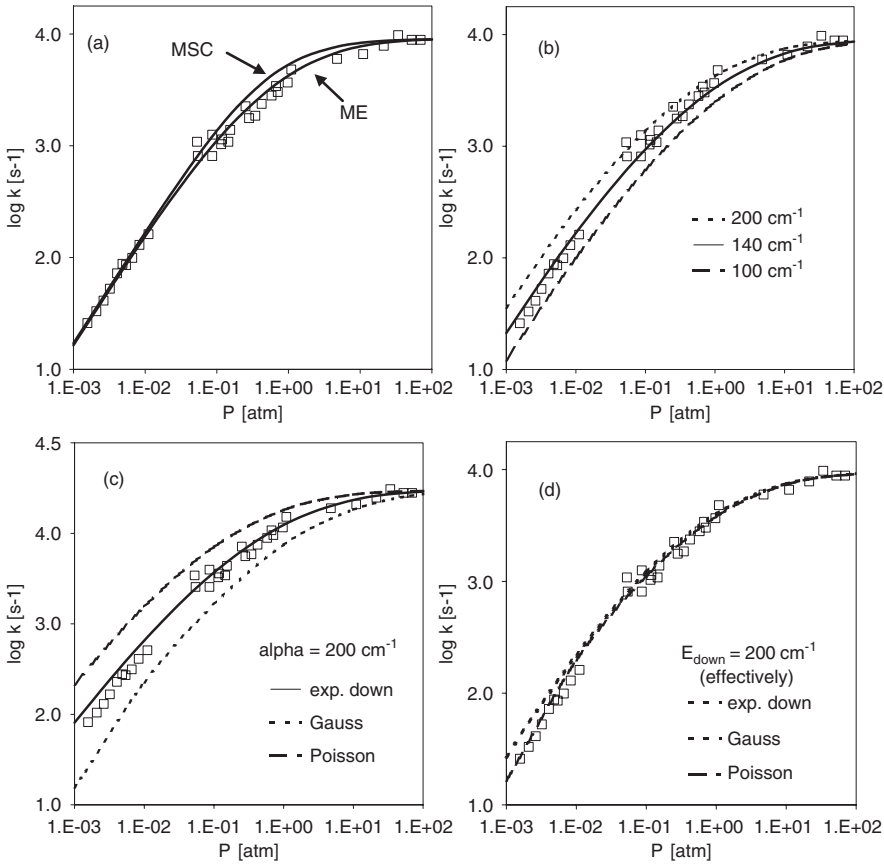

Fig. 6. Demonstration of the influence of collision parameters and energy transfer models on the fall-off prediction for the thermal dissociation of ethoxy at 406 K. (a) MSC (CARRA_MSC) versus ME (CARRA_ME) approach. (b) Impact of the $\langle E_{\text{down}} \rangle$ value (calculation done with ChemRate). (c) Impact of the energy transfer model for a given value of α (see text) (calculation done with Unimol). (d) Impact of the choice of the energy transfer model if α is adjusted to yield numerically $\langle \Delta E_{\text{down}} \rangle = 200\,\text{cm}^{-1}$ (calculation done with Unimol).

although the fall-off curve obtained with the ME treatment is somewhat flatter. At least for this example, the MSC formalism appears to provide a good alternative to the ME approach.

Fig. 6b contains results from ChemRate calculations with various $\langle \Delta E_{\text{down}} \rangle$ values. The relation between this parameter and the predictions is obvious: a larger $\langle \Delta E_{\text{down}} \rangle$ value leads to an increase in the unimolecular dissociation rate at low pressures and in the fall-off region. A consequence of this observation is that for each program an optimal $\langle \Delta E_{\text{down}} \rangle$ value can be found that leads to good agreement with the

data. For ChemRate this value is $\sim 140\,\mathrm{cm}^{-1}$ and for Unimol it is $\sim 150\,\mathrm{cm}^{-1}$. Another indication for the uncertainty of energy transfer parameters is that the original analysis by Caralp *et al.*—done in the framework of the Troe formalism—yielded a $\langle \Delta E_{\mathrm{all}} \rangle$ value of $-24\,\mathrm{cm}^{-1}$, which is—as the authors admit—surprisingly low. As discussed above, we used in our CARRA_MSC analysis a four times larger value for $\langle \Delta E_{\mathrm{all}} \rangle$ and obtained good agreement with the data.

Even if we restrict ourselves to a ME analysis, we still have the choice of many different collision models. In the review section we only discussed the exponential down model (60),

$$P(E, E') = \frac{1}{N(E')} \exp\left(-\frac{E' - E}{\alpha}\right), \quad \text{with } E < E' \text{(exponential down)}$$

but this is just one of many functional forms of $P(E, E')$ that are used in ME calculations.[12] Other models, for example, assume a Poisson or Gaussian distribution of the energy transfer probability. The corresponding expressions are

$$P(E, E') = \frac{1}{N(E')} \frac{E' - E}{\alpha} \exp\left(-\frac{E' - E}{\alpha}\right), \quad \text{with } E < E' \text{ (Poisson)}$$

$$P(E, E') = \frac{1}{N(E')} \exp\left(-\frac{(E' - E)^2}{\alpha^2}\right), \quad \text{with } E < E' \text{ (Gaussian)}$$

All these functions contain only one parameter, α, which in the case of the exponential down model equals $\langle E_{\mathrm{down}} \rangle$. In Fig. 6c, we compare fall-off curves for the ethoxy dissociation at 406 K calculated with each of these energy transfer models and a constant α value of $200\,\mathrm{cm}^{-1}$. At first glance we would conclude that the choice of the energy transfer model has a huge impact on the predictions. However, α has a different meaning in all three energy transfer models and thus it is not immediately clear that its value should be the same for all cases. Fortunately, the Unimol software, which was used for this subset of calculations, provides the average amount of energy transferred in a down collision (meaning a numerically obtained effective $\langle E_{\mathrm{down}} \rangle$ value) as part of the output. We find for our calculations effective $\langle E_{\mathrm{down}} \rangle$ values of $190.4\,\mathrm{cm}^{-1}$, $407\,\mathrm{cm}^{-1}$, and $108\,\mathrm{cm}^{-1}$, respectively,[13] for the exponential

[12] The current version of MultiWell handles 10 pre-defined collision models. See also the recent review by Barker *et al.* [17].

[13] The difference between the provided and effective $\langle \Delta E_{\mathrm{down}} \rangle$ values in the exponential down model can be explained with numerical errors due to the finite energy grain size.

down, Poisson, and Gaussian models. The calculated higher rate constant for the Poisson model is consistent with the earlier observation that a higher energy transfer value results in an increased rate constant in the low-pressure region. In Fig. 6d we adjusted the α parameters for all three cases in such a way that approximately the same numerical $\langle E_{\text{down}} \rangle$ value resulted. Now all predictions essentially overlap, proving that the specific choice of the model is of little impact.

Finally, we use MultiWell to study the change of the energy distribution function of ethoxy while it dissociates. To do so we carry out the following computer experiment: we assume that ethoxy is formed completely thermalized at 900 K and 1 atm and that it only dissociates to $CH_3 + CH_2O$. (It would be trivial to incorporate additional channels but we try to keep it simple.) The top of Fig. 7 depicts the distribution of ethoxy radicals with respect to the total amount of vibrational energy. At $t = 0$ sec the maximum population is found at $\sim 3000\,\text{cm}^{-1}$ (8.6 kcal/mol), but the long exponential tail in the energy distribution reveals that a significant fraction of ethoxy radicals possess substantially much more vibrational energy (up to and above $10{,}000\,\text{cm}^{-1}$). The barrier for dissociation is $\sim 5860\,\text{cm}^{-1}$ (16.8 kcal/mol), hence well inside the ethoxy population at this temperature. All profiles provided at longer times are clearly distinguished from the initial population in that the exponential tail is nearly completely depleted and only a very small fraction of ethoxy exists at energies above the barrier. The shapes of these later profiles are all similar and it appears as if only the area under the profiles diminishes. The bottom part of Fig. 7 depicts the integrated mole fractions versus time. Initially the mole fraction of ethoxy drops nearly instantaneously by 20%. This is followed by an exponential steady decay of the reactant and formation of the products. Since the time-dependent unimolecular rate constant is defined as $-\text{d}\ln(x)/\text{d}t$ at each point in time, we can qualitatively see that the rate constant is initially not independent of time. At later times, however, the rate constant becomes time independent and the populations are at steady state. More precisely, the distribution among different energy levels remains steady but the absolute amount of ethoxy declines due to reaction. MultiWell's output of the distributions visualizes the transition from a time regime where energy redistribution is important to the time domain where only chemically significant processes occur. The inset clarifies that the ethoxy decay is exponential after some time and a truly time-independent rate constant is defined.

Although Fig. 7 clearly shows that we can assign a time-independent rate constant for the thermal dissociation of ethoxy, it is also obvious that the initial fast decay is ignored. This is a consequence of waiting

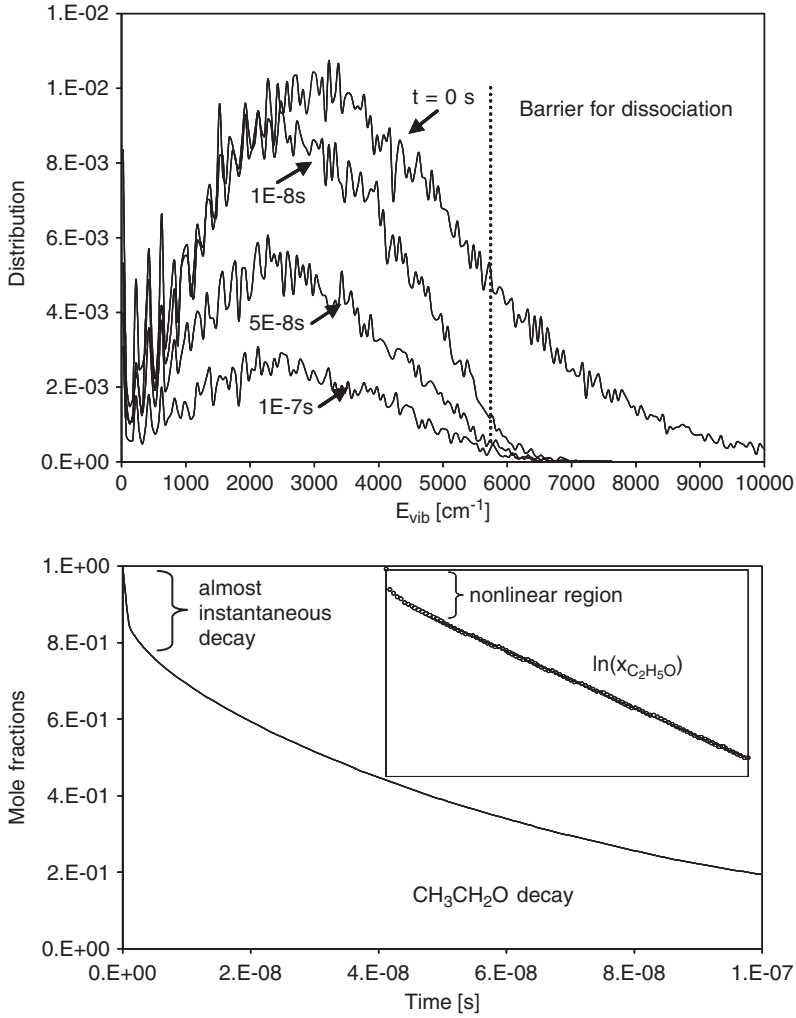

Fig. 7. Study of the unimolecular dissociation of ethoxy to $CH_3 + CH_2O$ at 900 K and 1 atm with MultiWell. (Top) Change of the distribution and population of vibrational energy levels as a function of time. (Bottom) Integrated C_2H_5O profiles versus time; (inset) ln(C_2H_5O) versus time. Notice the statistical noise inherent to all stochastic calculations.

until steady state is achieved. In this example, ~20% of the decay is not captured if we only use the apparent rate constant. Since the initial dissociation proceeds more or less instantly, this decay would have to be accounted for in the description of the formation reaction of ethoxy by assigning 20% of the yield directly to the products. For example, if we

envision that ethoxy is formed *via*

$$C_2H_5OH + F \rightarrow C_2H_5O + HF$$

we could assign an 80% yield to this channel and include

$$C_2H_5OH + F \rightarrow CH_3 + CH_2O + HF$$

as a 20% channel to account for the initial fast decay.

4.2 Example 2: the isomerization reaction n-C_3H_7 ⇌ i-C_3H_7

Our second example is the unimolecular isomerization of propyl radicals. We have chosen this reaction to address the question of how well does a steady-state analysis describe isomerizations. This will be done in three steps: first, we perform a steady-state kinetic analysis with the CARRA software (ME and MSC) for 1200 K with Ar as collider. Next we repeat the analysis with the stochastic MultiWell program to understand which time scales are involved in the overall process. Finally we compare predicted species profiles from both approaches.

The two isomers *n*-C_3H_7 and *i*-C_3H_7 are separated by a barrier of ~37 kcal/mol (measured with respect to *n*-C_3H_7) and they can easily interconvert at sufficiently high temperatures. Although in reality both radicals dissociate to propene + H and ethylene + CH_3 (see Fig. 8), we will ignore these channels here and focus exclusively on the isomerization part. The steady-state analysis with CARRA yields one apparent pressure-dependent rate constant, since the rate constant for the reverse reaction is determined by the equilibrium constant. The predictions with both versions (MSC and ME) for $T = 1200$ K and various pressures are shown in Fig. 9. The results are very similar and show the expected fall-off behavior. The MSC treatment—despite its simplicity—captures the pressure dependence well.

Next, we look at the results from MultiWell. Instead of focusing at the population distribution function, as we did in the first example, we use this time the results for the average energy ($\langle E_{vib} \rangle$) stored in the vibrational modes of both isomers. The change of $\langle E_{vib} \rangle$ with time is a measure of the energy transfer during the isomerization. Fig. 10 presents $\langle E_{vib} \rangle$ as a function of time for three different pressures and $T = 1200$ K. Initially *n*-C_3H_7 is thermalized and $\langle E_{vib} \rangle$ is at $t = 0$ sec in equilibrium with the thermal energy. (Note that $\langle E_{vib} \rangle_{t=0\,sec} = \sim 8200\,cm^{-1}$, which means that on average ~23.5 kcal/mol of energy is stored in these modes.) Shortly thereafter we see a clear drop of $\langle E_{vib} \rangle$. The lower the pressure, the larger this drop. The reason is clear: part of the *n*-C_3H_7 population at high energies quickly isomerizes to *i*-C_3H_7 and

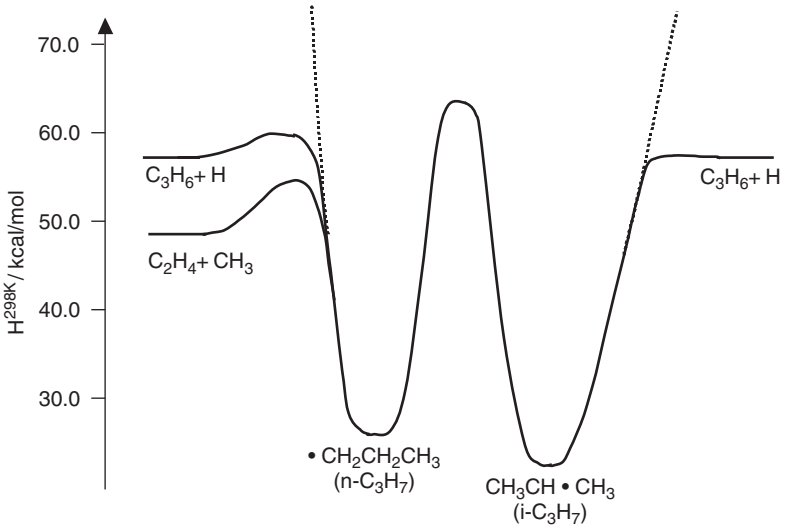

Fig. 8. PES surface for the isomerization of C_3H_7 radicals. The dotted lines indicate the cases in which the dissociation channels are ignored. The energies were calculated *ab initio* at CBS-QB3 level.

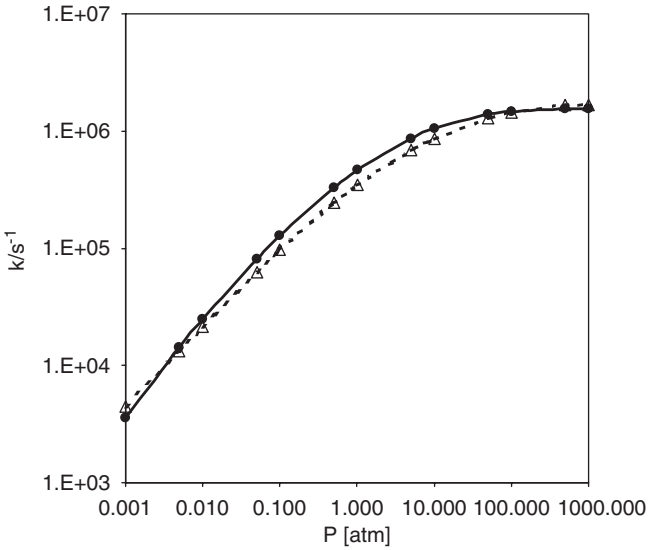

Fig. 9. Predicted rate constant for the isomerization of *n*-C_3H_7 to *i*-C_3H_7 as a function of pressure at 1200 K. Solid line with filled circles: QRRK/MSC prediction (with CARRA_MSC); broken line with open triangles: QRRK/ME predictions (with CARRA_ME).

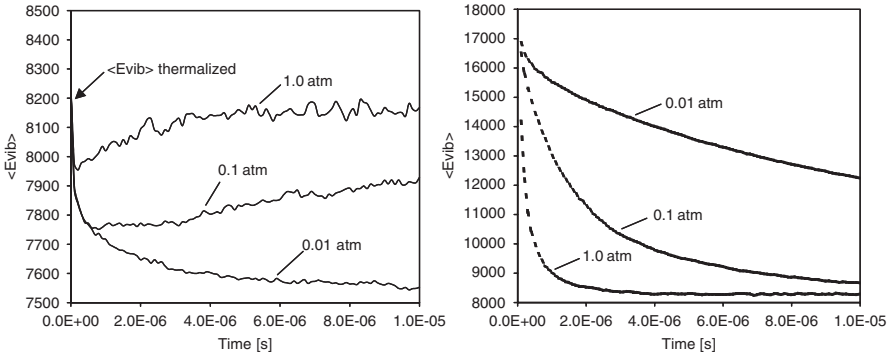

Fig. 10. Average vibrational energy E_{vib} of n-C_3H_7 (left) and i-C_3H_7 (right) as a function of reaction time. Conditions: 1 atm (Ar) and 1200 K; calculations with MultiWell. $\langle E_{vib} \rangle$ is given in cm^{-1}; 1 kcal/mol = 349 cm^{-1}.

thus is lost. If the pressure is high, the missing population is easily regenerated *via* collisions and the Boltzmann distribution is nearly maintained, while this is not possible at low pressures.

The barrier for isomerization is ~14,500 cm^{-1} (41.5 kcal/mol) above the zero-point energy of i-C_3H_7. Therefore, i-C_3H_7 is formed with a large amount of internal energy as seen in the right-hand side of Fig. 10. The initially formed highly excited i-C_3H_7 states are quickly deactivated (*via* collisions) so that the $\langle E_{vib} \rangle$ value decreases. Again, a lower pressure leads to a slower deactivation process. At equilibrium the $\langle E_{vib} \rangle$ values for both isomers should be very similar because they contain the same number of vibrations with similar frequencies. This can be seen for the results at 1 atm total pressure. At a reaction time of ~5E−6 sec the $\langle E_{vib} \rangle$ values for both, n-C_3H_7 (left) and i-C_3H_7 (right), have reached within the error limits their final values which can be seen to be ~8200 cm^{-1}. At the lower pressures the reaction is far from equilibrium and the $\langle E_{vib} \rangle$ values are far from the final value.

In Fig. 11 we compare predictions based on CARRA_MSC results with mole fraction profiles from MultiWell for two pressures at 1200 K. The steady-state code does not capture the initial drop seen at early times for the 0.01 atm profiles but agrees well at longer times. At 1 atm there is no initial drop apparent and steady-state rate constants could in principle describe the MultiWell data. The predicted profiles with both codes are rather close and small changes in the $-\langle E_{all} \rangle$ value used in CARRA_MSC can bring both plots even closer together. The major point to notice is again the characteristics of the steady-state assumption to ignore initial changes, which happen before the steady-state condition

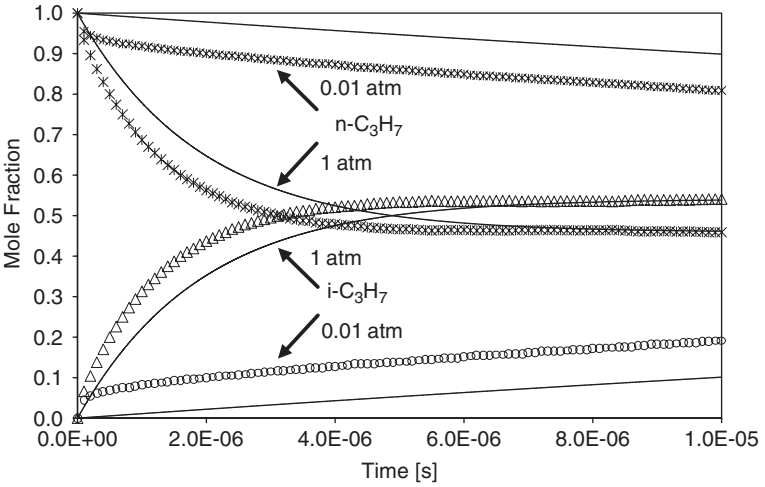

Fig. 11. Comparison of predicted MultiWell concentration profiles (symbols) for *n*-C_3H_7 and *i*-C_3H_7 with integrated profiles calculated from the CARRA_MSC results (lines) at 1 atm and 0.01 atm (Ar) and $T = 1200$ K.

is established. In this example the error is small, but one could imagine cases where the steady-state assumption is no longer a valid approach and time-dependent solutions to the ME must be used.

4.3 Example 3: the reaction $C_2H_5+O_2 \rightarrow$ products

The next example is a chemically activated reaction, the recombination of C_2H_5 radicals with O_2. This well-studied reaction [37,89–100] plays an important role in the low temperature oxidation of ethane. The underlying PES (Fig. 12) reveals that the initially formed ethyl peroxy complex, C_2H_5OO, can either undergo stabilizing collisions, react to bimolecular products such as ethylene and hydroperoxy or acetaldehyde and hydroxyl, isomerize to hydroperoxy ethyl, or redissociate back to the reactants. The isomerization product hydroperoxy ethyl, CH_2CH_2OOH, can also dissociate to ethylene and hydroperoxy or it can form ethylene oxide and hydroxyl radicals. Although this system appears to be a complex system, it is rather simple since—as we shall see—most of these channels are of minor importance. The barrier for the elimination of ethylene and hydroperoxy from ethyl peroxy is lower than the entrance channel but the corresponding rate constant has a significantly lower *A*-factor than the rate constant for the redissociation. The

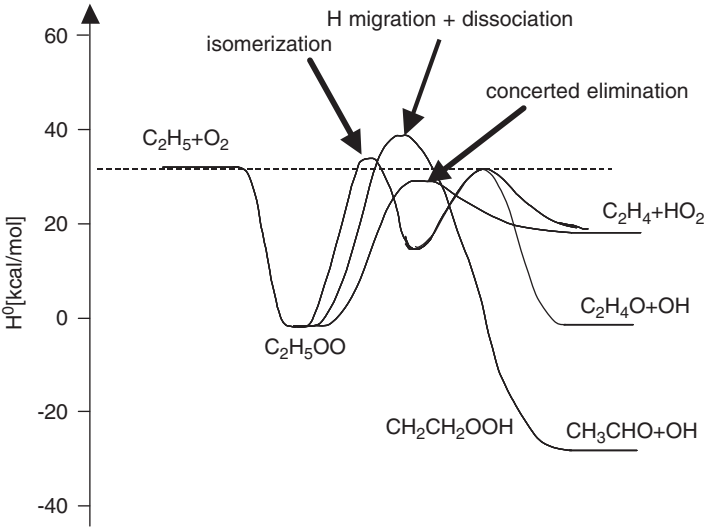

Fig. 12. PES for the reaction $C_2H_5 + O_2$.

barrier for the isomerization is slightly above the energy of the reactants and since this reaction has a low *A*-factor, too, it will be a minor channel under all conditions.

We will mainly use CARRA_MSC to analyze this system. Before looking at the results, we should address the question of how many apparent rate constants are required to fully describe this system. We have three sets of reactions: (a) reactions of $C_2H_5 + O_2$, (b) unimolecular reactions of stabilized C_2H_5OO, and (c) unimolecular reactions of CH_2CH_2OOH. These reactions are:

$$
\begin{aligned}
C_2H_5 + O_2 &\rightarrow CH_3CH_2OO \text{ (stabilization)} \\
&\rightarrow C_2H_4 + HO_2 \text{ (direct elimination)} \\
&\rightarrow CH_3CHO + OH \text{ (H migration to form } CH_3CHOOH, \\
&\quad \text{then rapid dissociation)} \\
&\rightarrow C_2H_4 + HO_2 \text{ (isomerization to form } CH_2CH_2OOH, \\
&\quad \text{then elimination)} \\
&\rightarrow C_2H_4O + OH \text{ (isomerization to form } CH_2CH_2OOH, \\
&\quad \text{then elimination)} \\
&\rightarrow CH_2CH_2OOH \text{ (isomerization to form } CH_2CH_2OOH, \\
&\quad \text{then stabilization)}
\end{aligned}
$$

$$
\begin{aligned}
CH_3CH_2OO \rightarrow\ & C_2H_5 + O_2 \text{ (reverse of recombination)}^* \\
\rightarrow\ & C_2H_4 + HO_2 \text{ (direct elimination)} \\
\rightarrow\ & CH_3CHO + OH \text{ (H migration to form} \\
& CH_3CHOOH, \text{ then rapid dissociation)} \\
\rightarrow\ & C_2H_4 + HO_2 \text{ (isomerization to form} \\
& CH_2CH_2OOH, \text{ then elimination)} \\
\rightarrow\ & C_2H_4O + OH \text{ (isomerization to form} \\
& CH_2CH_2OOH, \text{ then elimination)} \\
\rightarrow\ & CH_2CH_2OOH \text{ (isomerization to form} \\
& CH_2CH_2OOH, \text{ then stabilization)}
\end{aligned}
$$

$$
\begin{aligned}
CH_2CH_2OOH \rightarrow\ & C_2H_5 + O_2 \text{ (reverse of recombination)}^* \\
\rightarrow\ & C_2H_4 + HO_2 \text{ (direct elimination)} \\
\rightarrow\ & C_2H_4O + OH \text{ (direct elimination)} \\
\rightarrow\ & C_2H_4 + HO_2 \text{ (isomerization to form} \\
& CH_3CH_2OO, \text{then elimination)} \\
\rightarrow\ & CH_3CHO + OH \text{ (isomerization to form} \\
& CH_3CH_2OO, \text{then H migration to form} \\
& CH_3CHO + OH, \text{then dissociation)} \\
\rightarrow\ & CH_3CH_2OO \text{ (isomerization to form} \\
& CH_3CH_2OO, \text{then stabilization)}^*
\end{aligned}
$$

Three out of these 18 apparent reactions are marked with an asterisk "*", because they are the reverse reactions of already listed ones and thus do not present independent rate constants. This leaves 15 independent reactions to describe this example reaction. This number could be further reduced if channels with insignificant contributions to the overall product spectrum were eliminated. One more word of clarification to the reaction list: reactions labeled with "isomerization …, then elimination" are different from those labeled with "direct elimination," because they follow a different reaction path. For example, the two $CH_2CH_2OOH \rightarrow C_2H_4 + HO_2$ product channels are:

1. $CH_2CH_2OOH \xrightarrow{\text{elimination barrier}} C_2H_4 + HO_2.$
2. $CH_2CH_2OOH \xrightarrow{\text{isomerization barrier}} CH_3CH_2OO^*$
   $CH_3CH_2OO^* \xrightarrow{\text{elimination barrier}} C_2H_4 + HO_2.$

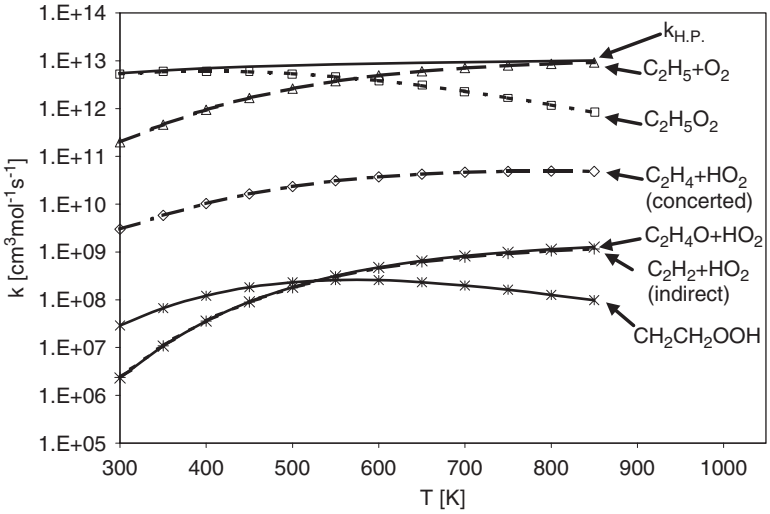

Fig. 13. Temperature-dependent apparent rate constants for chemically activated reactions of the $C_2H_5 + O_2$ system ($CH_3CHO + OH$ channel is not included). In addition, the redissociation channel (formally $C_2H_5 + O_2 \Rightarrow C_2H_5 + O_2$) and the high-pressure rate constant (k_{HP}) are shown. The calculations were done at 1 atm He.

The second apparent rate constant is different from those for CH_3CH_2OO because the $CH_3CH_2OO^*$ is not stabilized.

In Fig. 13 we present results for the chemically activated reactions at 1 atm (He) as a function of temperature. In addition to the apparent rate constants (the unimportant $CH_3CHO + OH$ channel is omitted), the redissociation rate constant and the high-pressure rate constant are plotted. At low temperatures, stabilization to ethyl peroxy dominates all other channels. With increasing temperature, the redissociation rate constant becomes increasingly more important and at 850 K this channel is more than one order of magnitude faster than stabilization. Effectively this means that the observable $C_2H_5 + O_2$ rate decreases drastically with temperature under these conditions. Among the bimolecular products the concerted elimination channel has the highest yield, followed by the formation of $C_2H_4O + OH$ and $C_2H_4 + HO_2$ from the isomerization channel.

The initially stabilized ethyl peroxy adduct is not stable at higher temperatures. Predictions of its unimolecular reactions for the same conditions are presented in Fig. 14. The major dissociation channel leads to $C_2H_5 + O_2$ and the only other important reaction path produces $C_2H_4 + HO_2$. Due to the higher A-factor, the dominance of the redissociation channel increases with temperature. For the dissociation

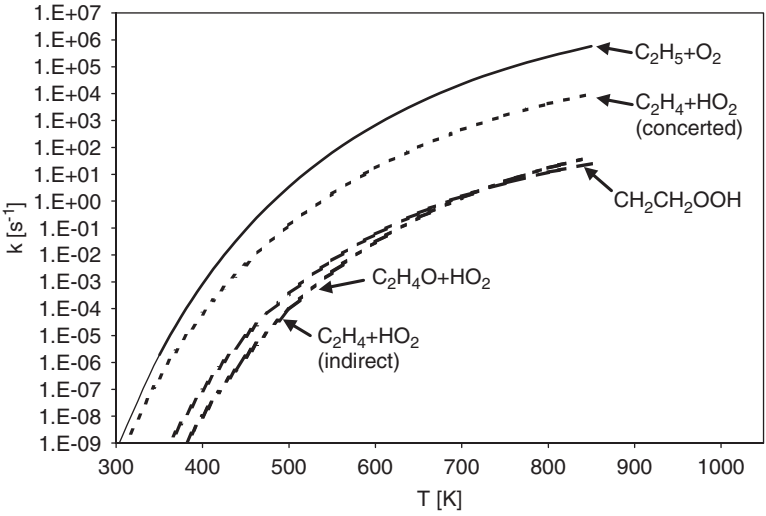

Fig. 14. Apparent rate constants for major channels of the unimolecular dissociation of ethyl peroxy at 1 atm (He).

of the second isomer, similar results are obtained, although they are not shown.

The work by Sheng *et al.* [101] demonstrated that results obtained with the QRRK/ME approach are very similar to the predictions from this QRRK/MSC analysis. The separation of the $C_2H_5 + O_2$ reaction into two steps: (1) prompt chemically activated reactions and (2) delayed thermal dissociation reactions, might appear unphysical or arbitrary. A justification why this approach is reasonable can be obtained from time-dependent solutions of the ME. We use MultiWell to illustrate this for one specific case (700 K, 1 atm). The results are presented in Fig. 15. We can clearly see that $C_2H_5O_2$ is consumed on two very different time scales: ~90% of it dissociates very rapidly to $C_2H_5 + O_2$, thereby competing with collision stabilization. In contrast, the stabilized $C_2H_5O_2$ fraction dissociates several orders of magnitudes slower. The appearance of two completely separated time domains provides the justification to break the entire process down into two separate steps as it is done in the QRRK/MSC analysis presented before. Fig. 15 also shows the minor $C_2H_4 + HO_2$ channels (magnified by 100). Under these conditions, MultiWell predicts that $C_2H_4 + HO_2$ is nearly exclusively produced on the prompt time scale. However, the noise of the profile is too high to allow any conclusions as to whether small amounts of delayed $C_2H_4 + HO_2$ are being produced on longer time.

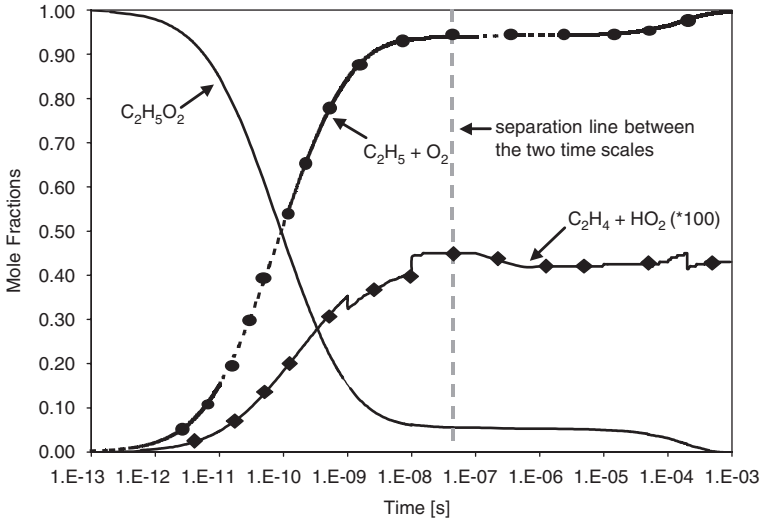

Fig. 15. MultiWell results of the decay of chemically activated ethyl peroxy at 700 K and 1 atm He. The separation line divides the time range into the "prompt" (left) and the "delayed" (right) regions.

4.4 Example 4: the reaction $C_2H_3+O_2 \rightarrow$ products

While the previous example is basically a single-well reaction (the isomerization and therefore reactions of the second well play only a very minor role), this final example deals with a multi-well multiple channel reaction. The reaction between vinyl radicals + O_2 was studied by several groups [102–104] and we will present here an analysis close to that provided by Bozzelli and Dean [102][14]. A schematic PES is shown in Fig. 16. It is characterized by the existence of several product and isomerization channels with barriers clearly below the entrance channel. If one considers only the energetic properties, the most favorable products would be CH_2O + HCO and OHCCOH (glyoxal) + H. However, these products can only be formed after two isomerization steps with relatively low *A*-factors.

In contrast, vinoxy ($\bullet CH_2CHO$) has the highest barrier but it is formed from the initial complex and the *A*-factor for this bond fission is expected to be high. Therefore, based on this qualitative analysis of the PES, one would expect a competition of these different channels.

[14]An improved surface is available in Klippenstein *et al.* [104]. Note that the use of a different PES will lead to different results.

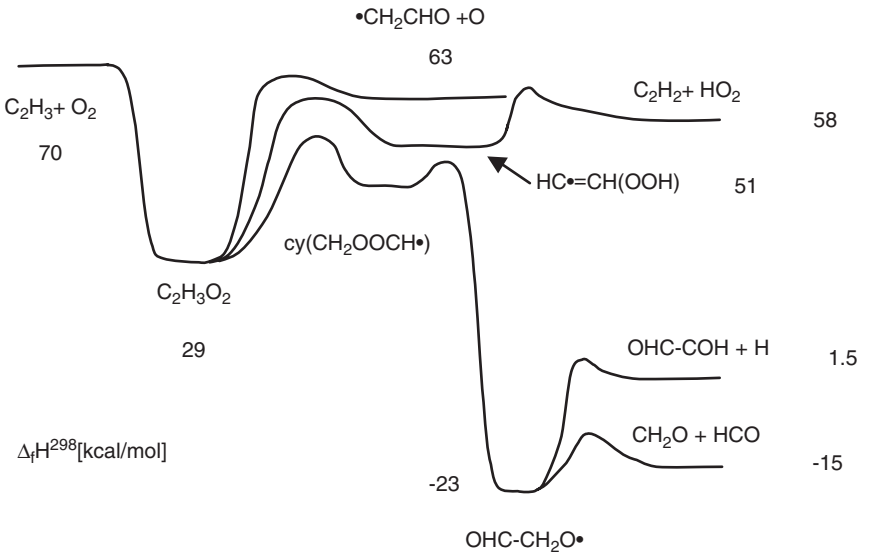

Fig. 16. Schematic representation of the PES for the reaction $C_2H_3 + O_2$ (taken from Bozzelli and Dean [102]).

Predicted apparent rate constants for various channels of the $C_2H_3 + O_2$ reaction are shown in Fig. 17. The plots at the top were calculated with CARRA_MSC for $T = 300\,K$. Apart from specific details about individual rate constants one can generally see two different types of profiles: (1) rate constants that decline with increasing pressure and (2) those that increase (at least over a certain pressure range) if the pressure rises. A closer look at the results reveals that all bimolecular product channels belong to the first category while stabilization channels form the second type. Since the $HC\bullet = CH(OOH)$ isomer is stabilized after isomerization from chemically activated $C_2H_3O_2$, this profile contains a maximum. At low pressures, a pressure increase leads to more collision stabilization of $HC\bullet = CH(OOH)$ and prevents it from further reaction to $C_2H_2 + HO_2$. This explains the initial increase of the production rate with pressure. At a certain pressure, a further pressure increase prevents the isomerization step from happening because the collisional stabilization of $C_2H_3O_2$ becomes too fast. Therefore, at this point a pressure increase leads to a reduction of the $HC\bullet = CH(OOH)$ formation rate.

The bottom part of Fig. 17 shows similar calculation results at 1300 K. As discussed earlier in the theory section an increase of the temperature shifts the fall-off region toward higher pressure. The magnitude of such a shift can be seen here: while the apparent rate constants at 300 K

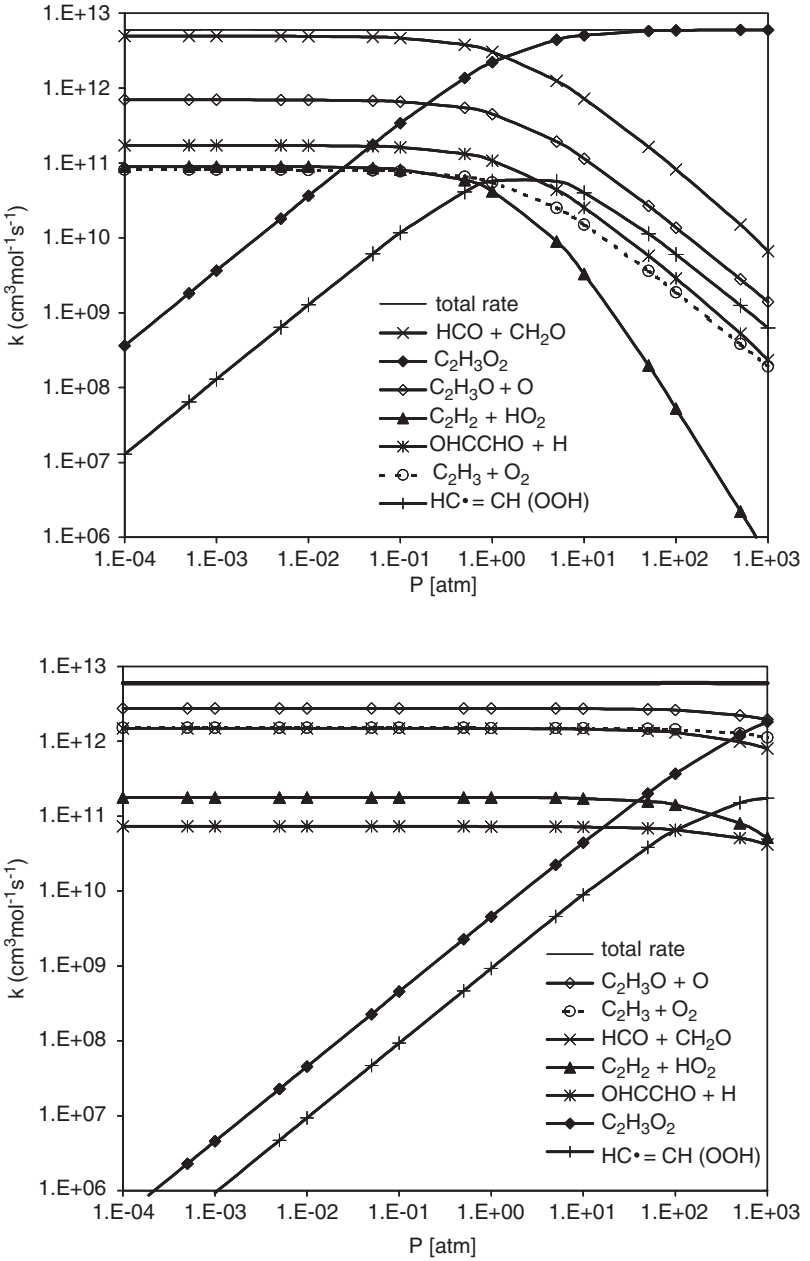

Fig. 17. Pressure dependence of the apparent rate constants for various channels in the reaction of C_2H_3 with O_2 at 300 K (top) and 1300 K (bottom).

approach the high-pressure limit somewhere ~100 atm, we notice that at 1300 K even a pressure of 1000 atm is too low to come close to the high-pressure limit[15]. Therefore, the 1300 K results are similar to the low-pressure results at 300 K. Now the nearest product channel (vinoxy + O) dominates. Another change is that the redissociation rate constant increased significantly compared to the results at 300 K.

We present only results from the chemically activated analysis, but the complete set of reactions would again include apparent rate constants for the thermal dissociation of all isomers as well.

5 REPRESENTATION OF $k(T, p)$ RATE COEFFICIENTS FOR MODELING

From the viewpoint of modeling, the ultimate goal of the kinetic analysis of pressure-dependent reaction systems is to provide reliable time-independent rate expressions $k(T, p)$ which can be incorporated into large kinetic models. The functional forms of these rate expressions can be rather complicated for multi-channel multiple wells systems, since—as we saw from the examples—the competition of product channels leads to strongly non-Arrhenius behavior. On the other hand, pressure-dependent rate constants for single-well single-channel reaction systems are comparably easy to describe. Therefore, we will divide this discussion into two sections going from simple fall-off systems to complex systems.

5.1 Single-well single-channel systems

Simple fall-off reactions are reasonably well described by Lindemann's collision activation model discussed in Section 2. It leads to an expression for the rate constant $k(T, p)$ based on k_0, k_∞, and [M] (see equation (8)). Improved treatments of single-well single-channel reactions differ only in details from the Lindemann model. Therefore, it seems natural to base a general fall-off description on an extension of equation (8):

$$k(T,p) = k_\infty(T)\frac{p_r}{1+p_r}F; \quad p_r = \frac{k_0(T)[M]}{k_\infty(T)} \tag{163}$$

Here, the "form or broadening factor" F is introduced. Both, k_0 and k_∞, are well-defined functions of the temperature and typically expressed in modified Arrhenius form. Thus, the role of the form factor is to correct

[15]At the high-pressure limit, the stabilization rate constant for $C_2H_3O_2$ is equal to the total rate constant.

the shape of the Lindemann fall-off curve to match the experimental data. Gilbert *et al.* [14] and Stewart *et al.* [105] provide parameterizations of this form factor that are implemented in modeling software such as Chemkin. Based on solutions of the MEs for a series of unimolecular reactions, Gilbert *et al.* define the broadening factor in terms of the so-called Troe formalism (or F_{cent} method) *via*

$$\log(F) = \frac{\log(F_{\text{cent}})}{1 + [(\log(p_{\text{r}}) + c)/(n - d(\log(p_{\text{r}}) + c))]^2} \tag{164}$$

with

$$c = -0.4 - 0.67\log(F_{\text{cent}})$$
$$n = 0.75 - 1.27\log(F_{\text{cent}})$$
$$d = 0.14$$

$$F_{\text{cent}} = (1 - a)\exp\left(-\frac{T}{T^{***}}\right) + a\exp\left(-\frac{T}{T^{*}}\right) + \exp\left(-\frac{T^{**}}{T}\right) \tag{165}$$

The approximation (165) contains four adjustable parameters (a, T^{***}, T^{*}, and T^{**}). Together with modified Arrhenius parameters (A, n, E_{a}) for both the low- and the high-pressure rate constants, the overall fall-off representation requires 10 parameters.

The second parameterization by Stewart *et al.* is commonly referred as the SRI formula. Here, the broadening factor F is given by

$$F = \left[a\exp\left(-\frac{b}{T}\right) + \exp\left(-\frac{T}{c}\right)\right]^{x} \tag{166}$$

which also contains four adjustable parameters (a, b, c, x). The implementation of this method in Chemkin provides even a fifth parameter, d, which scales F by d. In total 11 parameters are available to provide a good fit to the data.

In addition to the methods mentioned above, several other parameterizations to represent pressure-dependent rate constants based on k_0 and k_∞ are known; see, for example, the work by Wang and Frenklach [106], Gardiner [107], and Poole and Gilbert [108]. However, these methods did not find their way into modeling software such as Chemkin.

5.2 *Multi-well multi-channel systems*

Despite the rather large number of adjustable parameters, neither the Troe formalism nor the SRI method allows an adequate description of

the temperature and pressure dependences of apparent rate constants for multiple well, multiple channel systems [109,110]. A main reason for this is that these rate constants are not longer only determined by the physics that leads to the modified Arrhenius behavior of elementary rate constants or the simple fall-off predicted by the Lindemann concept. Instead, they are also strongly affected by the competition between different reaction channels. Since this competition can lead to a complicated function of temperature and pressure, the above methods fail.

Given that the apparent rate constants for complex reaction systems might strongly deviate from Lindemann-type rate expressions, the concept of correcting the Lindemann expression for $k(T, p)$ leads to problems.[16] Based on this conclusion, Venkatesh *et al.* [110] proposed the use of a purely mathematical approximation, Chebyshev polynomials, to represent the temperature and pressure dependences of apparent rate constants. Briefly, a Chebyshev polynomial of degree $i-1$ is defined as

$$\Phi_i(x) = \cos((i - l)\arccos(x)), \quad \text{with } x \in [-1, 1] \text{ and } i = 1, 2, \ldots \tag{167}$$

An arbitrary function $f(x)$ defined in the interval [–1, 1] can be well approximated *via*

$$f(x) \approx \sum_{k=1}^{N} c_k \Phi_k(x) \tag{168}$$

Provided $f(x)$ is known for certain values of x, the Chebyshev coefficients can be calculated analytically. Therefore, this approximation is not a fitting procedure. A second important feature is that the approximation is still good if only $M<N$ coefficients are used for the approximation.

For the representation of $k(T, p)$ data in terms of $1/T$ and $\log(P)$ we obtain the following relations:

$$\tilde{T} \leftarrow \frac{2T^{-1} - T_{\min}^{-1} - T_{\max}^{-1}}{T_{\min}^{-1} - T_{\max}^{-1}}, \quad \text{with } T_{\min} \le T \le T_{\max} \tag{169}$$

$$\tilde{p} \leftarrow \frac{2\log(p) - \log(p_{\min}) - \log(p_{\max})}{\log(p_{\max}) - \log(p_{\min})}, \quad \text{with } \log(p_{\min}) \le \log(p) \le \log(p_{\max}) \tag{170}$$

[16] However, Kazakov *et al.* [109] proposed a parameterization method, which is a generalization of the Lindemann formulation and which provides in many—though not all—cases a good description of $k(T, p)$.

$$\log(k(T,p)) = \log(k(\tilde{T},\tilde{p})) = \sum_{i=1}^{N_T}\sum_{j=1}^{N_p} \alpha_{ij}\Phi_i(\tilde{T})\Phi_j(\tilde{p}) \tag{171}$$

Equations (169) and (170) project the temperature ($1/T$) and pressure ($\log(p)$) to the required $[-1, 1]$ interval. Equation (171) formulates the approximation as a double sum over N_T Chebyshev polynomials in T and N_p Chebyshev polynomials in p. This representation thus requires $N_T N_p$ coefficients. In practice, $N_T = 7$ and $N_p = 3$ often provide excellent approximations of $k(T, p)$ rate constants over large temperature (300–2000 K) and pressure (0.001–100 atm) ranges. The Chebyshev representation is implemented in recent Chemkin releases and the program CARRA provides rate expressions in form of Chebyshev polynomials as an output option. More details can be found in Naik *et al.* [111].

6 SUMMARY AND LOOK TO THE FUTURE

Successful modeling of complex reaction systems strongly depends on the availability of accurate temperature- and pressure-dependent rate constants. We discussed the well-known basic theory starting with single-well systems and expanding to complex multiple-channel multiwell problems. Different treatments of these systems may be distinguished by two points: (1) the method to calculate $k(E)$ and $\rho(E)$ and (2) the energy transfer model. This leads to two extreme cases of sophistication. The most accurate and physically fundamental analysis utilizes RRKM theory to calculate $k(E)$ and $\rho(E)$ and solves the time-dependent ME to describe the energy transfer process. The ME may be solved in a deterministic or stochastic way. To serve the modeling community, the results of these calculations must be translated into time-independent rate constants. Though the RRKM/ME approach is in principle the most accurate method, it comes with a price: it requires detailed knowledge of molecular properties of the reactants as well as of the transition states involved. In contrast, a QRRK/MSC analysis can yield $k(T, p)$ data based on estimated thermodynamic and kinetic data of the reactants alone. Such an approach can be very useful as a screening method to identify crucial pressure-dependent reactions in mechanism, which later may be reanalyzed more thoroughly with RRKM/ME programs. The main advantage of such a strategy is to be able to focus on crucial reactions while less important ones can still be treated in a pressure-dependent manner.

Having said this, one should note that the example cases presented here as well as several other comparisons in the literature indicated that

results from the QRRK/MSC analysis compare remarkably well with more sophisticated programs. Just because the method is simple, it does not have to give bad predictions.

Given that the theoretical background is well established one might ask what the future will bring. At least four areas that need improvements can be identified:

(1) Molecule parameters can now be obtained from *ab initio* calculations. These still have large error margins despite the enormous progress made in the last few decades. Such errors translate into large uncertainties of the kinetic input data, thus making the predictions unreliable. For example, a realistic error in the activation entropy, $\Delta S^{\#}$, of 1 entropy unit changes the corresponding rate constant by a factor of 2.7. Many factors, such as the neglect of anharmonicity effects due to the HO–RR assumption, the neglect of coupling between internal modes, the use of single determinant (HF)-based methods to calculate the electronic energy, and so on, contribute to these deficiencies. Further increases of CPU power and advances in algorithms will certainly lead to continued improvements of *ab initio* results, which in turn will improve kinetic calculations.

(2) A precise description especially of loose transition states requires the formulation of microcanonical rate constants as function of E and J, since the conservation laws for both energy and total angular momentum must be obeyed. Unimol can handle $k(E, J)$ rate constants but most kinetic studies neglect effects of the angular momentum. In the future we expect that more attention will be paid to this issue.

(3) The energy transfer process is not well understood and energy transfer values such as $\langle E_{\text{down}} \rangle$ are frequently treated as adjustable parameters and not as well-defined input data for rate prediction. Continued advances in experimental methods and more sophisticated simulations (e.g., trajectory studies) will steadily improve our basic knowledge of energy transfer mechanisms. New models such as the BRW model and similar concepts indicate that progress has been made in this field. Nevertheless, a lot of work needs to be done to make energy transfer processes truly predictable.

(4) Finally, there is clearly a need for guidelines or evaluation methods to determine the criteria a reaction system needs to fulfill in order to be described by time-independent apparent rate constants. Vice versa, it would be useful to have a list of criteria at

hand that would allow to determine under which circumstances constant rate expressions fail to provide an adequate description of the chemistry and therefore time-dependent rate expressions are needed. The example calculations presented earlier clearly demonstrate that apparent rate constants are often a very good approximation—especially if all other sources of errors are taken into account. On the other hand, the observation of incubation times in certain shock tube experiments makes clear that these systems can only be modeled with a time-dependent description of the reaction rates. Hence, it would be desirable to have tools or criteria in hand that allow a kineticist to decide for which cases conventional reaction mechanisms are appropriate or, vice versa, which problems can only adequately described by formulating and solving the underlying time-dependent ME.

Even though the kinetic analysis of pressure-dependent reactions can clearly be improved, even at this point the kineticist is already in the position to provide relatively accurate pressure-dependent rate constants. We hopefully showed that such calculations are straightforward to perform, and we anticipate that $k(T, p)$ data for many more important reactions will soon be available for modeling studies.

REFERENCES

[1] K.A. Holbrook, M.J. Pilling, S.H. Robertson, *Unimolecular Reactions*. Wiley, Chichester, 1996.
[2] R.G. Gilbert, S.C. Smith, *Theory of Unimolecular and Recombination Reactions*. Blackwell Scientific Publications, Oxford, 1990.
[3] J. Troe, H.G. Wagner, *Berichte der Bunsengesellschaft für physikalische Chemie*, **71** (1967) 937–979.
[4] D.M. Golden, R.K. Solly, S.W. Benson, *J. Phys. Chem.*, **75** (1971) 1333–1338.
[5] R.E. Weston Jr., *Int. J. Chem. Kinet.*, **18** (1986) 1259–1276.
[6] H.W. Schranz, S. Nordholm, N.D. Hamer, *Int. J. Chem. Kinet.*, **14** (1982) 543–564.
[7] A.Y. Chang, J.W. Bozzelli, A.M. Dean, *Zeitschrift fuer Physikalische Chemie*, **214** (2000) 1533–1568.
[8] J.W. Bozzelli, A.Y. Chang, A.M. Dean, *Int. J. Chem. Kinet.*, **29** (1997) 161–170.
[9] S.C. Smith, M.J. McEwan, R.G. Gilbert, *J. Chem. Phys.*, **90** (1989) 4265–4273.
[10] S.C. Smith, M.J. McEwan, J.I. Brauman, *J. Phys. Chem. A*, **101** (1997) 7311–7314.
[11] J. Troe, *J. Phys. Chem.*, **83** (1979) 114–126.
[12] J. Troe, *Berichte der Bunsengesellschaft für physikalische Chemie*, **87** (1983) 161–169.
[13] J. Troe, *J. Chem. Phys.*, **66** (1977) 4758–4775.
[14] R.G. Gilbert, K. Luther, J. Troe, *Berichte der Bunsengesellschaft für physikalische Chemie*, **87** (1983) 169–177.
[15] G.Z. Whitten, B.S. Rabinovitch, *J. Chem. Phys.*, **38** (1963) 2466–2473.

[16] I.S. Gradshteyn, I.M. Ryzhik, *Table of Integrals, Series, and Products*. Academic Press, New York, 1965.
[17] J.R. Barker, L.M. Yoder, K.D. King, *J. Phys. Chem. A*, **105** (2001) 796–809.
[18] M.J. Pilling, S.H. Robertson, *Annu. Rev. Phys. Chem.*, **54** (2003) 245–275.
[19] N.S. Snider, *J. Chem. Phys.*, **42** (1965) 548–555.
[20] S.J. Klippenstein, J.A. Miller, *J. Phys. Chem. A*, **106** (2002) 9267–9277.
[21] J.A. Miller, S.J. Klippenstein, *J. Phys. Chem. A*, **107** (2003) 2680–2692.
[22] V.M. Bedanov, W. Tsang, M.R. Zachariah, *J. Phys. Chem.*, **99** (1995) 11452–11457.
[23] V.D. Knyazev, W. Tsang, *J. Phys. Chem. A*, **103** (1999) 3944–3954.
[24] H.W. Schranz, S. Nordholm, *Chem. Phys.*, **87** (1984) 163–177.
[25] D.T. Gillespie, *J. Comput. Phys.*, **22** (1976) 403.
[26] D.T. Gillespie, *J. Phys. Chem.*, **81** (1977) 2340–2361.
[27] J.R. Barker, *Chem. Phys.*, **77** (1983) 301–318.
[28] R.G. Gilbert, M.F.T. Jordan, S.C. Smith, G.P. Knight, *UNIMOL*. School of Chemistry, Sydney University, NSW, Australia, 1994.
[29] K.F. Lim, R.G. Gilbert, *J. Chem. Phys.*, **84** (1986) 6129–6140.
[30] V. Mokrushin, V. Bedanov, W. Tsang, M. Zachariah, V. Knyazev, *ChemRate*. NIST, Gaithersburg, MD, 1996–2002.
[31] V.D. Knyazev, W. Tsang, *J. Phys. Chem. A*, **104** (2000) 10747–10765.
[32] J. R. Barker, N. F. Ortiz, J. M. Preses, L. L. Lohr, A. Maranzana, P. J. Stimac. MultiWell Program Suite. Department of Atmospheric, Oceanic and Space Sciences, Department of Chemistry, University of Michigan Ann Arbor, MI 48109-2143, USA.
[33] J.R. Barker, *Int. J. Chem. Kinet.*, **33** (2001) 232–245.
[34] J.R. Barker, N.F. Ortiz, *Int. J. Chem. Kinet.*, **33** (2001) 246–261.
[35] A.M. Dean, *J. Phys. Chem.*, **89** (1985) 4600–4608.
[36] A.M. Dean, J.W. Bozzelli, E.R. Ritter, *Combust. Sci. Technol.*, **80** (1991) 63–85.
[37] C.Y. Sheng, J.W. Bozzelli, A.M. Dean, A.Y. Chang, *J. Phys. Chem. A*, **106** (2002) 7276–7293.
[38] For inquiries on the status/availability of this code, please send an email to hcarsten@mines.edu
[39] S.J. Klippenstein, A.F. Wagner, R.C. Dunbar, D.M. Wardlaw, S.H. Robertson, J.A. Miller, *VARIFLEX*. 1999.
[40] M. Garcia-Viloca, C. Alhambra, J. Corchado, M.L. Sanchez, J. Villa, J. Gao, D.G. Truhlar. CHARMMRATE. Department of Chemistry and Supercomputer Institute, University of Minnesota, Minneapolis, MN 55455-0431, USA, 2002.
[41] J.T. McKinnon, G. Murray, MarkNimlos, D. Hodgson, Z. Zhang, P. Guzman, B. Scroggs, B. Vandermeer, D. Ward, *OpenChem Workbench*. Colorado School of Mines, Golden, CO 80401, USA, 2003.
[42] T.N. Truong, T. Cook, M. Nayak, C. Boonyasiriwat, L.-T.T. Tran, S. Zhang, *CSEO*. 2003.
[43] M.W. Chase, Jr., C.A. Davies, J.R. Downey Jr., D.J. Frurip, R.A. McDonald, A.N. Syverud, *J. Phys. Chem. Ref. Data* (Suppl. 14) (1985) 1.
[44] http://webbook.nist.gov/chemistry
[45] R. Atkinson, D.L. Baulch, R.A. Cox, J.N. Crowley, R.F. Hampson, R.G. Hynes, M.E. Jenkin, M.J. Rossi, J. Troe, *Atmos. Chem. Phys.*, **4** (2004) 1461–1738.
[46] http://kinetics.nist.gov/index.php
[47] B.E. Poling, J.M. Prausnitz, O'J.P. Connell, *The Properties of Gases and Liquids*. McGraw-Hill, New York, 2000.

[48] R.J. Kee, F.M. Rupley, J.A. Miller, M.E. Coltrin, J.F. Grcar, E. Meeks, H.K. Moffat, A.E. Lutz, G. Dixon-Lewis, M.D. Smooke, J. Warnatz, G.H. Evans, R.S. Larson, R.E. Mitchell, L.R. Petzold, W.C. Reynolds, M. Caracotsios, W.E. Steward, P. Glarborg, C. Wang, O. Adigun, *Chemkin Collection*. Reaction Design, Inc., San Diego, CA, 2000.
[49] S.W. Benson, *Thermochemical Kinetics*. Wiley, New York, 1976.
[50] E.R. Ritter, J.W. Bozzelli, *Int. J. Chem. Kinet.*, **23** (1991) 767–778.
[51] T.H. Lay, J.W. Bozzelli, A.M. Dean, E.R. Ritter, *J. Phys. Chem.*, **99** (1995) 14514–14527.
[52] R. Sumathi, H.-H. Carstensen, W.H. Green Jr., *J. Phys. Chem. A*, **105** (2001) 6910–6925.
[53] R. Sumathi, H.-H. Carstensen, W.H. Green Jr., *J. Phys. Chem. A*, **105** (2001) 8969–8984.
[54] R. Sumathi, H.-H. Carstensen, W.H. Green Jr., *J. Phys. Chem. A*, **106** (2002) 5474–5489.
[55] R. Sumathi, W.H. Green Jr., *Theor. Chem. Acc.*, **108** (2002) 187–213.
[56] H.-H. Carstensen, A.M. Dean, unpublished data, 2006.
[57] W. Forst, *J. Phys. Chem.*, **76** (1972) 342–348.
[58] R.S. Brokaw, *Ind. Eng. Chem. Prog. Des. Dev.*, **8** (1969) 240–253.
[59] H. Wang, M. Frenklach, *Combust. Flame*, **96** (1994) 163–170.
[60] D.A. McQuarrie, J.D. Simon, *Molecular Thermodynamics*. University Science Books, Sausalito, CA, 1999.
[61] A.L.L. East, L. Radom, *J. Chem. Phys.*, **106** (1997) 6655–6674.
[62] K.S. Pitzer, W.D. Gwinn, *J. Chem. Phys.*, **10** (1942) 428–440.
[63] R.B. McClurg, R.C. Flagan, W.A. Goddard III, *J. Chem. Phys.*, **106** (1997) 6675–6680.
[64] P.Y. Ayala, H.B. Schlegel, *J. Chem. Phys.*, **108** (1998) 2314–2325.
[65] M.J. Frisch, G.W. Trucks, H.B. Schlegel, G.E. Scuseria, M.A. Robb, J.R. Cheeseman, V.G. Zakrzewski, J.A. Montgomery Jr., R.E. Stratmann, J.C. Burant, S. Dapprich, J.M. Millam, A.D. Daniels, K.N. Kudin, M.C. Strain, O. Farkas, J. Tomasi, V. Barone, M. Cossi, R. Cammi, B. Mennucci, C. Pomelli, C. Adamo, S. Clifford, J. Ochterski, G.A. Petersson, P.Y. Ayala, Q. Cui, K. Morokuma, D.K. Malick, A.D. Rabuck, K. Raghavachari, J.B. Foresman, J. Cioslowski, J.V. Ortiz, A.G. Baboul, B.B. Stefanov, G. Liu, A. Liashenko, P. Piskorz, I. Komaromi, R. Gomperts, R.L. Martin, D.J. Fox, T. Keith, M.A. Al-Laham, C.Y. Peng, A. Nanayakkara, M. Challacombe, P.M.W. Gill, B. Johnson, W. Chen, M.W. Wong, J.L. Andres, C. Gonzalez, M. Head-Gordon, E.S. Replogle, J.A. Pople, *Gaussian 98*. Gaussian, Inc., Pittsburgh, PA, 1998.
[66] A. Nicolaides, A. Rauk, M.N. Glukhovtsev, L. Radom, *J. Phys. Chem.*, **100** (1996) 17460–17464.
[67] L.A. Curtiss, K. Raghavachari, P.C. Redfern, J.A. Pople, *J. Chem. Phys.*, **106** (1997) 1063–1079.
[68] L.A. Curtiss, K. Raghavachari, P.C. Redfern, B.B. Stefanov, *J. Chem. Phys.*, **108** (1998) 692–697.
[69] K. Raghavachari, B.B. Stefanov, L.A. Curtiss, *J. Chem. Phys.*, **106** (1997) 6764–6767.
[70] C.F. Melius, *Proc. Combust. Inst.*, **21** (1986) 1953.
[71] G.A. Petersson, D.K. Malick, W.G. Wilson, J.W. Ochterski, J.A. Montgomery Jr., M.J. Frisch, *J. Chem. Phys.*, **109** (1998) 10570–10579.

[72] M. Saeys, M.-F. Reyniers, G.B. Marin, V.V. Speybroeck, M. Waroquier, *J. Phys. Chem. A*, **107** (2003) 9147–9159.
[73] E. Wigner, *Zeitschrift fuer Physikalische Chemie B*, **19** (1932) 203–216.
[74] W.H. Miller, *J. Am. Chem. Soc.*, **101** (1979) 6810–6814.
[75] M. Schwartz, P. Marshall, R.J. Berry, C.J. Ehlers, G.A. Petersson, *J. Phys. Chem. A*, **102** (1998) 10074–10081.
[76] T.V. Albu, J.C. Corchado, D.G. Truhlar, *J. Phys. Chem. A*, **105** (2001) 8465–8487.
[77] B.J. Lynch, D.G. Truhlar, *J. Phys. Chem. A*, **106** (2002) 842–846.
[78] W.-P. Hu, Y.-P. Liu, D.G. Truhlar, *J. Chem. Soc., Faraday Trans.*, **90** (1994) 1715–1725.
[79] I.G. Pitt, R.G. Gilbert, K.R. Ryan, *J. Phys. Chem.*, **99** (1995) 239–247.
[80] L.B. Harding, Y. Georgievskii, S.J. Klippenstein, *J. Phys. Chem. A*, **109** (2005) 4646–4656.
[81] S.J. Klippenstein, Y. Georgievskii, L.B. Harding, *Phys. Chem. Chem. Phys.*, **8** (2006) 1133–1147.
[82] T. Beyer, D.F. Swinehart, *Commun. Assoc.*, **16** (1973) 379.
[83] S.E. Stein, B.S. Rabinovitch, *J. Chem. Phys.*, **58** (1973) 2438–2445.
[84] R. Cambi, D. Cappelletti, G. Liuti, F. Pirani, *J. Chem. Phys.*, **95** (1991) 1852–1861.
[85] J.C. Slater, J.G. Kirkwood, *Phys. Rev.*, **37** (1931) 682–697.
[86] P. Paul, J. Warnatz, *Proc. Combust. Inst.*, **27** (1998) 495–504.
[87] K.F. Lim, R.G. Gilbert, *J. Chem. Phys.*, **92** (1990) 1819–1830.
[88] F. Caralp, P. Devolder, C. Fittschen, N. Gomez, H. Hippler, R. Mereau, M.T. Rayez, F. Striebel, B. Viskolcz, *Phys. Chem. Chem. Phys.*, **1** (1999) 2935–2944.
[89] J.W. Bozzelli, A.M. Dean, *J. Phys. Chem.*, **94** (1990) 3313–3317.
[90] J.D. DeSain, S.J. Klippenstein, J.A. Miller, C.A. Taatjes, *J. Phys. Chem. A*, **107** (2003) 4415–4427.
[91] J.A. Miller, S.J. Klippenstein, S.H. Robertson, *Proc. Combust. Inst.*, **28** (2000) 1479–1486.
[92] J.A. Miller, S.J. Klippenstein, *Int. J. Chem. Kinet.*, **33** (2001) 654–668.
[93] E.W. Kaiser, T.J. Wallington, J.M. Andino, *Chem. Phys. Lett.*, **168** (1990) 309–313.
[94] E.W. Kaiser, I.M. Lorkovic, T.J. Wallington, *J. Phys. Chem.*, **94** (1990) 3352–3354.
[95] E.W. Kaiser, *J. Phys. Chem.*, **99** (1995) 707–711.
[96] E.W. Kaiser, *J. Phys. Chem. A*, **106** (2002) 1256–1265.
[97] T.J. Wallington, J.M. Andino, E.W. Kaiser, S.M. Japar, *Int. J. Chem. Kinet.*, **21** (1989) 1113–1122.
[98] I.R. Slagle, E. Ratajczak, D. Gutman, *J. Phys. Chem.*, **90** (1986) 402–407.
[99] A.F. Wagner, I.R. Slagle, D. Sarzynski, D. Gutman, *J. Phys. Chem.*, **94** (1990) 1853–1868.
[100] I.C. Plumb, K.R. Ryan, *Int. J. Chem. Kinet.*, **13** (1981) 1011–1028.
[101] C. Sheng, J.W. Bozzelli, A.M. Dean, Presented at *2nd Joint Meeting of the U.S. Sections of the Combustion Institute*, Oakland, CA, 2001.
[102] J.W. Bozzelli, A.M. Dean, *J. Phys. Chem.*, **97** (1993) 4427–4441.
[103] A.M. Mebel, E.W.G. Diau, M.C. Lin, K. Morokuma, *J. Am. Chem. Soc.*, **118** (1996) 9759–9771.
[104] S.J. Klippenstein, J. Georgievskii, J.A. Miller, J.A. Nummela, B.K. Carpenter, P.R. Westmoreland, Presented at *Joint Meeting of the U.S. Sections of the Combustion Institute*, 2003.
[105] P.H. Stewart, C.W. Larson, D.M. Golden, *Combust. Flame*, **75** (1989) 25–31.
[106] H. Wang, M. Frenklach, *Chem. Phys. Lett.*, **205** (1993) 271–276.

[107] W.C. Gardiner, Presented at *12th IMACS World Congress on Scientific Computations*, Paris, 1988.
[108] J.S. Poole, R.G. Gilbert, *Int. J. Chem. Kinet.*, **26** (1994) 273–281.
[109] A. Kazakov, H. Wang, M. Frenklach, *J. Phys. Chem.*, **98** (1994) 10598–10605.
[110] P.K. Venkatesh, A.Y. Chang, A.M. Dean, M.H. Cohen, R.W. Carr, *AIChE J.*, **43** (1997) 1331–1340.
[111] C. Naik, H.-H. Carstensen, A.M. Dean, Presented at *WSS 2002 Spring Meeting of the Combustion Institute*, San Diego, CA, 2002. An executable (DOS) converting k(P,T) data into Chebyshev polynomials can be found on the companion CD or requested by sending an email to hcarsten@mines.edu